PB89-127484

Effects of Sorbent Injection for Sulfur Dioxide Removal on Particulate Control Systems for Coal-Fired Boilers

Southern Research Inst., Birmingham, AL

Prepared for

Environmental Protection Agency
Research Triangle Park, NC

Nov 88

U.S. Department of Commerce
National Technical Information Service
NTIS

TECHNICAL REPORT DATA

(Please read Instructions on the reverse before completing)

1. REPORT NO.: EPA/600/7-88/023

2.

3. RECIPIENT'S ACCESSION NO.: PB89 127484/AS

4. TITLE AND SUBTITLE: Effects of Sorbent Injection for Sulfur Dioxide Removal on Particulate Control Systems for Coal-fired Boilers

5. REPORT DATE: November 1988

6. PERFORMING ORGANIZATION CODE

7. AUTHOR(S): J. P. Gooch, J. L. DuBard, M. G. Faulkner, G. H. Marchant, Jr., R. S. Dahlin, and R. Beittel

8. PERFORMING ORGANIZATION REPORT NO.: SRI-ENV-88-620-5676

9. PERFORMING ORGANIZATION NAME AND ADDRESS:
Southern Research Institute
Birmingham, Alabama 35255

10. PROGRAM ELEMENT NO.

11. CONTRACT/GRANT NO.: CR811683

12. SPONSORING AGENCY NAME AND ADDRESS:
EPA, Office of Research and Development
Air and Energy Engineering Research Laboratory
Research Triangle Park, NC 27711

13. TYPE OF REPORT AND PERIOD COVERED: Final; 10/84 - 10/87

14. SPONSORING AGENCY CODE: EPA/600/13

15. SUPPLEMENTARY NOTES: AEERL project officer is Louis S. Hovis, Mail Drop 4, 919/541-3374. Initial project officer was Samuel L. Rakes.

16. ABSTRACT

The report describes studies undertaken to quantify the effects of dry SO2 sorbent injection on ESP operation with a coal-burning utility boiler. The specific operation of interest was EPA's limestone injection, multistage burners (LIMB) process. The combination of spent sorbent and fly ash has a higher resistivity, a higher mass concentration, and a finer particle-size distribution than the ash alone; all of these factors diminish the effectiveness of ESP. Also investigated was chemical conditioning to reduce the resistivity problem, the only one of three concerns stemming from sorbent injection that can be readily mitigated. Other topics studied were: the recycle, disposal, and utilization of waste-ash/sorbent mixtures; the selection and modification of sorbents to improve SO2 capture in the furnace; and the reactivation of spent sorbent by humidification to achieve supplemental post-furnace capture of SO2.

17. KEY WORDS AND DOCUMENT ANALYSIS

a. DESCRIPTORS		b. IDENTIFIERS/OPEN ENDED TERMS	c. COSATI Field/Group	
Pollution	Coal	Pollution Control	13B	21D
Sorbents	Utilities	Stationary Sources	11G	
Sulfur Dioxide	Boilers	Particulate	07B	13A
Particles	Limestone	Limestone Injection Multistage Burners (LIMB)	14G	08G
Fly Ash	Humidification		21B	13H
Electrostatic Precipitators			13I	

18. DISTRIBUTION STATEMENT: **Release to Public**

19. SECURITY CLASS (This Report): Unclassified

20. SECURITY CLASS (This page): Unclassified

21. NO. OF PAGES: 131

22. PRICE: PC 21.95/MF 6.95

EPA Form 2220-1 (9-73)

PB89-127484

EPA/600/7-88/023
November 1988

EFFECTS OF SORBENT INJECTION FOR SULFUR DIOXIDE REMOVAL ON PARTICULATE CONTROL SYSTEMS FOR COAL-FIRED BOILERS

by
John P. Gooch
James L. DuBard
M. Greg Faulkner
G. H. Marchant, Jr.
Robert S. Dahlin
Roderick Beittel
Southern Research Institute
Birmingham, Alabama 35255

Cooperative Agreement No. CR 811683

EPA Project Officer
Louis S. Hovis
Air and Energy Engineering Research Laboratory
U.S. Environmental Protection Agency
Research Triangle Park, North Carolina 27711

AIR AND ENERGY ENGINEERING RESEARCH LABORATORY
OFFICE OF RESEARCH AND DEVELOPMENT
U.S. ENVIRONMENTAL PROTECTION AGENCY
RESEARCH TRIANGLE PARK, NC 27711

REPRODUCED BY
U.S. DEPARTMENT OF COMMERCE
NATIONAL TECHNICAL INFORMATION SERVICE
SPRINGFIELD, VA. 22161

NOTICE

This document has been reviewed in accordance with U.S. Environmental Protection Agency policy and approved for publication. Mention of trade names or commercial products does not constitute endorsement or recommendation for use.

ABSTRACT

This report describes a research project concerned with the effects of sorbent injection for SO_2 control on the performance of electrostatic precipitators (ESPs). The report relates specifically to the LIMB process (Limestone Injection, Multistage Burners) of the U.S. Environmental Protection Agency, whereby limestone or hydrated lime is injected into the furnace of a coal-burning utility boiler. Much of the work described was performed to support EPA's demonstration of LIMB at Ohio Edison's power station at Lorain, OH.

The project work was organized under five tasks. The scope and results of each are described in the following paragraphs:

Task 1. Development of a predictor of the electrical resistivity of mixtures of fly ash and LIMB sorbent. The principal positive contribution from this task was finding the need for a new procedure to meet the measurement requirements on the resistivity of ash-sorbent mixtures. Funding limitations on this project led to the development of the new procedure under a different EPA-sponsored project. The development of the predictor is an objective that has not yet been satisfied.

Task 2. Determination of the effect of high mass loadings of ash and sorbent on ESP performance. This task was approached both experimentally and theoretically. The deterioration of ESP performance as a consequence of high mass loadings and related effects (high resistivity and high fine-particle concentrations) was demonstrated experimentally. The need for a revised ESP model for calculating the effects of LIMB on ESP performance was satisfied through theoretical developments.

Task 3. Pilot-scale testing of LIMB impacts on an ESP. This task required use of a pilot scale ESP with a large furnace with a LIMB modification operating over a long term. The site finally selected for this task, in the Canadian province of New Brunswick, was initially characterized but finally deemed unsuitable for further work. The test program in Canada was thus canceled; a similar program will be conducted as part of the LIMB demonstration at Edgewater.

Task 4. Investigation of recycle, disposal, and utilization of LIMB ash-sorbent mixtures. Successful developments were made in all three aspects of this task. Perhaps the most definitive conclusion is that LIMB waste poses no hazard for landfill disposal under present regulations. LIMB waste can be activated by hydration; to acquire useful sorbent for recycle, however, requires separation of sorbent from ash. No satisfactory method has yet been demonstrated for this separation. Utilization of LIMB waste for synthetic aggregate seems promising, as for highway construction, but further research is required.

Task 5. Pilot-scale combustor studies to characterize LIMB sorbents. This was a multifaceted task. The primary positive developments were 1) a confirmation of the value of lignosulfonate as an additive to hydrated lime; 2) the definition of the conditions under which furnace-injected sorbent may be activated with a water spray in a low-temperature duct, to achieve enhanced SO_2 capture; and 3) confirmation of the adaptability of LIMB ash-sorbent mixtures to conditioning by water vapor, to overcome their high electrical resistivities.

This report was submitted in fulfillment of Cooperative Agreement No. CR 811683 by Southern Research Institute under the sponsorship of the U.S. Environmental Protection Agency. This report covers the period form October 1984 to October 1987.

CONTENTS

Abstract iii
Figures vii
Tables x
Acknowledgments xi

1. Introduction 1-1
2. Summary, Conclusions, and Recommendations 2-1
3. Task 1. Development of a Resistivity Predictor for Ash-Sorbent Mixtures 3-1
   - Introduction 3-1
   - Collection and Characterization of Samples 3-1
   - Experimental Analyses 3-1
   - Experimental Results 3-3
   - Changes in the Sample Properties during Measurements 3-12
   - Conclusion 3-18
4. Task 2. Investigation of the Effect of High Mass Loading on Fly Ash Precipitators 4-1
   - Introduction 4-1
   - Laboratory Experiments 4-1
     - Fly Ash with Lime Injection 4-3
     - Fly Ash with Lime Injection and SO_3 Addition 4-3
     - Application of Results 4-8
   - Theoretical Work 4-8
     - Mathematical Structure 4-11
     - Comparison of Results 4-17
   - Summary 4-26
5. Task 3. Pilot-Scale Investigation of ESP Performance with Furnace Sorbent Injection 5-1
6. Task 4. Studies of LIMB Ash Recycle, Disposal, and Utilization 6-1
   - Introduction 6-1
   - Objectives and Scope 6-1
   - Results and Discussion 6-3
     - Recycle 6-3
     - Disposal 6-10
     - Utilization 6-13
   - Conclusions and Recommendations 6-17
7. Task 5. Characterization of Sorbents through Pilot-Scale Combustor Studies 7-1
   - Introduction 7-1
   - Objectives and Scope 7-1

CONTENTS (Continued)

Results and Discussion 7-2
Screening of Hydrated Lime for Reactivity with SO_2 7-2
Comparison of Lignosulfonate Formulations as Additives in Hydrated Lime 7-6
Investigation of Post-Furnace Humidification to Achieve Sorbent Activation 7-10
Investigation of Charge-Augmented Humidification (CASH) 7-18
Study of Conditioning for Resistivity Control 7-24
8. References 8-1

APPENDIX

Quality Control Evaluation Report A-1

FIGURES

Number		Page
3-1	Resistivity versus temperature for an ash-sorbent sample from Hallmark (Lot No. 3) coal and Longview hydrated lime.	3-8
3-2	Resistivity versus temperature for an ash-sorbent sample from Pittsburgh No. 8 (EPA Demo) coal and Marblehead hydrated lime.	3-9
3-3	Resistivity versus temperature for an ash-sorbent sample from Pittsburgh No. 8 (EPA Demo) coal and Marblehead hydrated lime.	3-10
3-4	Resistivity versus Li + Na concentration for ash-sorbent mixtures at 85 °C and 7% H_2O.	3-13
3-5	Resistivity versus Li + Na concentration for ash-sorbent mixtures at 112 °C and 7% H_2O.	3-14
3-6	Resistivity versus Li + Na concentration for ash-sorbent mixtures at 144 °C and 7% H_2O.	3-15
3-7	Effect of increasing temperature on the surface area of selected ash-sorbent mixtures.	3-17
4-1	Segmented-plate electrostatic precipitator.	4-2
4-2	Variation in current with time for fly ash and hydrated lime at 45 kV. Lime injection began at time = 0 min.	4-4
4-3	Current on each plate strip for fly ash and lime at 45 kV.	4-5
4-4	V-I curves for fly ash and fly ash plus hydrated lime plus SO_3.	4-6
4-5	Variation in current with time for fly ash with hydrated lime and SO_3 conditioning at 45 kV.	4-7
4-6	Current on each plate strip for fly ash with hydrated lime and SO_3 conditioning at 45 kV.	4-9
4-7	Outlet mass loading as a function of SCA for an ESP collecting coal with hydrated lime and SO_3.	4-10
4-8	Logic diagram for the standard version of the ESP Model (Revision 3).	4-15
4-9	Logic diagram for the revised version of the ESP Model.	4-16
4-10	Particulate charge calculated by the standard and revised versions of the ESP Model.	4-18

FIGURES (continued)

Number Page

4-11 Calculated electric fields for the standard and revised versions of the ESP Model. 4-19

4-12 Total space charge density calculated by the standard and revised versions of the ESP Model. The calculation is at the plate directly opposite the wire. 4-21

4-13 Particulate and ionic components of the space charge calculated by the revised version of the ESP Model. The calculation point is at the plate directly opposite the wire. 4-22

4-14 Ionic and particulate current densities predicted by the standard and revised versions of the ESP Model. 4-23

4-15 Mass penetration calculated by the standard and revised versions of the ESP Model. 4-24

4-16 Fractional penetration calculated by the standard and revised versions of the ESP Model compared to measured data. 4-25

4-17 Outlet particle migration velocities calculated by the standard and revised versions of the ESP Model. 4-27

5-1 ESP trailer and ductwork. Base Gagetown, Oromocto, N.B. 5-3

5-2 ESP control trailer and ductwork. Base Gagetown, Oromocto, N.B. 5-4

5-3 Test facility, Base Gagetown, Oromocto, N.B. 5-5

5-4 Inlet ductwork, heater exchanger, heater and humidification chamber. Base Gagetown, Oromocto, N.B. 5-6

5-5 Schematic drawing of Gagetown facility. 5-7

6-1 SO_2 removal as a function of Ca/S ratio for Longview hydrate and rehydrated ash-sorbent mixture (from demonstration coal and Tenn-Luttrell coarse limestone). 6-5

6-2 Size dependence of elemental concentrations in an ash-sorbent mixture produced by addition of Longview hydrated lime during combustion of Indiana coal. 6-6

6-3 Effect of reaction flask temperature on degree of hydration. 6-8

6-4 Effect of steam flow on ash elutriation. 6-9

FIGURES (concluded)

Number Page

7-1 Particle-size distributions (by sedimentation) of commercial calcitic hydrates. 7-4

7-2 Enhancement of the utilization of Longview hydrate with Lignosite powder or liquid (Ca/S = 2). 7-8

7-3 Utilization of additive-free Marblehead hydrate versus temperature as revealed by gas and solids analysis. 7-9

7-4 Enhancement of the utilization of Marblehead hydrate with Lignosite powder or liquid (Ca/S = 2). 7-11

7-5 Humidification chamber showing injection and sampling points. 7-13

7-6 Schematic representation of humidification modes 7-15

7-7 Spray chamber and residence time chamber. 7-20

7-8 Apparatus for drop charging and charge measurement. 7-22

7-9 Charge augmentation of humidification to enhance SO_2 capture with limestone. 7-23

7-10 Resistivity of fly ash and ash-sorbent mixture with and without SO_3 conditioning. 7-26

7-11 Resistivity of ash-sorbent mixture with water conditioning. 7-27

7-12 Resistivity of ash-sorbent mixture as a function of temperature and humidification. 7-28

7-13 Pilot ESP voltage-current curves. 7-30

7-14 ESP electrical performance during sorbent injection, with and without humidification. 7-31

TABLES

Number Page

3-1 Summary of ash-sorbent samples and data. 3-2

3-2 Summary of chemical analyses for ash-sorbent mixtures. 3-4

3-3 Chemical and electrical characteristics of ash-sorbent mixtures at 7% H_2O. 3-5

3-4 Chemical and electrical characteristics of ash-sorbent mixtures at 11% H_2O. 3-6

3-5 Chemical and electrical characteristics of ash-sorbent mixtures at 15% H_2O. 3-7

3-6 Summary of various tests for ash-sorbent mixtures. 3-11

3-7 Effect of heat on ash-sorbent mixtures. 3-16

4-1 Glossary of variables used in Section 4. 4-12

5-1 Gagetown Unit 2 boiler data. 5-8

5-2 Gagetown proximate and ultimate coal analyses. 5-9

5-3 Gagetown solids concentrations. 5-10

5-4 Gagetown gas characteristics during mass loading tests. 5-11

5-5 Gagetown gas analyses at ESP inlet. 5-12

5-6 Gagetown chemical analysis of solids. 5-13

6-1 Leachate data for an ash-sorbent mixture from the pilot-scale combustor. 6-11

6-2 Wetting tests with Edgewater demonstration modified ash. 6-12

6-3 Analysis of runoff from landfill test site. 6-14

6-4 Analysis of liquid and extracts of solids at landfill test site. 6-15

6-5 Results of Aardelite's tests on LIMB fly ash pellets. 6-16

6-6 EP toxicity data for extracts from LIMB ash pellets. 6-18

7-1 Properties of commercial calcitic hydrates. 7-3

ACKNOWLEDGEMENTS

The authors wish to acknowledge the guidance and support of the management and staff of the Engineering Applications Division of EPA's Air and Energy Engineering Research Laboratory. Louis S. Hovis served as project officer. Sam L. Rakes, Norman Kaplan, and Leslie E. Sparks provided assistance on various aspects of project administration. James H. Abbott and Dennis C. Drehmel provided general guidance and support.

The authors also wish to acknowledge the contributions of the technical staff within the Environmental Sciences Department of Southern Research Institute. The main contributors were John D. Carlton, C. Chrissy Clark, Walter R. Dickson (deceased February 1988), Bruce A. Morgan, and E. Alexander Stokes, III.

This report was assembled by Edward B. Dismukes from material supplied by the individual task leaders.

SECTION 1

INTRODUCTION

This is the final report of research performed by Southern Research Institute (SRI) under Cooperative Agreement No. CR 811683, "Effects of Sorbent Injection for Sulfur Oxide Removal on Particulate Control for Coal-Fired Boilers." This work was monitored initially by the Particulate Technology and LIMB Technology Branches and later by the Technology Development Branch of the Air and Energy Engineering Research Laboratory (AEERL), the U.S. Environmental Protection Agency; Research Triangle Park, NC. The research was conducted over a 3-year period beginning in October 1984 and terminating in October 1987.

The technology known as LIMB (Limestone Injection, Multistage Burners) is being developed by EPA as a means of controlling SO_2 emissions from coal-fired boilers. This technology is one of several based in dry-sorbent injection that are expected to be adaptable in retrofit applications with boilers that predate new-source performance standards. It provides only partial reduction of SO_2 emissions at economical operating costs; however, it requires a lesser capital investment than more efficient conventional processes, such as wet scrubbing, and is thus a candidate for application where old boilers continue in service. One of the problems in implementing LIMB technology is the difficulty of maintaining acceptable levels of particulate emissions. The concentration of suspended solid matter that must be removed is greatly increased; moreover, the fraction of the solids that is small in particle size and thus especially difficult to remove is substantially increased. These changes in suspended solids will have unfavorable consequences in any particulate-control device. Their impact is most serious, however, in terms of the performance of electrostatic precipitators (ESPs), since most of the boilers where LIMB may be applied operate in conjunction with ESPs for particulate control.

The research effort under the cooperative agreement was organized to address five principal tasks:

1. Development of a predictor of the electrical resistivity of mixtures of fly ash and sorbent, which result from sorbent injection into coal-fired boilers.

2. Determination of the effect of high mass loadings of ash-sorbent mixtures on ESPs.

3. Designing and implementing a pilot-scale program of electrostatic precipitation with furnace sorbent injection.

4. Investigation of recycle, disposal, and utilization of LIMB ash-sorbent mixtures.

5. Studies with a pilot-scale combustor to characterize sorbents that may be applicable in the LIMB process.

The research performed was a combination of laboratory and pilot-scale investigations. The pilot-scale studies were primarily accomplished at SRI's one-million-Btu/h (300-kW) coal-burning research combustor in Birmingham, AL; this combustor is referred to in this report as the Coal Combustion Facility. In particular, samples of ash and sorbent that were generated for laboratory study under Task 1, 2, and 4 came from that combustion facility. Moreover, the research performed under Task 5 was performed at that facility. The research required under Task 3, on the other hand, required a source of combustion gas and LIMB ash that was larger in size and operable far more continuously without major change in conditions than the pilot-scale combustor in Birmingham. Two preliminary sites for studies under Task 3, to be conducted with a portable trailer-mounted pilot-scale precipitator, were considered and then abandoned – facilities of the Energy and Environmental Research Corporation near Irvine, CA, and the Homer City Station of the Pennsylvania Electric Company. Later, a third site at the Canadian Defence Forces at Base Gagetown in New Brunswick was selected and used for certain preliminary research; ultimately, however, the work at Gagetown was terminated prior to completion, due to unforeseen problems with the boiler performance that adverse- impacted the ability to conduct ESP experiments.

This report will make it clear that the term "limestone" in the acronym LIMB was broadened to cover $Ca(OH)_2$ as well as $CaCO_3$ as a relevant form of a calcium-based sorbent. This broadening of the LIMB concept accompanied EPA's decision to make the first full-scale demonstration of LIMB with $Ca(OH)_2$ as the sorbent. (This sorbent is also known as "hydrate" or hydrated lime — a term that signifies the chemical hydration of CaO.) As the research program evolved, much of the work performed was related specifically to the LIMB demonstration, which is underway at the Edgewater Station of Ohio Edison Company at Lorain, OH.

SECTION 2

SUMMARY, CONCLUSIONS, AND RECOMMENDATIONS

The details of the work performed under five major tasks are presented in the five following sections of this report. The scope of each phase of study and the principal conclusions and recommendations reached are as follows:

Task 1. Development of a resistivity predictor for ash-sorbent mixtures. The first step was to obtain a variety of samples of ash-sorbent mixtures and characterize them with respect to mineral composition, particle size, surface area, density, and electrical resistivity. Efforts were then made to establish correlations between resistivity and one or more of the other properties. In particular, an attempt was made to establish a relationship between resistivity and the sum of lithium and sodium contents, which is the basis of an earlier correlation for ordinary fly ash; this attempt failed. In the course of the work performed, the discovery was made that the procedure used for resistivity measurements altered the surface area of the ash-sorbent mixtures and thus altered the resistivity.

The need for a revised procedure for measuring resistivity was thus evident. By mutual agreement between EPA and SRI, work toward that end was undertaken under another cooperative agreement (CR 812282) and will be described in a report under that agreement. The effort to develop the resistivity predictor, however, remains unfulfilled; the prospects for completing this effort successfully cannot be evaluated from the data now available.

Task 2. Investigation of high mass loadings in ESPs. This task was addressed through both experimental and theoretical approaches. The experimental effort centered on the use of a specially instrumented ESP that was operated in conjunction with SRI's pilot-scale combustion facility, which produced an ash of high resistivity (2×10^{12} ohm-cm), an elevated concentration (higher by a factor of three), and a particle-size distribution with a much greater proportion of fine material. The primary observations were that 1) there was an ESP malfunction owing to the high mass resistivity and 2) there was a strong space-charge suppression of the corona (observable when the ash resistivity was lowered with SO_3) due to the fineness of the particle-size distribution. The data were used in the existing ESP model to project the effect on ESP emissions of adding the LIMB process to a typical boiler.

The theoretical study consisted of the development of a revised version of the ESP model, which is responsive to a wider range of ESP operating conditions. Comparisons of the revised model with a limited number of field data sets indicate that the revised model functions satisfactorily as a predictive tool. Nevertheless, there was an indicated need for certain further refinements in the model, to be undertaken under Cooperative Agreement CR 812282. Specific recommendations in this regard appear at the conclusion of Section 4.

Task 3. Performance of a pilot-scale program of ESP performance with furnace sorbent injection. Arrangements for pursuing this task at Base Gagetown of the Canadian armed forces in New Brunswick were completed, and certain background data were obtained, as documented in Section 5 of this report. Ultimately, however, the pilot facilities assembled at Gagetown were dismantled at EPA's direction before the planned measurement program could be completed. A crucial factor that led to this action was the abnormally high carbon content (LOI) of the ash produced in the Gagetown burners, which would have had a serious impact on ESP performance, regardless of the impact of sorbent injection.

An alternate to the program planned at Gagetown will now be carried out as part of the LIMB demonstration at the Edgewater plant in Lorain, OH, under Cooperative Agreement CR 812811.

Task 4. Studies of LIMB ash recycle, disposal, and utilization. The results of these studies demonstrate that LIMB ash can be reactivated by hydration and can then be reinjected to achieve further utilization for SO_2 capture. A principal stumbling block to this approach, however, is the excessive mass loadings that will occur unless somehow the sorbent can be separated from the fly ash. Potential separation methods that deserve further study are based on a cyclone or an ESP, a dense-phase classifier, or a steam elutriator.

Both laboratory and field tests showed that LIMB ash can be safely handled and used for landfilling. Cementitious reactions in the moist ash produce a nearly impermeable product, which has a minimal potential for groundwater contamination. LIMB ash cannot be classified as a hazardous waste under any of the RCRA criteria.

Synthetic aggregates represent one of the most promising uses for LIMB ash. Such aggregates are likely to conform to highway specifications; however, further development of aggregate technology and testing of aggregate in a highway test section are needed.

Task 5. Studies of sorbent characterization in the SRI pilot-scale combustor. There was a diversity of topics investigated under this task. The principal subjects of study and the results obtained were as follows:

- A set of commercial hydrated limes was collected and characterized with respect to physical properties and chemical reactivity (with respect to SO_2 capture during furnace injection). Correlations between physical properties and chemical reactivity could not be established, even though significant variations in properties presumed to be important (particle size and surface area, for example) were encountered. The range in furnace utilization was relatively narrow — less than 20% on a relative basis. The economic significance of even such a narrow range, however, justifies ongoing efforts to clarify the relationship of physical properties to utilization.

- The effectiveness of calcium lignosulfonate as an additive in hydrated lime, for increasing utilization during furnace injection, was confirmed, specifically through demonstration of the utility of this dispersant as either a dry powder or an aqueous solute.

- Certain fundamental studies of SO_2 capture by hydrated lime at low gas temperatures, under the influence of humidification, were studied. A primary conclusion is that water vapor alone cannot activate the solid appreciably. Physical wetting, on the other hand, which occurs when dry entrained sorbent particles and water spray droplets collide, has the potential for strongly activating the solid. The practical limitation of the wetting process is the infrequency of particle-droplet collisions, which allows most of the sorbent particles to remain dry and hence unreactive.

- A brief study of charge-augmented sorbent humidification (referred to by the acronym CASH) was performed. In this process, sorbent particles were charged negatively and water droplets positively, to enhance the collision frequency. Further study of the concept was pursued under Cooperative Agreement CR 812811; in the final analysis, no beneficial result of the process seems to be in the offing.

- A comparison was made of the effects of SO_3 gas and water vapor as conditioning agents, to alleviate the concern with high resistivity of ash-sorbent mixtures in an ESP. At concentrations of about 60 ppm, SO_3 was found largely ineffective — much less promising than had been indicated by prior studies. At addition levels around 5% by volume (which gave an approach to adiabatic saturation of 20 °F or 11 °C), water vapor, on the other hand, produced a much more promising result — a reduction in resistivity from 1×10^{13} to 1×10^{11} ohm-cm.

SECTION 3

TASK 1. DEVELOPMENT OF A RESISTIVITY PREDICTOR FOR ASH-SORBENT MIXTURES

INTRODUCTION

The objective of this task was to develop a mathematical model for predicting the bulk electrical resistivity of particulate matter composed of ash-sorbent mixtures. A resistivity predictor model was available for ordinary fly ash from pulverized coal combustion (1). This mathematical predictor had been widely accepted and used in the electric utility industry. However, no comparable predictive tool was available for combinations of fly ash and sorbent.

COLLECTION AND CHARACTERIZATION OF SAMPLES

The first step in this task was to obtain as many samples as possible that were composed of fly ash and sorbent. The number and type of samples were determined by the work which was going on in the Coal Combustion Facility at Southern Research Institute. This task did not have combustor operating expense included in its budget. Therefore, the samples were generated in the combustor for various other projects. The samples were collected from either the baghouse discharge or from a sample probe. Table 3-1 lists the samples that were collected in sufficient quantity to permit at least a mineral analysis and a laboratory resistivity measurement.

The table gives the sample number, notebook number, coal type, sorbent type, and analyses that were performed. The ash-sorbent samples are divided into two categories. Samples in the first category were generated with hydrated lime injection and are designated by a two-digit code number. Samples in the second category were generated with limestone injection and are designated by a three-digit code number.

EXPERIMENTAL ANALYSES

Various tests were performed on the collected ash-sorbent samples (mineral analysis, laboratory resistivity, Bahco particle sizing, BET surface area, and helium pycnometry density) to determine if correlations existed between the resistivity and other properties.

The laboratory resistivity measurement was performed according to IEEE Standard 548-1984 (descending temperature), which had been developed for fly ash. The procedure for this measurement begins by placing each sample in a special test cell. These cells are placed in an oven and the sample is annealed overnight at 450 °C. The following day, a specified water concentration is added and the oven temperature is allowed to descend while current and voltage values are measured at various temperatures. From these current and voltage values a resistivity value is calculated for each corresponding

TABLE 3-1. SUMMARY OF ASH-SORBENT SAMPLES AND DATA

Code Number	Coal Type	Sorbent Type	Analyses[a]	Resistivity Data[b]
103	Illinois	Eldorado (Limestone)		L
104	Pittsburgh #8	Lowellville (Limestone)	CU	L
106	Kentucky #9	Reed (Limestone)		L
108 C0059-1-2C	Indiana (Lot No. 2)	Vicron 45-3 (Limestone)	CU/AM	S/L
110	Freeman #6 (Illinois)	Vicron 45-3 (Limestone)	CU/AM	S
112 RPC-5/27C	Illinois (Cilco)	Vicron 45-3 (Limestone)	CU/AM	S/L
03	Indiana (Lot No. 3)	Longview (Hydrated Lime)	CU/AM	S/L
105 C0751-137	Hallmark (Lot No. 1)	Vicron 45-3 (Limestone)	CU/AM	S/L
111 C0890-30	Hallmark (Lot No. 2)	Marianna #3 (Limestone)	CU/AM	S/L
12 C0890-80	Hallmark (Lot No. 3)	Longview (Hydrated Lime)	CU/AM	S/L
02 D0127-61	HC Deep Cleaned (Penelec)	Longview (Hydrated Lime)	CU/AM	S/L
01 D0249-107&109	Hallmark (Lot No. 3)	Longview (Hydrated Lime)	CU/AM	S/L
14 D0292-37	Pittsburgh #8 (EPA Demo)	Marblehead (Hydrated Lime)	CU/AM	S/L
04 D0316-103,104&106	Indiana No. 7 (PSI)	Longview (Hydrated Lime)	CU/AM	S/L
107 D0316-136	Indiana No. 7 (PSI)	Marianna #3 (Limestone)	CU/AM	S/L
08 D0292-114	Pittsburgh #8 (EPA Demo)	Mercer (Hydrated Lime)	CU/AM	S/L
15 D0292-118	Pittsburgh #8 (EPA Demo)	Huron (Hydrated Lime)	CU/AM	S/L
13 C0890-105	Hallmark (Lot No. 3)	Longview (Hydrated Lime)	CU/AM	S/L
16 AWOL08	Ontario Hydro		AM	L
109	Gagetown	Limestone	AM	L
17 D0292-46-5	Pittsburgh #8 (EPA Demo)	Marblehead (Hydrated Lime)	AM	L
18 D0687-28-1	Pittsburgh #8 (EPA Demo) Lot 2	Marblehead (Hydrated Lime)	AM	L
119 D0687-13-2	Pittsburgh #8 (EPA Demo) Lot 2	Tenn.-Luttrell (Limestone)	AM	L
101 D0687-128-1	Pittsburgh #8 (EPA Demo)	Tenn.-Luttrell (Limestone)	AM	L
102 D0687-118-3	Pittsburgh #8 (EPA Demo)	Tenn.-Luttrell (Limestone)	AM	L
20 D0393-154-2		Corson PHDL	CU/AM	L
21 D0393-114,116&118	Indiana No. 7 (PSI)	Corson PHDL	CU/AM	S/L
22 D0393-137&139	Indiana No. 7 (PSI)	Corson PHDL	CU/AM	S/L
23 D0393-120,122&124	Indiana No. 7 (PSI)	Corson PHDL	CU/AM	S/L
24 D0393-142&144	Indiana No. 7 (PSI)	Corson PHDL	CU/AM	S/L
113 860211	Malmo, Sweden	Ignaberga (Limestone)	AM	L
114 860212	Malmo, Sweden	Skovde (Limestone)	AM	L
115 860213	Malmo, Sweden	Ignaberga (Limestone)	AM	L

a. CU - Coal Ultimate. AM - Ash Mineral.
b. S - in situ. L - laboratory.

temperature. After all the resistivity values are measured, the oven is once again turned up and the samples are again annealed overnight at 450 °C. The following day a new water concentration is added. The oven temperature is once again allowed to descend, and the current and voltage values are measured. This process continues for each water concentration that is desired.

Other sample characterizations consisted of determinations of 1) BET surface area with a Quantachrome Monosorb analyser, 2) aerodynamic particle size with a Bahco classifier, and 3) intrinsic density with a Quantachrome helium pycnometer.

EXPERIMENTAL RESULTS

The collection of data began with the mineral analyses of selected samples. The results from these analyses are given in Table 3-2. The ash-sorbent code number is given along the top row. The chemical components are listed vertically under each representative code number and are reported in weight percentages. In each sample, there is a high concentration of calcium due to the sorbent injection.

Table 3-3 illustrates data from the laboratory resistivity measurements. The values of laboratory resistivity are listed for each ash-sorbent mixture. For each sample, there are six resistivity values corresponding to specified temperatures along the top of the table. The atomic concentrations of Li + Na, Mg + Ca, and Fe are also listed for each ash. Tables 3-3, 3-4, and 3-5 are alike except that the water concentrations are 7%, 11%, and 15%, respectively.

Figures 3-1, 3-2, and 3-3 are example graphs of laboratory resistivity plotted versus temperature, at three water concentrations, for three different ash-sorbent samples. The sample number and water concentrations are given at the top of each graph. From Table 3-1, the coal and sorbent types can be found by using the sample number in the top right hand corner of each graph. Figure 3-1 is a set of resistivity curves like those for regular fly ash. These curves are normal in appearance due to the fact that as the water concentration increases the corresponding resistivity values decrease. In Figure 3-2, however, there appears some strange behavior. This is especially noticeable at 144 °C where the resistivity values are reversed from what would be expected. At this temperature, as the water concentration increases the resistivity also increases. The peaks of the curves are also shifted to lower temperature with increasing water concentrations. Figure 3-3 is similar to Figure 3-2 with an increase in resistivity with increasing water and a shift of the curve to lower temperature with increasing water. Most of the laboratory resistivity measurements showed some strange behavior, and the actual trends in the change in resistivity were hard to map.

Additional tests were performed to determine if there were some physical property that was causing the unusual results in resistivity measurements. Table 3-6 gives the results of several tests which were performed on a select

TABLE 3-2. SUMMARY OF CHEMICAL ANALYSES FOR ASH-SORBENT MIXTURES

Ash Parameter	Sample Code Number								
	01	02	04	105	107	08	15	17	101
Li_2O	0.01	0.03	0.01	0.02	0.01	0.01	0.01	0.01	0.02
Na_2O	0.15	0.32	0.30	1.3	0.29	0.11	0.17	0.11	0.20
K_2O	0.57	1.9	1.3	0.69	1.4	0.60	0.74	0.53	1.1
MgO	3.2	2.3	3.9	0.58	1.0	1.5	1.1	0.77	0.73
CaO	38.5	21.9	38.4	44.2	37.6	40.2	41.1	46.4	52.9
Fe_2O_3	20.9	8.6	10.0	21.4	12.5	12.7	10.9	8.6	8.3
Al_2O_3	6.4	22.0	9.6	7.8	10.1	8.5	8.4	6.7	7.5
SiO_2	8.1	35.1	24.2	11.7	27.6	17.5	17.4	14.4	16.3
TiO_2	0.33	1.2	0.58	0.56	0.75	0.58	0.50	0.50	0.50
P_2O_5	0.13	0.36	0.10	0.29	0.18	0.07	0.10	0.04	0.19
SO_3	19.8	6.5	9.9	11.7	8.5	16.6	19.2	21.6	11.1
LOI	9.4	8.8	10.4	10.2	5.8	7.6	4.2	2.9	1.9

Ash Parameter	Sample Code Number							
	102	18	119	20	111	12	13	14
Li_2O	0.02	0.01	0.02	0.01	~0.01	~0.01	~0.01	~0.01
Na_2O	0.24	0.10	0.25	0.24	0.03	0.22	0.18	0.13
K_2O	1.3	0.51	1.0	1.1	0.13	1.2	1.0	0.75
MgO	0.75	0.75	0.74	19.4	0.72	1.2	1.1	0.69
CaO	54.2	48.1	54.1	27.6	48.5	27.5	29.0	33.9
Fe_2O_3	8.6	6.3	7.8	6.8	0.78	18.3	18.3	13.1
Al_2O_3	8.1	6.5	8.0	7.6	1.1	11.5	10.0	8.9
SiO_2	17.3	14.3	17.9	19.6	5.9	20.2	18.7	20.4
TiO_2	0.58	0.50	0.58	0.50	0.05	0.44	0.43	0.39
P_2O_5	0.21	0.08	0.19	0.08	0.03	0.47	0.48	0.38
SO_3	7.6	20.8	7.5	15.0	0.15	10.4	14.0	15.5
LOI	0.80	5.9	5.2	3.6	42.2	8.2	6.3	5.4

TABLE 3-3. CHEMICAL AND ELECTRICAL CHARACTERISTICS OF ASH-SORBENT MIXTURES AT 7% H_2O

				Measured Resistivity in Ohm-cm at Various Temperatures					
				1000/T(K) 2.8	2.6	2.4	2.2	2.0	1.6
Ash	Atomic Percentage			°C 84	112	144	182	227	352
No.	Mg+Ca	Fe	Li+Na	°F 183	233	291	359	441	666
01	28.3	3.9	0.14	3.6E10	1.1E12	6.7E12	2.1E13	2.7E13	3.1E12
02	15.7	1.5	0.29	2.5E09	6.5E10	2.4E11	2.7E11	1.4E11	8.3E09
04	26.2	1.7	0.23	2.0E10	5.8E11	8.6E12	2.2E13	9.1E12	3.0E11
105	28.8	3.9	1.04	8.0E10	5.3E11	1.3E12	8.2E12	2.7E13	3.1E11
107	23.7	2.1	0.23	2.4E11	2.3E12	9.4E12	1.5E13	1.0E13	6.2E11
08	26.3	2.2	0.10	1.1E11	5.9E12	3.6E13	3.9E13	1.2E13	4.0E11
111	44.1	0.2	0.05	3.4E12	4.2E13	9.5E13	8.7E13	4.3E13	2.1E12
12	21.0	3.7	0.21	5.2E11	3.3E12	6.2E12	6.4E12	3.5E12	2.1E11
13	21.5	3.6	0.17	2.5E11	1.9E12	4.3E12	6.3E12	1.4E13	4.0E11
14	23.2	2.4	0.12	7.1E09	2.2E11	3.3E12	2.2E13	2.8E13	9.8E11
15	25.6	1.6	0.11	1.3E10	1.1E12	4.2E13	8.7E13	4.5E13	7.7E11
16	14.5	2.3	0.51	3.2E11	4.1E12	1.8E13	2.9E13	2.3E13	1.6E12
17	28.4	1.4	0.09	3.7E09	1.2E11	5.0E12	3.8E13	5.9E13	1.2E12
18	29.4	1.1	0.09	3.0E09	8.5E10	1.1E12	7.5E12	1.6E13	1.5E12
119	32.2	1.3	0.21	4.8E10	4.2E11	2.1E12	5.1E12	4.4E12	2.2E11
20	28.9	1.2	0.18	3.2E10	9.2E11	9.8E12	3.5E13	4.1E13	3.5E12

TABLE 3-4. CHEMICAL AND ELECTRICAL CHARACTERISTICS OF ASH-SORBENT MIXTURES AT 11% H_2O

				Measured Resistivity in Ohm-cm at Various Temperatures					
				1000/T(K) 2.8	2.6	2.4	2.2	2.0	1.6
Ash	Atomic Percentage			°C 84	112	144	182	227	352
No.	Mg+Ca	Fe	Li+Na	°F 183	233	291	359	441	666
01	28.3	3.9	0.14	4.7E09	2.6E11	2.4E12	9.4E12	1.5E13	1.6E12
02	15.7	1.5	0.29	3.1E08	1.7E10	1.2E11	2.1E11	1.5E11	1.1E10
04	26.2	1.7	0.23	5.6E09	5.4E11	1.1E13	1.4E13	5.2E12	2.0E11
105	28.8	3.9	1.04	5.5E10	5.0E11	1.5E12	2.0E12	1.5E12	1.6E11
107	23.7	2.1	0.23	4.7E10	7.8E11	4.2E12	8.9E12	7.4E12	5.5E11
08	26.3	2.2	0.10	2.4E11	1.6E13	3.2E13	2.6E13	8.3E12	2.8E11
111	44.1	0.2	0.05	3.6E11	1.4E13	5.5E13	6.0E13	2.8E13	1.8E12
12	21.0	3.7	0.21	2.4E11	2.6E12	5.4E12	5.4E12	2.3E12	1.2E11
13	21.5	3.6	0.17	1.8E11	1.9E12	4.2E12	4.7E12	2.8E12	1.9E11
14	23.2	2.4	0.12	2.2E09	2.1E11	1.1E13	4.1E13	2.6E13	6.3E11
15	25.6	1.6	0.11	1.7E11	2.2E13	6.0E13	6.8E13	2.8E13	5.6E11
16	14.5	2.3	0.51	3.2E11	4.1E12	1.8E13	2.9E13	2.3E13	1.6E12
17	28.4	1.4	0.09	1.9E09	4.2E11	2.3E13	8.4E13	4.9E13	6.8E11
18	29.4	1.1	0.09	4.1E09	1.2E12	3.4E13	8.7E13	4.2E13	6.0E11
119	32.2	1.3	0.21	1.4E10	2.3E11	1.6E12	4.5E12	4.5E12	2.3E11
20	28.9	1.2	0.18	4.4E09	2.7E11	4.1E12	1.4E13	1.4E13	1.6E12

TABLE 3-5. CHEMICAL AND ELECTRICAL CHARACTERISTICS OF ASH-SORBENT MIXTURES AT 15% H_2O

Ash	Atomic Percentage			Measured Resistivity in Ohm-cm at Various Temperatures					
				1000/T(K) 2.8	2.6	2.4	2.2	2.0	1.6
				°C 84	112	144	182	227	352
No.	Mg+Ca	Fe	Li+Na	°F 183	233	291	359	441	666
01	28.3	3.9	0.14	9.1E08	7.3E10	9.4E11	5.2E12	1.1E13	6.7E11
02	15.7	1.5	0.29	4.3E07	4.9E09	6.3E10	1.6E11	1.4E11	1.4E10
04	26.2	1.7	0.23	1.7E10	1.7E12	9.1E12	9.7E12	3.7E12	1.3E11
105	28.8	3.9	1.04	2.5E10	3.1E11	9.4E11	1.4E12	1.1E12	2.1E11
107	23.7	2.1	0.23	1.9E10	3.9E11	2.6E12	6.6E12	5.9E12	3.2E11
08	26.3	2.2	0.10	2.7E11	1.4E13	2.4E13	2.1E13	6.9E12	1.9E11
111	44.1	0.2	0.05	1.2E11	7.5E12	3.7E13	4.0E13	2.1E13	1.6E12
12	21.0	3.7	0.21	7.5E10	1.5E12	3.9E12	3.7E12	1.8E12	9.4E10
13	21.5	3.6	0.17	5.5E10	9.6E11	2.5E12	3.0E12	1.9E12	2.1E11
14	23.2	2.4	0.12	6.8E09	2.5E12	2.2E13	3.7E13	1.7E13	4.6E11
15	25.6	1.6	0.11	5.2E11	2.3E13	5.2E13	4.9E13	1.8E13	3.5E11
17	28.4	1.4	0.09	1.3E10	9.4E12	4.8E13	6.5E13	2.5E13	4.5E11
18	29.4	1.1	0.09	5.4E10	1.5E13	4.9E13	6.4E13	2.3E13	4.0E11
119	32.2	1.3	0.21	8.1E09	2.2E11	1.6E12	4.4E12	4.2E12	2.1E11
20	28.9	1.2	0.18	3.8E09	2.8E11	2.9E12	6.5E12	5.8E12	7.8E11

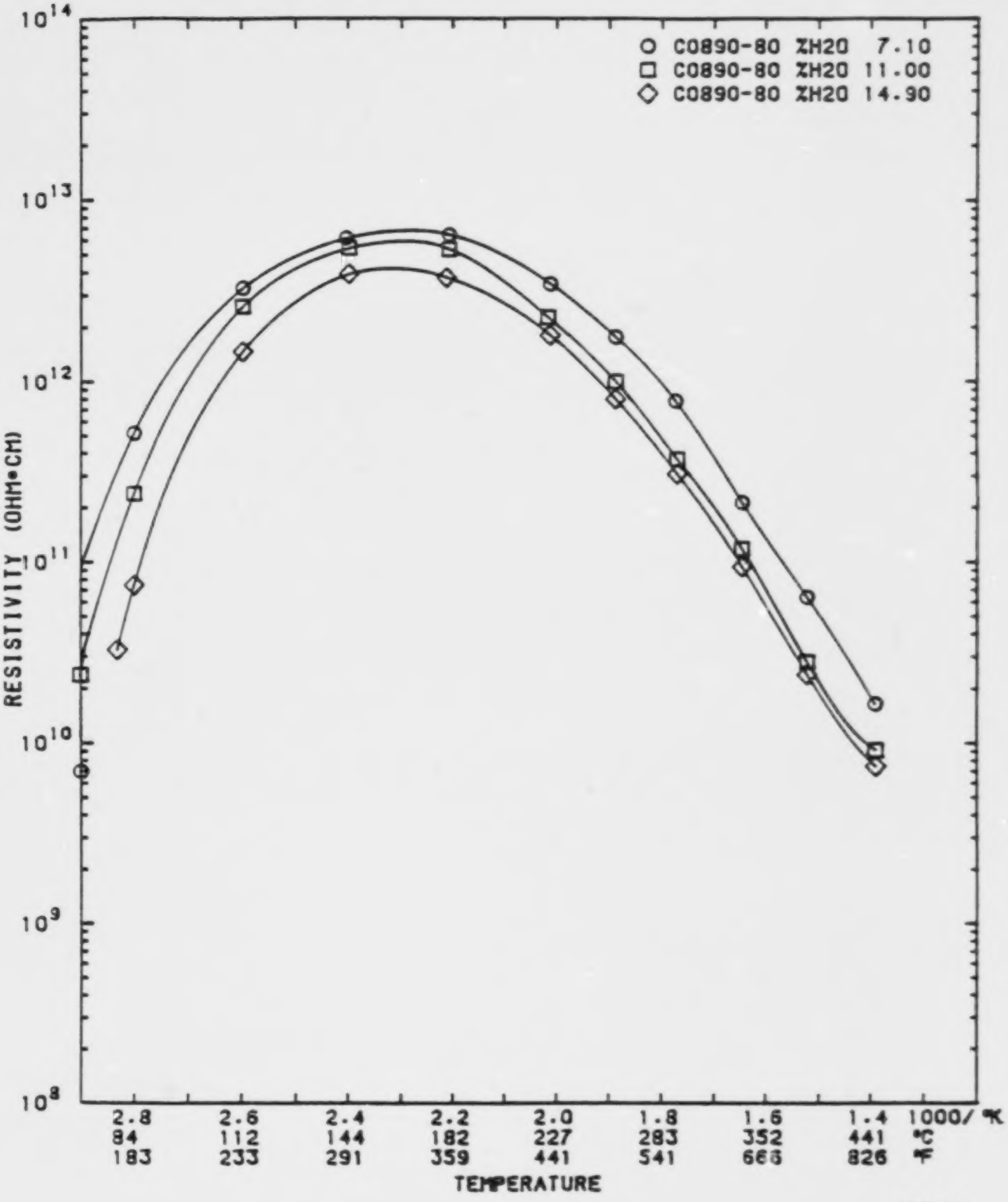

5676-142

Figure 3-1. Resistivity versus temperature for an ash-sorbent sample from Hallmark (Lot No. 3) coal and Longview hydrated lime.

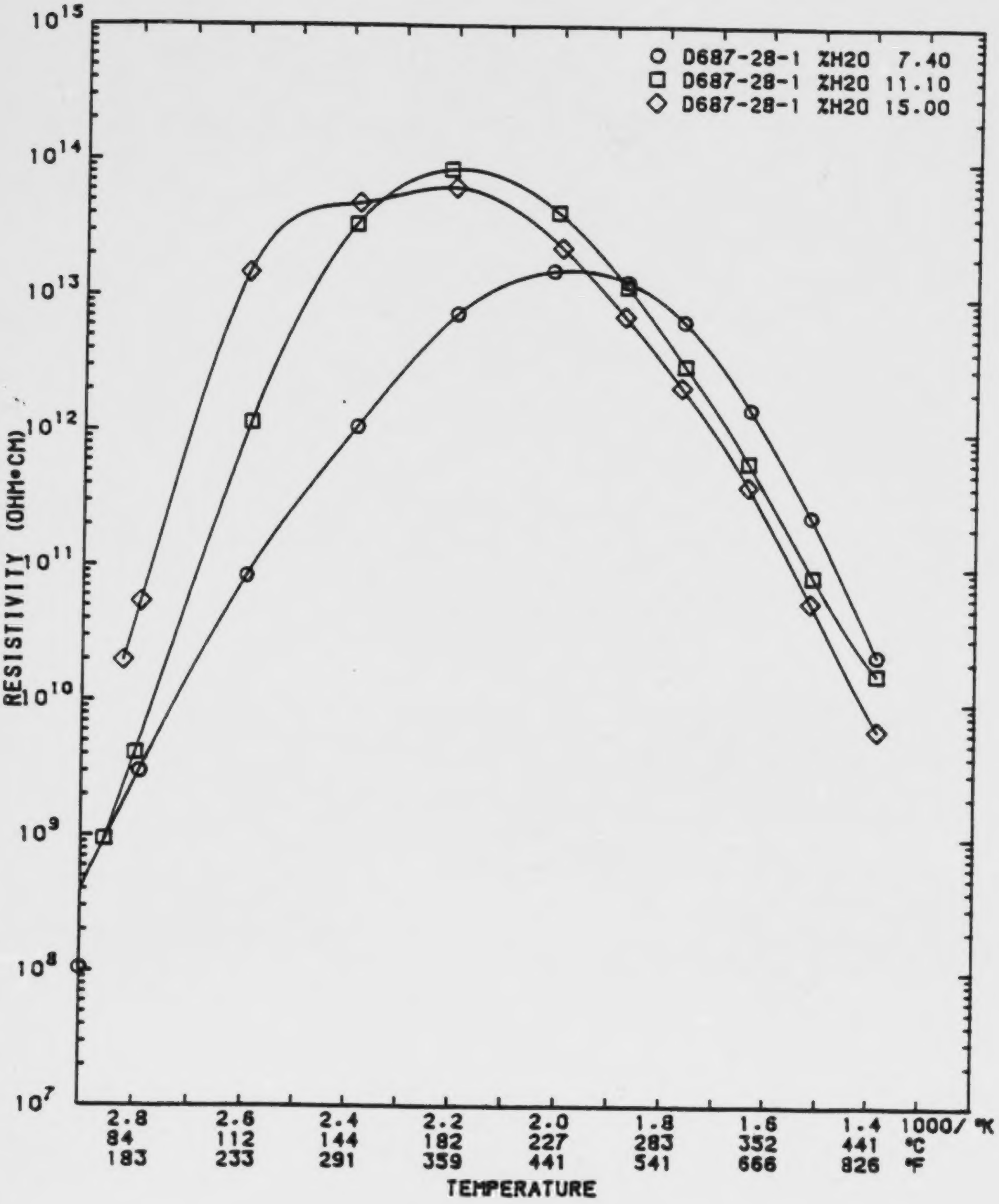

5676-143

Figure 3-2. Resistivity versus temperature for an ash-sorbent sample from Pittsburgh No. 8 (EPA Demo) coal and Marblehead hydrated lime.

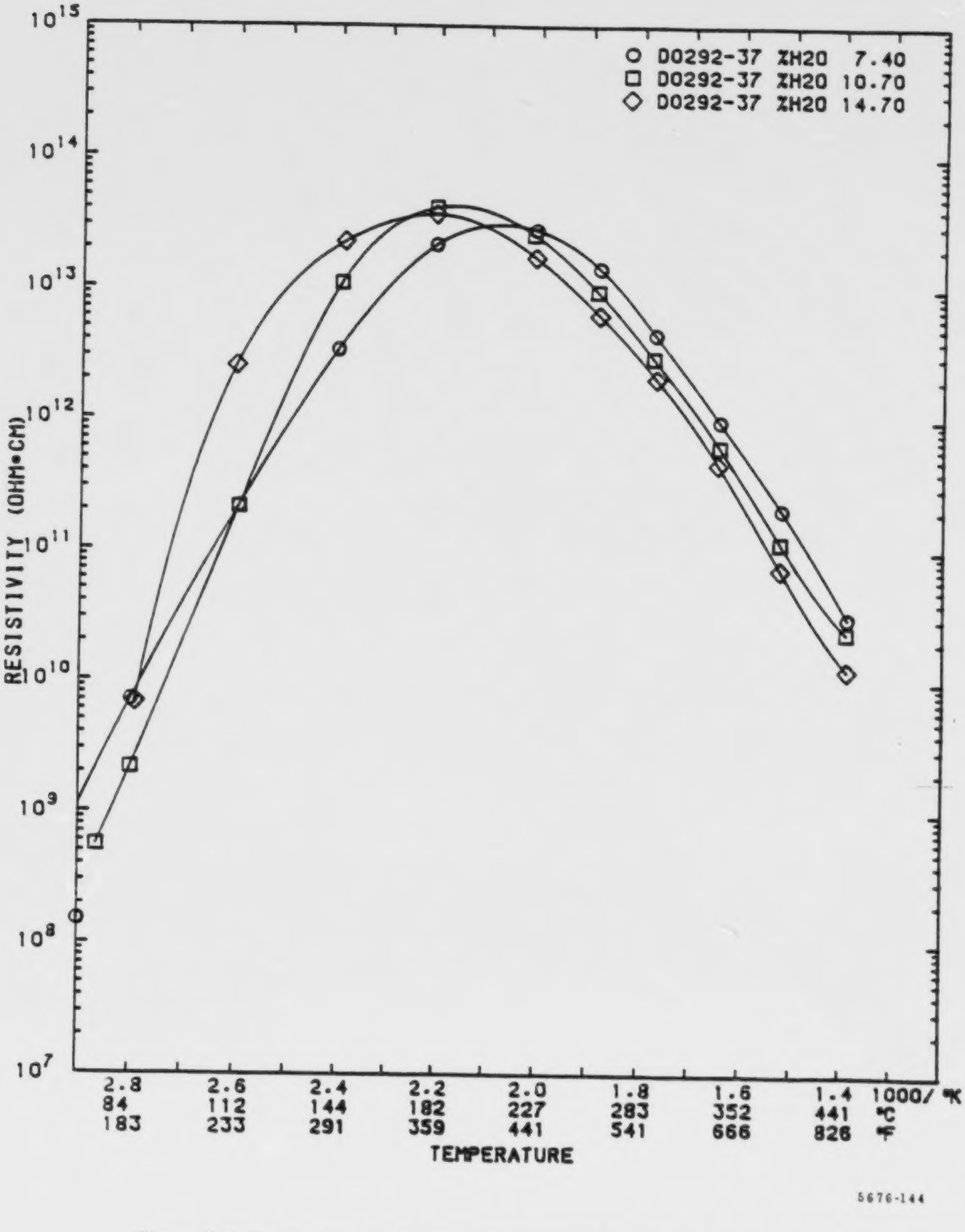

Figure 3-3. Resistivity versus temperature for an ash-sorbent sample from Pittsburgh No. 8 (EPA Demo) coal and Marblehead hydrated lime.

TABLE 3-6. SUMMARY OF VARIOUS TESTS FOR ASH-SORBENT MIXTURES

Code No.	BET, m^2/g (surface area)	Density, g/cm^3 (helium pycnometry)	Particle Size, mmd	(BAHCO) σ
01	2.9	2.70	5.8166	2.3694
02	3.9	–	–	–
08	2.3	2.74	4.8979	2.0308
12	3.0	2.75	7.1351	2.4622
13	4.0	2.73	6.8479	2.3353
14	4.0	–	–	–
15	3.5	2.78	3.9703	1.6319

group of samples. The results of these tests showed no significant difference in physical properties that might cause the unexpected resistivity data.

An attempt was made to correlate the chemical composition of the ash-sorbent samples with the laboratory resistivity values. The first step was to calculate the Li + Na concentration in atomic percent for each of the samples. These values were then plotted versus resistivity to determine if a correlation existed between them. Previous experiments have shown that the Li and Na ions are the principal charge carriers in fly ash and, thus, have a dominant effect on its resistivity. After the plots were made, a linear regression analysis was performed on each graph and it was found that there were no correlations between the Li + Na concentration and the resistivity. Figures 3-4, 3-5, and 3-6 are the graphs of resistivity plotted versus the Li + Na concentrations for 84 °C, 112 °C, and 144 °C, respectively, with a water concentration of 7%. From these graphs it is obvious that there are no correlations.

CHANGES IN THE SAMPLE PROPERTIES DURING MEASUREMENTS

The unusual laboratory resistivity data raised the question as to whether the experimental procedure was causing large changes in the samples during the experimental process. The strange behavior in the resistivity curves could be due to large changes in the surface area of the samples. This change in surface area could be due to both drying and the calcination of $Ca(OH)_2$. This calcining occurs at approximately 350 °C, well below 450 °C, which is the annealing temperature for each sample before the laboratory resistivity measurement. Another factor that could cause changes in the surface area is the sintering effect. The exact temperature at which sintering begins was unknown.

An experiment was designed to determine the effect of temperature on the surface area of ash-sorbent mixtures. This test was performed by placing five ash-sorbent samples and one regular fly ash sample in an oven and allowing them to anneal overnight at a specified temperature. After each annealing, a portion of each sample was collected and submitted for BET surface area analysis. The first night, the samples were allowed to anneal at 150 °C for a 24-h period. For each additional night, the temperature was increased in 50 °C increments until a temperature of 450 °C was reached. The results of the test are given in Table 3-7 and are shown graphically in Figure 3-7. The upper graph is a plot of oven temperature for the duration of the experiment. The lower graph is a plot of surface area versus elapsed time in days. The oven temperature on the top graph corresponds to a specific surface area value on the bottom graph. The samples numbered 101, 102, and 119 are ash-sorbent samples created with limestone injection. Those which are numbered 17 and 18 are samples created with hydrated lime injection. The sample numbered 308 is a high calcium fly ash sample.

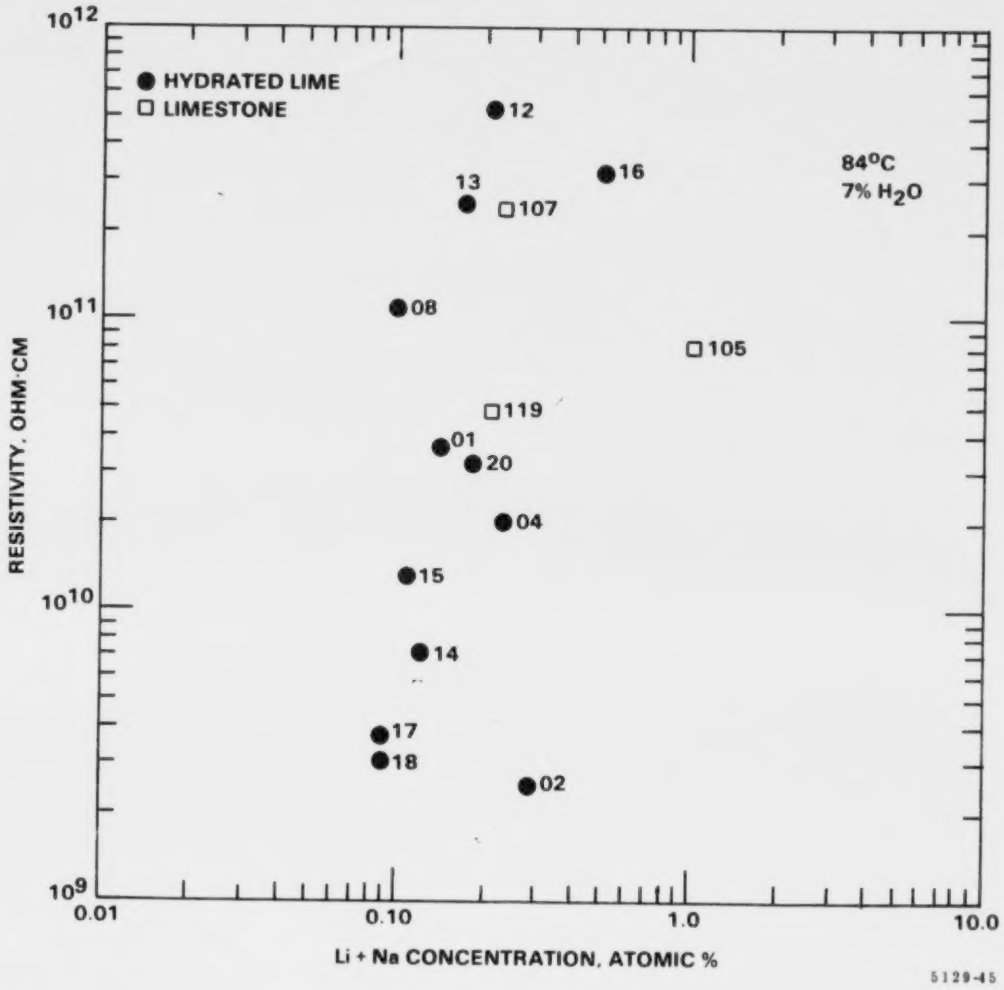

Figure 3-4. Resistivity versus Li + Na concentration for ash-sorbent mixtures at 84°C and 7% H_2O.

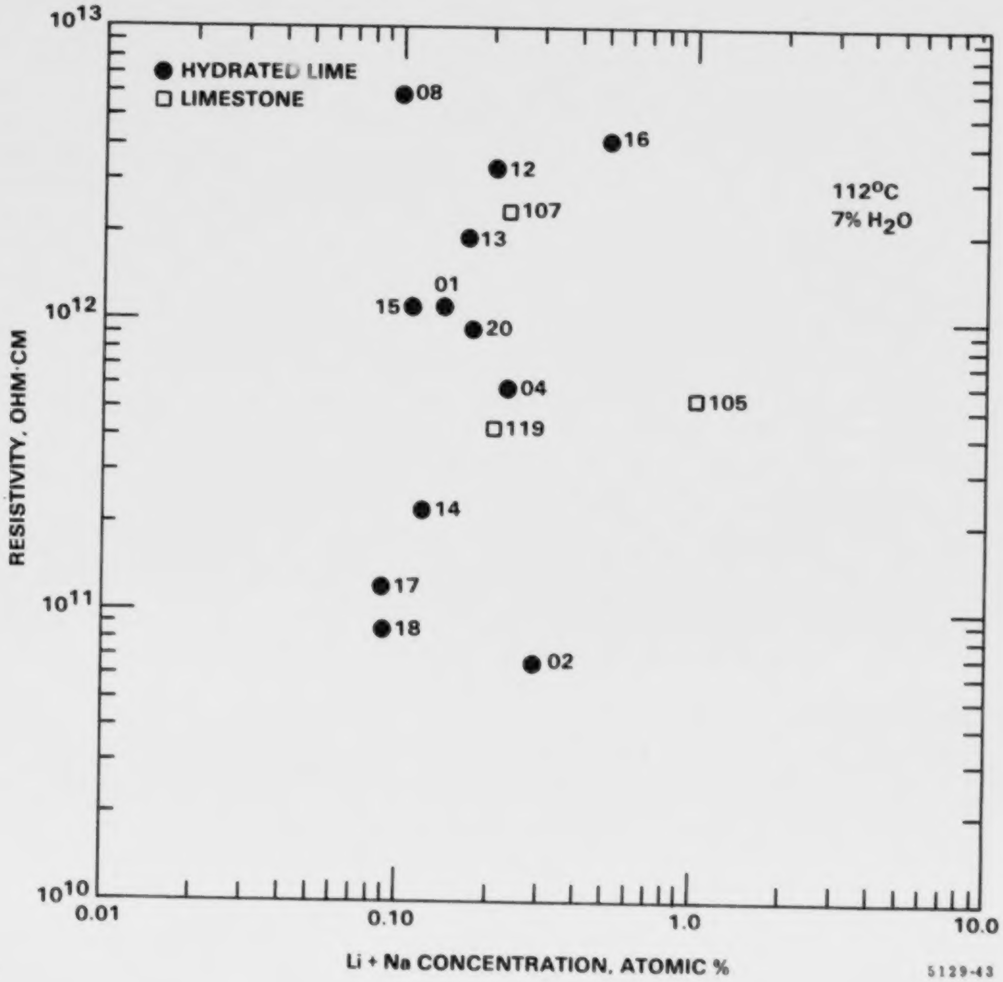

Figure 3-5. Resistivity versus Li + Na concentration for ash-sorbent mixtures at 112°C and 7% H_2O.

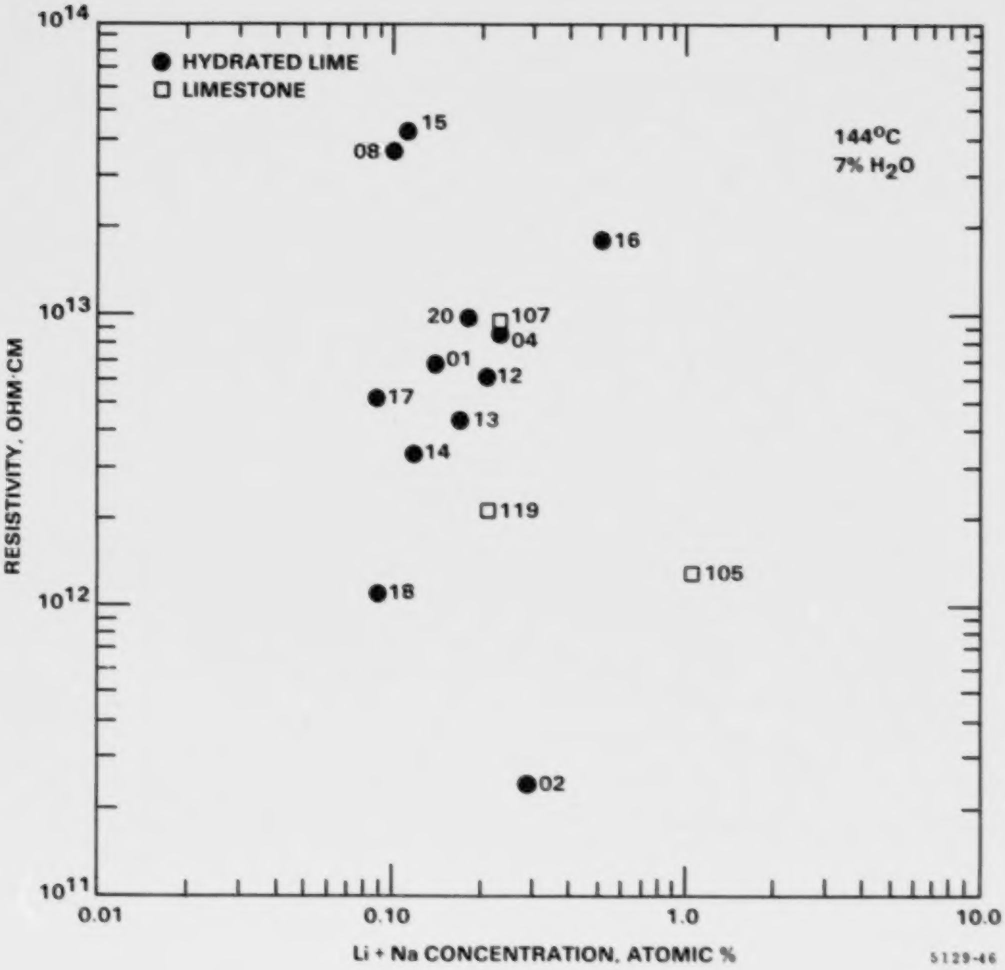

Figure 3-6. Resistivity versus Li + Na concentration for ash-sorbent mixtures at 144°C and 7% H_2O.

TABLE 3-7. EFFECT OF HEAT ON ASH-SORBENT MIXTURES

	Surface area, m2/g, for Tests No.										
Sample Number	0	1	2	2.5	3	4	5	5.5	6	7	7.5
(D0292-46-5) 17	4.2	4.4	4.4	5.3	6.0	7.7	13.4	8.3	6.7	2.2	2.0
(D0687-28-1) 18	4.6	4.9	5.0	5.8	6.8	10.7	14.6	14.8	9.8	2.6	2.3
(D0687-128-1) 101	2.0	2.1	2.1	2.3	2.6	3.1	3.4	3.3	2.4	1.7	1.6
(D0687-118-3) 102	1.3	1.3	1.4	1.4	1.5	1.8	2.0	2.0	1.3	1.0	1.0
(D0687-13-2) 119	3.0	3.2	3.6	4.0	4.7	8.0	10.8	10.7	3.4	1.3	1.2
(Sunoco) 308	1.4	1.4	1.4	1.4	1.5	1.4	1.4	1.4	1.4	1.4	1.3

The list below gives the operating conditions of the oven during the entire experiment and corresponds to the upper graph in Figure 3-7 and the tabulation above.

Test No.	Annealing Temperature
0	Original Sample
1	150 °C overnight
2	200 °C overnight
2.5	200 °C over the weekend
3	250 °C overnight
4	300 °C overnight
5	350 °C overnight
5.5	200 °C over the weekend
6	400 °C overnight
7	450 °C overnight
7.5	450 °C overnight

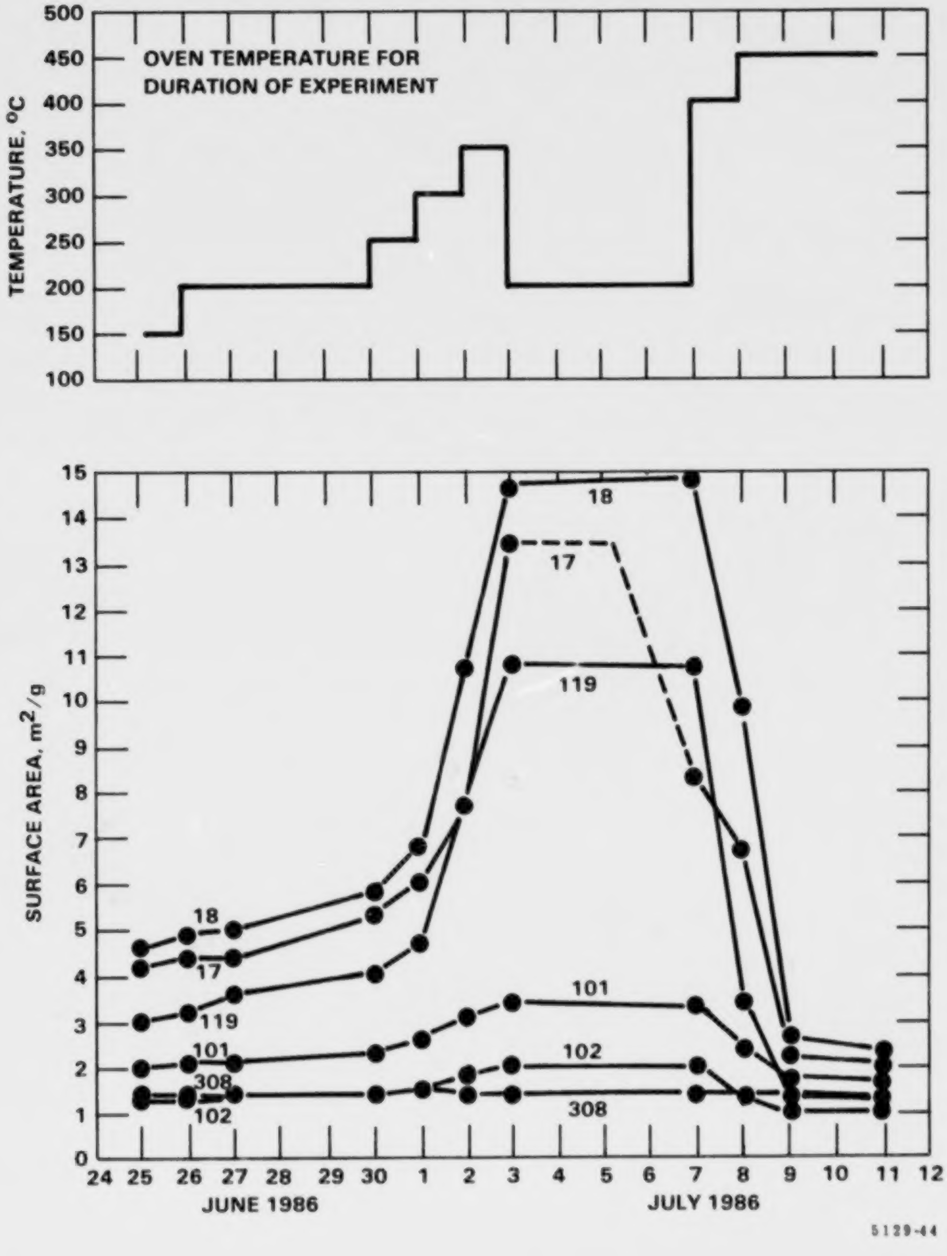

Figure 3-7. Effect of increasing temperature on the surface area of selected ash-sorbent mixtures.

The graph shows that as the temperature increases, there is a definite change in surface area. Samples 17 and 18 show the greatest amount of change and seem to reach their peak somewhere around 350 °C. This large change in surface area is due to driving off water and calcining the $Ca(OH)_2$. There is evidence of sintering at the temperatures above 400 °C. Samples 101 and 102 show very little change at all in surface area, but the general trend is the same as for the other samples. Sample 119 shows a large change in surface area and appeared to behave very much like samples 17 and 18. However, its chemical composition is almost exactly like those of samples 101 and 102. Sample 308, which is just a fly ash sample, acted very much as expected and showed little or no change in surface area during the duration of the test. From these results it is apparent that the IEEE Standard 548-1984 laboratory resistivity measurement is not applicable to samples which are composed of ash-sorbent mixtures because it profoundly alters surface area and, hence, resistivity.

CONCLUSION

The experimental work led to the conclusion that the original objective could not be accomplished by using standard laboratory techniques. The development and validation of new laboratory techniques, and a second experimental program using those techniques, were estimated to require a level of effort much greater than what could be accomplished within the fixed project budget. Therefore, the work under the task was terminated at this point, and the remaining funds were redirected to Task 2, which is discussed in the next section.

The development and validation of new laboratory techniques for measuring ash-sorbent resistivity were pursued successfully under the subsequent EPA Cooperative Agreement CR 812282.

SECTION 4
TASK 2. INVESTIGATION OF THE EFFECT OF HIGH MASS LOADING ON FLY ASH PRECIPITATORS

INTRODUCTION

The technique of concern for the control of SO_2 in flue gas is the furnace injection of a dry sorbent material such as hydrated lime (LIMB). One of the results of sorbent injection is the addition of a large quantity of small particles to the flue gas. These additional particles affect the operation of the ESP used to clean the gas in the following ways:

1. The particles increase the total dust load on the ESP.

2. The particles fall in the size band where ESPs are least effective.

3. As the particles are charged, they form a space charge cloud which may suppress the corona in the ESP.

4. The sorbent material may change the resistivity of the collected particulate layer.

This section describes a combination of experimental and theoretical work in development of more reliable performance projections for fly ash precipitators operating under the high inlet mass loading caused by sorbent injection.

LABORATORY EXPERIMENTS

In order to study the effects of increased space charge with sorbent injection, a laboratory ESP was modified so that the plate current could be measured in small increments along its length. A schematic of the segmented plate ESP is shown in Figure 4-1. The ESP has six wires on 6 in. (15 cm) centers. The wires may be powered by a single supply or by multiple supplies. One of the collection plates is a 26 x 48 in. (66 x 122 cm) circuit board that was machined into conductive strips as shown in Figure 4-1. There are 43 conductive strips measuring 0.875 x 20.25 in. (2.2 x 51 cm) and 2 end strips measuring 2.375 x 20.25 in. (6 x 51 cm). The length of the conductive strips corresponds to the length of the corona wires. Each of the narrow strips has an area of 0.123 ft^2 (114 cm^2). The area of all 45 strips is 6 ft^2 (5560 cm^2). The other collection plate is a grounded stainless steel sheet. The duct width is 9 in. (23 cm).

The segmented plate ESP is located in the SRI Coal Combustion Facility. The combustor is a 1×10^6 Btu/h (300 kW) down-fired furnace which burns pulverized coal to produce fly ash that is very similar to the ash produced by a full-scale utility boiler. The furnace has provisions for the injection of hydrated lime to test the LIMB process. The ESP processes the entire gas stream, with a typical SCA of 27 $ft^3/[1000\ ft^3/min]$ (5.3 $m^2/[m^3/s]$) at 300 °F (150 °C).

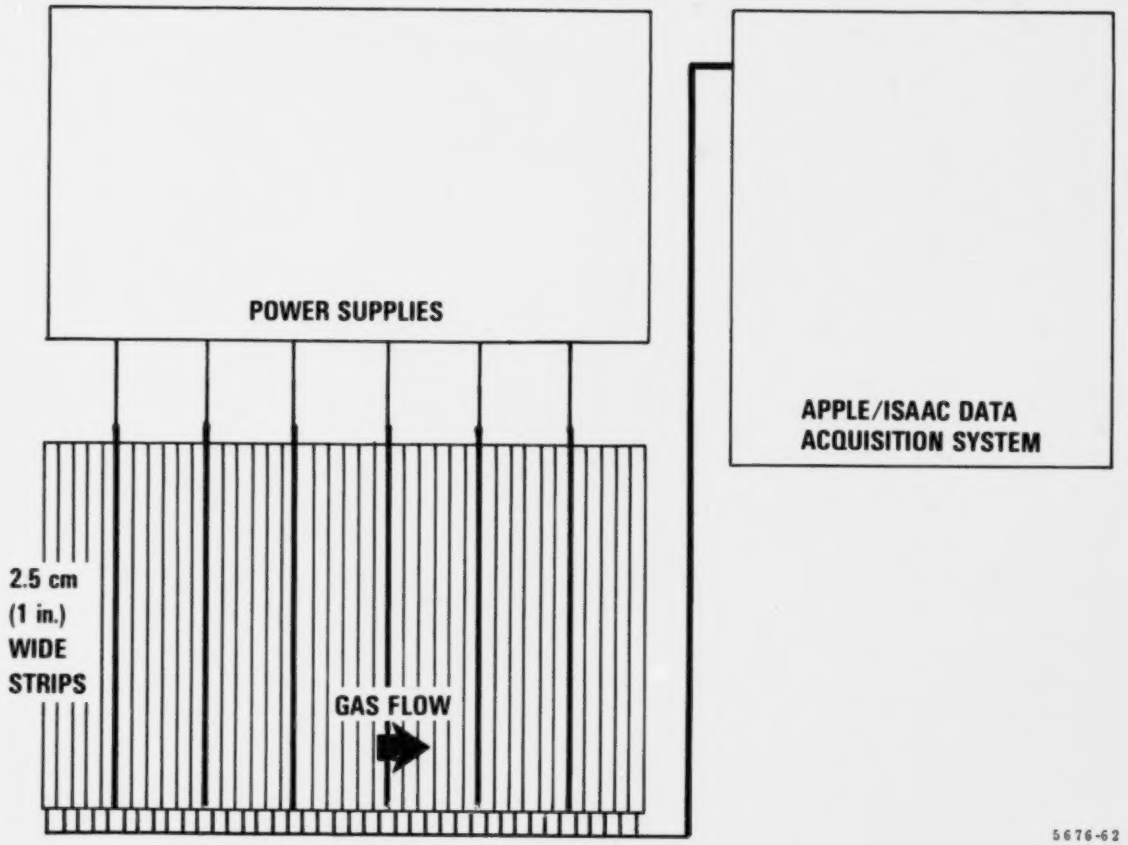
POWER SUPPLIES
APPLE/ISAAC DATA ACQUISITION SYSTEM
2.5 cm (1 in.) WIDE STRIPS
GAS FLOW
5676-62

Figure 4-1. Segmented-plate electrostatic precipitator.

Each of the 45 plate segments in the ESP is monitored by an electrometer circuit which produces a voltage proportional to the current on the plate strip. The 45 voltages are then scanned by a Cyborg/Isaac relay multiplexer, converted to a digital signal, and processed and stored by an Apple IIe computer. Some representative experimental data are reported here.

Fly Ash with Lime Injection

The segmented plate ESP was used with hydrated lime ($Ca[OH]_2$) injected into the furnace at $Ca/S \approx 2$. Figure 4-2 shows the total plate current as a function of time for this test. The current shown for time $t < 0$ was for fly ash only. At $t = 0$, when lime injection began, the current density dropped by about 50%. The times during which the two 45 channel current measurements were made are shown by the horizontal lines in the figure. The duration of the first measurement was 6 min, during which the 45 channels were read 10 times and averaged. During this period, the current rose from 0.075 to 0.57 mA, which corresponds to a rise in the current density of 5 to 37 nA/cm^2. The second test was shortened to about one minute by reducing the number of times the data were averaged. During this test, the current rose from 2.0 to 2.7 mA, which corresponds to an increase in current density of 130 to 170 nA/cm^2. Previous in-situ resistivity data taken in the Coal Combustion Facility have shown that the addition of hydrated lime at the furnace raises the resistivity of the ash from 2×10^{10} to 2×10^{12} ohm cm. The high resistivity and the uncontrolled rise in current indicate that the system went into severe back corona during this test.

Figure 4-3 shows the 45 channel current measurements for this test. Figure 4-3a shows the data for fly ash only ($t < 0$). Figure 4-3b shows the first multi-channel data taken with lime injection (first test in Figure 4-2). Although the area around wires 2 and 3 may indicate corona suppression, wire 6 is showing the beginnings of back corona. By the second test (Figure 4-3c), the system is well into back corona. In an attempt to return to normal operation, the voltage was reduced and the plates were vibrated. A large drop in current occurred, after which the current rose again. Figure 4-3d shows data taken during this period. The voltage had been reduced from 45 to 37 kV. Wires 1 and 6 are still in back corona. There is no apparent emission from the inner wires. The current density rose from 13 to 22 nA/cm^2 during the test. The back corona problem was remedied only by opening the ESP and cleaning it.

Fly Ash with Lime Injection and SO_3 Addition

To counter the problems caused by high resistivity, the previous test was repeated with the addition of SO_3. The hydrated lime was again furnace-injected at $Ca/S \approx 2$. The estimated dust loadings for coal only and coal plus lime were 1 and 3 gr/ft^3 (2.3 and 6.9 g/m^3), respectively. The in-situ resistivity of the ash plus lime plus SO_3 mixture was 2×10^{10} ohm cm, which was very close to that of the fly ash alone. The V-I curves for this test are shown in Figure 4-4. The upper V-I curve is for fly ash. The irregularity in the curve is due to shutting the power off and checking the wires in the middle of taking V-I data. The lower curve is for ash plus lime plus SO_3. Figure 4-5 shows the ESP current at constant voltage (45 kV) during periods of operation with fly ash only and ash plus lime plus SO_3. The combination of sorbent injection

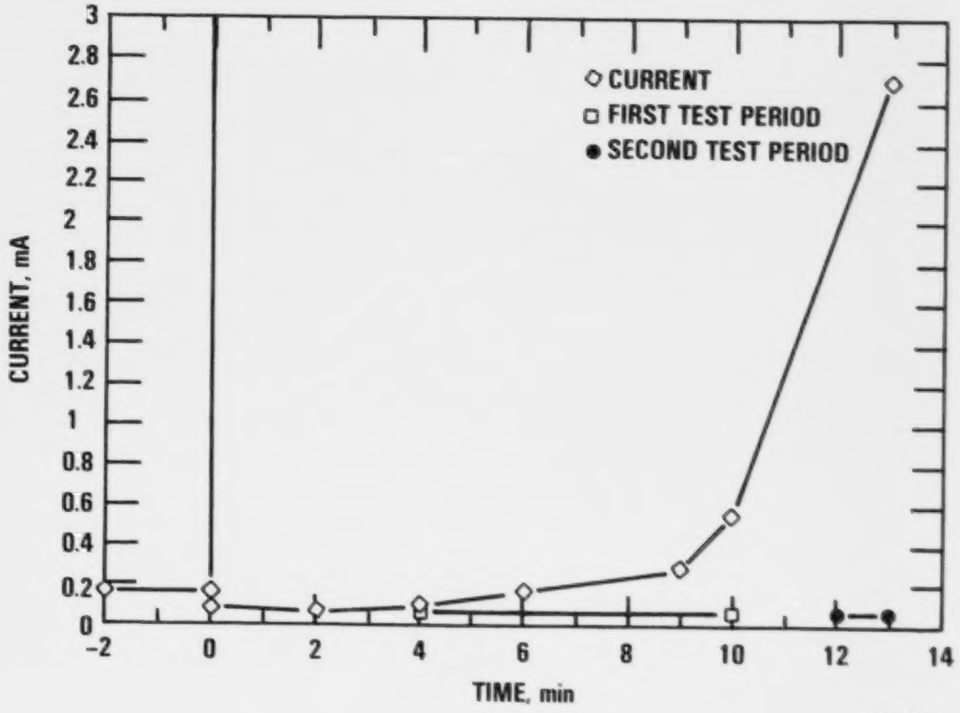

5676-141

Figure 4-2. Variation in current with time for fly ash and hydrated lime at 45 kV. Lime injection began at time = 0 min.

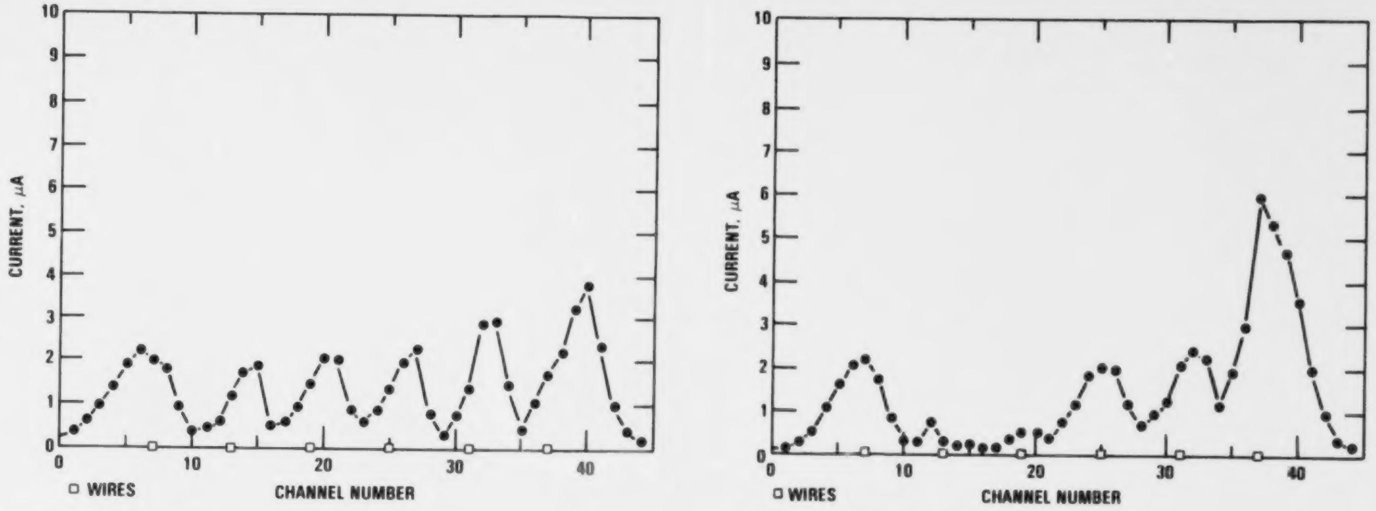

a. FLY ASH

b. FLY ASH + LIME, FIRST TEST

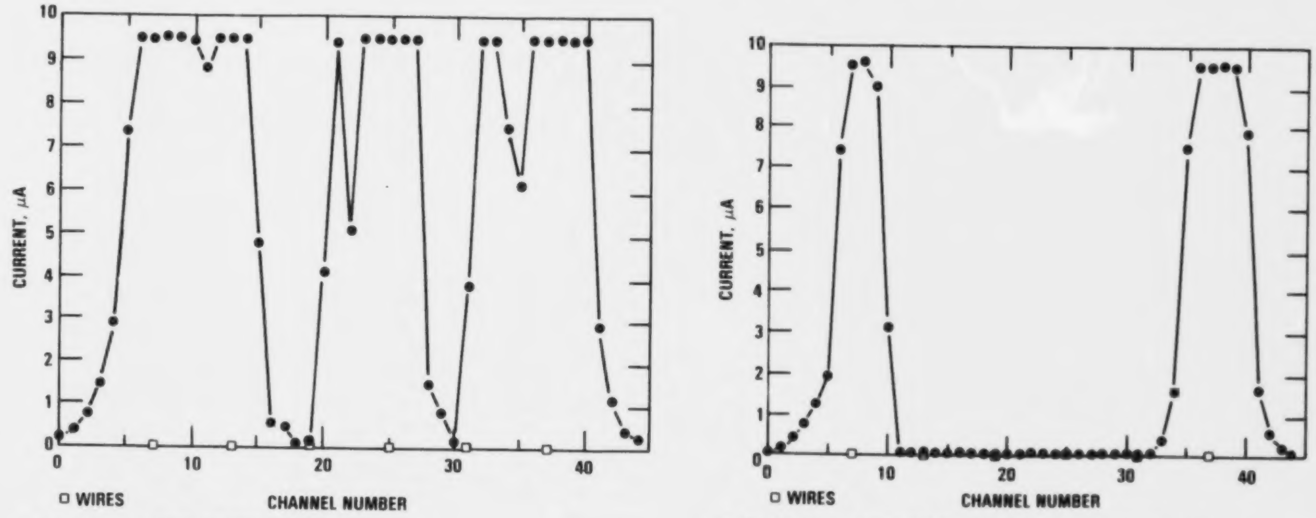

c. FLY ASH + LIME, SECOND TEST

d. FLY ASH + LIME AT REDUCED VOLTAGE (37 kV)

5676-44

Figure 4-3.. Current on each plate strip for fly ash and lime at 45 kV.

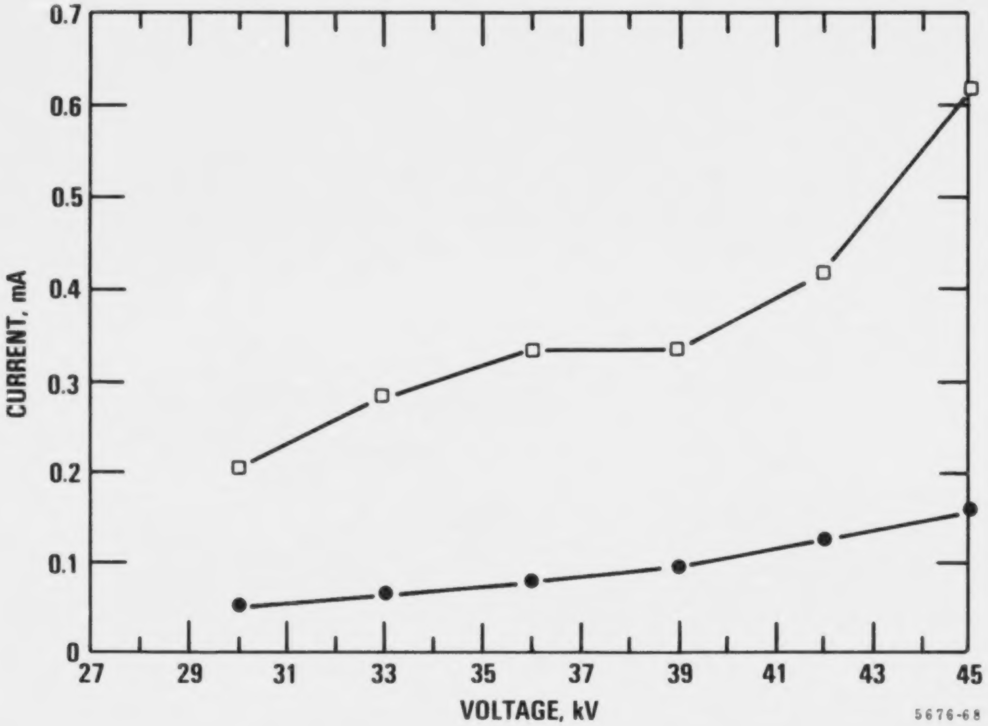

Figure 4-4. V-I curves for fly ash and fly ash plus hydrated lime plus SO_3.

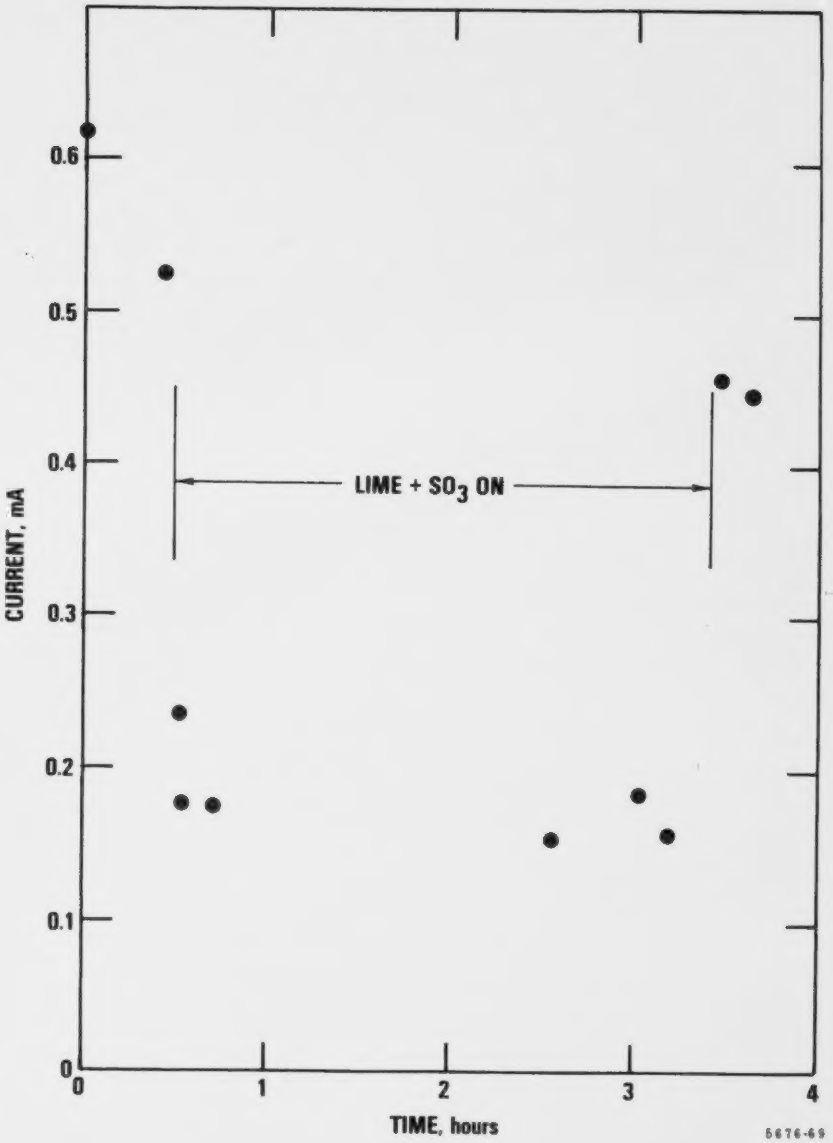

Figure 4-5. Variation in current with time for fly ash with hydrated lime and SO_3 conditioning at 45 kV.

and SO_3 conditioning reduced the current by about a factor of 3. The current was stable at the lower level for the 3 h of the injection test. When the injection was stopped, the current returned to the higher level. Figure 4-6 shows the 45 channel current measurements for the test, in which the current suppression during the lime-plus-SO_3 injection and the current recovery afterward are clearly illustrated. The current in Figure 4-6d may have been affected somewhat by an effort to clear the wires of deposits before the data were taken.

Application of Results

The EPA-SRI ESP Model, Revision 3 (2), has been used to estimate collection efficiency and outlet particulate emissions for a full-scale ESP based on the results of the tests with coal plus hydrated lime plus SO_3. The ESP was chosen to represent an older unit of the type that would be retrofitted for sorbent injection. The ESP has 9 in. (23 cm) plate spacing, weighted wires, and an SCA in the range 150 to 300 $ft^2/[1000\ ft^3/min]$ (30 to 60 $m^2/[m^3/s]$). The simulations were run for the four conditions listed below:

1. High-sulfur coal only. For this case the mass loading was assumed to be 2.3 gr/ft^3 (5.3 g/m^3).

2. Coal plus hydrated lime (Ca/S = 2) plus ≈100 ppm SO_3. For this case, the mass loading was increased by about a factor of 3 and the mass-median diameter of the particle size distribution was reduced from 30 to 15 μm to match data taken at the SRI Coal Combustion Facility. The electrical operating conditions were the same as for Case 1.

3. Coal plus hydrated lime plus SO_3. This case is the same as Case 2 except that the current in the first half of the first electrical section has been reduced in proportion to the V-I curves in Figure 4-4.

4. Coal plus hydrated lime plus SO_3. This case is the same as Case 2 except that the current in the first half of the ESP has been reduced in proportion to the V-I curves in Figure 4-4.

The results of the simulations are shown in Figure 4-7. The largest change in emissions was caused by the increase in the dust loading and the shift in the particle size distribution, which accounts for the large increase in the number of fine particles due to the hydrated lime. By comparison, the additional increase in emissions due to current suppression is small.

THEORETICAL WORK

The theoretical portion of this task consisted of the development of a more general and more powerful mathematical model of electrostatic precipitation. The standard version of the ESP Model developed by SRI for EPA (2), does a good job of simulating the performance of cold-side utility fly ash precipitators with typical values of inlet mass loading. To increase the responsiveness of the ESP Model to situations having high inlet mass loading and/or

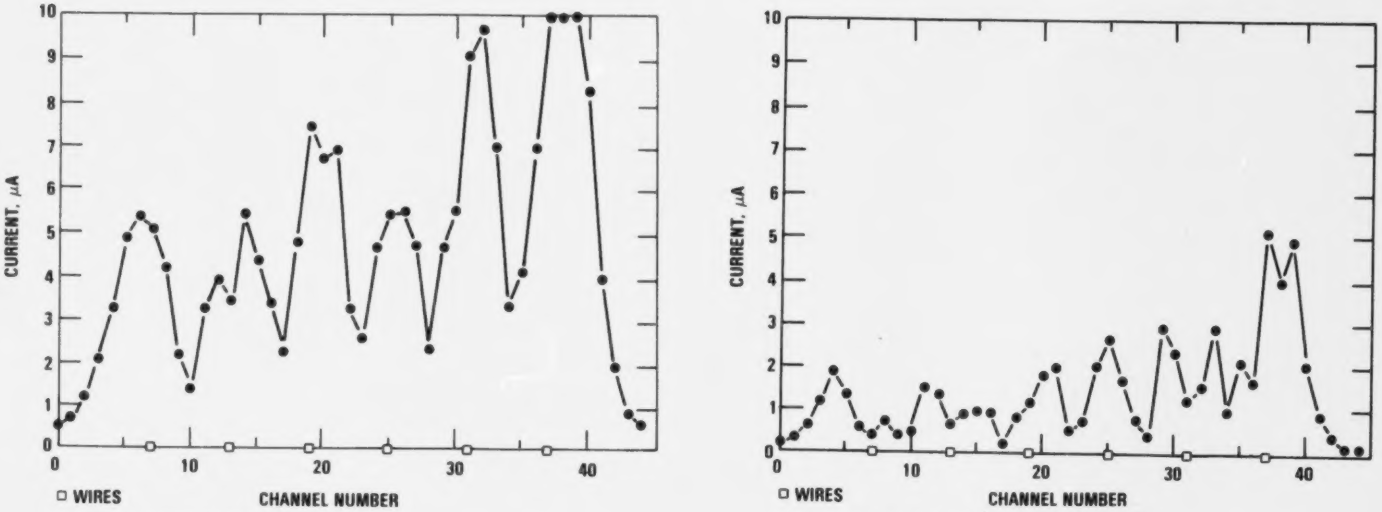

a. FLY ASH BEFORE CONDITIONING

b. INITIAL FLY ASH + LIME + SO_3 TEST

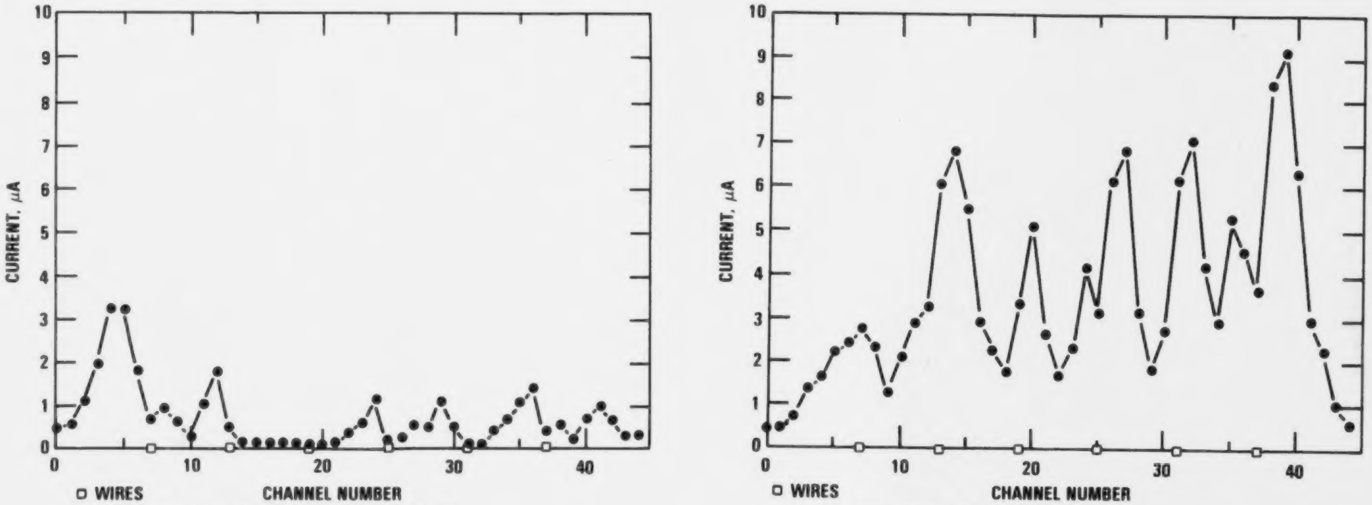

c. FLY ASH + LIME + SO_3 AFTER 3 HOURS

d. FLY ASH AFTER END OF CONDITIONING TEST

5676-70

Figure 4-6. Current on each plate strip for fly ash with hydrated lime and SO_3 conditioning at 45 kV.

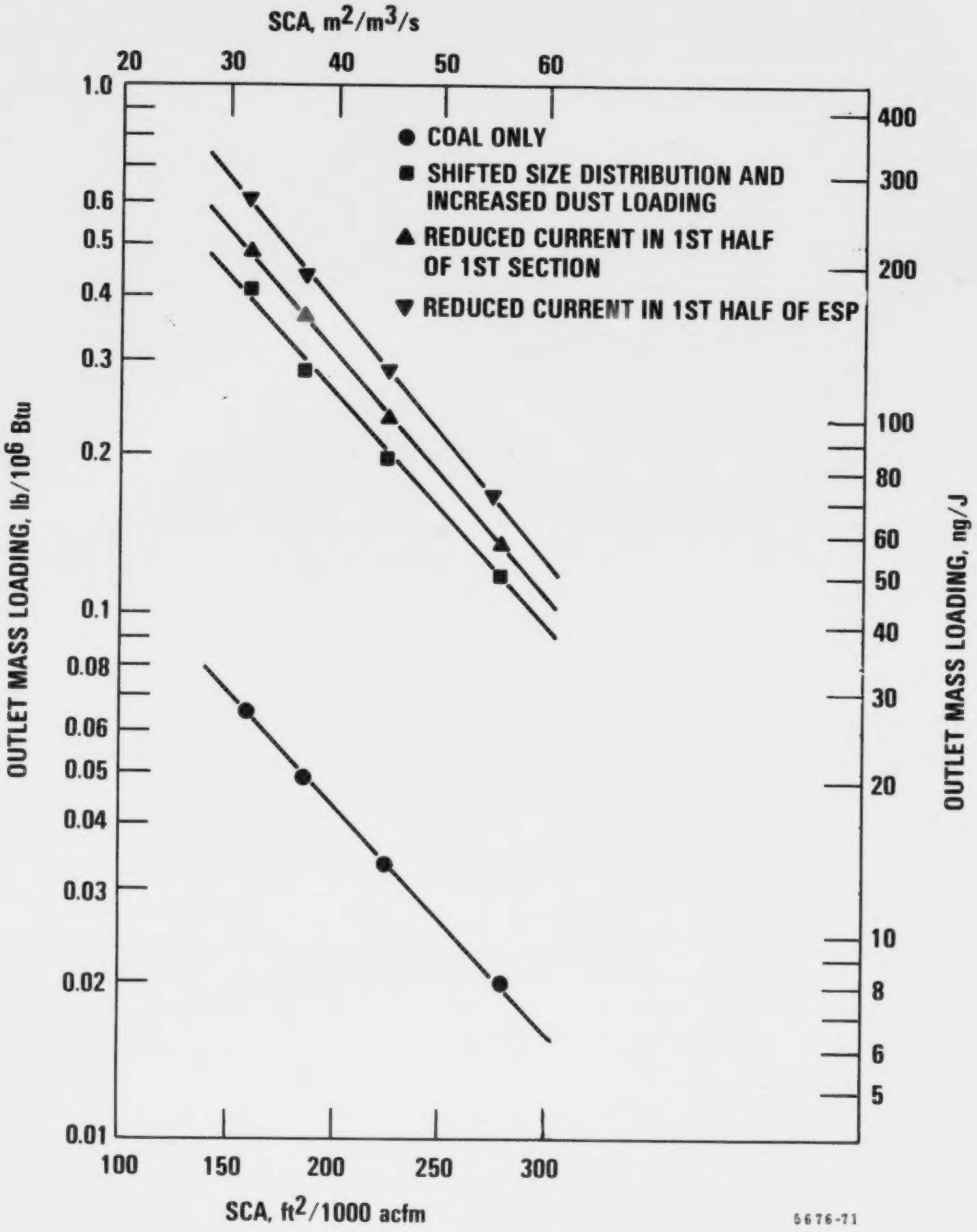

Figure 4-7. Outlet mass loading as a function of SCA for an ESP collecting coal with hydrated lime and SO_3.

abnormally low corona current, a revised version of the model was prepared. Both versions of the model apply the Deutsch equation to narrow particle size bands over short ESP length increments to determine particle collection efficiency. In the standard version, the effects of particulate space charge are estimated by a formula which predicts an effective mobility for combined ions and particles and a reduced ion density for particle charging. These estimated values are then used to calculate separately the electric field at the plate, E_{pl}, and the particle charge, Q, which are required for the Deutsch equation. The revised version differs from the standard version in that the particulate space charge is treated explicitly, which allows the interrelation of the particle charge and electric field calculations. The charge and field calculations are alternated until the charge used for the space charge in the field calculation is the same as the charge calculated using the results of the field calculation.

Mathematical Structure

The underlying assumptions for the revised version of the model are listed below. A glossary of the variables used in this section is presented in Table 4-1.

1. The space charge due to charged particles is constant in a given length increment and is uniformly distributed in the gas stream. This allows the development of a rigorously Deutschian model, as these were the conditions for which the Deutsch equation was derived. The assumption of uniformity is particularly good for fine particles in a turbulent gas flow. The fine particles are especially important in ESP modeling as these are the most difficult particles for an ESP to collect.

2. The space charge due to ions is neither uniformly distributed nor constant because the ions follow the electric field lines which are non-uniform in the interelectrode space.

3. The total space charge density is the sum of the particulate and ionic space charge densities ($\rho = \rho_p + \rho_i$). In the revised model, ρ_p and ρ_i are treated separately and explicitly, in contrast to the estimated treatment of a combined ionic and particulate space charge found in the standard version of the model.

4. The current is ionic except in the laminar boundary layer at the collection plate. This is due to the assumption that the particles are stationary in a given length increment. This is a good approximation since the particulate mobility is several orders of magnitude less than the mobility of the ions. Since the particles are stationary, only the ionic current density appears in the current continuity equation ($\nabla \cdot \vec{J}_i = 0$).

5. The ionic mobility, b_i, is used only in the calculation of the ionic current density on the plate ($J_i = E_{pl}\rho_i b_i$). The mobility drops out of the equations in the remainder of the interelectrode space.

TABLE 4-1. GLOSSARY OF VARIABLES USED IN SECTION 4

E_{pl}	Electric field at the collection plate (V/m)
E_{avg}	Average electric field in the interelectrode space (V/m)
Q	Particle charge (coulombs)
ρ	Total space charge density (coulombs/m^3)
ρ_p	Particulate component of ρ
ρ_i	Ionic component of ρ
J	Total current density on the collection plate (amp/m^2)
J_p	Particulate component of J
J_i	Ionic component of J
N_k	Number density of particles in the kth size band (number/m^3)
Q_k	Charge on the particles in the kth size band (coulombs)
ω_k	Deutsch migration velocity of the particles in the kth size band (m/s)
I	Measured plate current (amps)
A	Plate area (m^2)
V	Electric potential (volts)
FID	Free ion density used for charge calculation (coulombs/m^3)
e	Electron charge (1.6 E-19 coulombs)
ΔX	Wire-to-plate distance (m)
B	Scale factor to increase or decrease charging rate
Δt	Time over which charging takes place (s)
ρ(wire)	Total space charge density at the corona wire (coulombs/m^3)
b_i	Ionic mobility (m^2/V-s)

6. The particulate current density J_p is included when determining the total current density on the plate ($J = J_i + J_p$). J_p is computed from the calculated charges and Deutsch migration velocities of the different size particles ($J_p = \sum_k N_k Q_k \omega_k$).

7. Overall E field convergence is tested using the measured average plate current density ($J = I/A$).

8. The calculations of the electric field and the particle charge are alternated until self-consistency is obtained in each incremental length before proceeding to the next incremental length in the precipitator. The self-consistency is determined by comparing the changes in E_{avg} between successive field-charge iterations. When the change in the field is sufficiently small, the calculation is assumed to have converged.

The basic equations of the E field routine have been redefined, starting with Poisson's equation ($\nabla^2 V = -\rho/\epsilon_0$) and the current continuity equation ($0 = \nabla \cdot \vec{J}_i = \nabla \cdot [\rho_i b_i \vec{E}]$). The equations are solved for V and ρ on a calculation grid, called the V/ρ grid, which stretches from wire to mid-wire to plate. The following notation is used on the V/ρ grid:

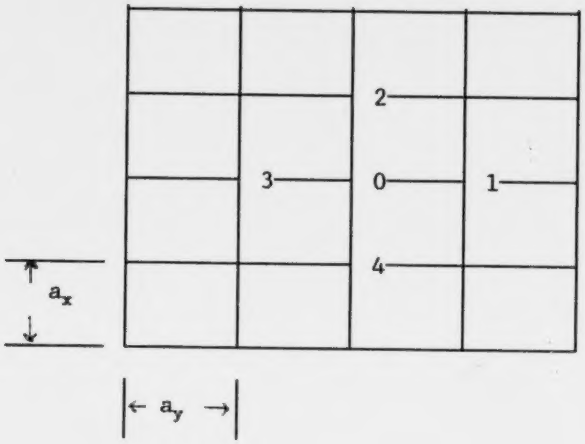

The equation for the potential at point 0 is

$$2\ (a_x{}^2 + a_y{}^2)\ V_0 = a_y{}^2\ (V_2 + V_4) + a_x{}^2\ (V_1 + V_3) + \frac{1}{\varepsilon_0}\ a_x{}^2\ a_y{}^2\ \rho_0 ,$$

which is unchanged from previous versions of the model, except that $\rho = \rho_i + \rho_p$ explicitly. The space charge density equation is

$$\rho_0 = -A \pm \mathrm{SQRT}\ [A^2 + \varepsilon_0 E_x \rho_2 / a_x + \varepsilon_0 E_y \rho_3 / a_y],$$

$$\text{where } A = (\varepsilon_0 E_x / a_x + \varepsilon_0 E_y / a_y - \rho_p)/2.$$

The equation for ρ is similar to that of the standard version of the model with the following exceptions:

1. In the revised version, the particulate and ionic space charge densities are treated explicitly and summed to find the total space charge ($\rho = \rho_p + \rho_i$).

2. Mobility does not appear in the revised equations. The only mobility which could occur in a stationary cloud of charged particles is the ionic mobility, and it cancels algebraically in the interelectrode space.

3. In the standard version of the model, A does not contain the $-\rho_p$ term, which arises from the explicit treatment of the space charge. The sign before the square root is taken as negative for negatively charged particles. The close similarity in the equations allows the use of the existing E field subroutine structure with only minor changes in the FORTRAN code.

Following the solution of the V/ρ grid and the subsequent calculation of E_{avg} and E_{pl}, the particle charge is calculated. Charging is done by the rigorous charging procedure used in the standard version of the model. To obtain correct charging in an iterative charging procedure, the charges on the particles are reduced to the values from the previous length increment in each iteration before recharging using the most recent values of E_{avg} and free ion density (FID). The value of the free ion density is obtained from FID = $-\rho_i/e*B$ where ρ_i is the average ionic space charge on the V/ρ grid, e is the elemental charge and B is a factor ≤ 1 which may be used to reduce the charge in a given E/Q iteration to avoid nonconvergence of the V/ρ calculation. Steps have been taken to ensure that the amount of charge reduction in a given E/Q iteration is less than in the previous iteration. This results in slow and steady growth of the particle charge until full charge is reached without causing nonconvergence of the V/ρ calculation. Full charge is defined as that charge that would be achieved if all of the available free ions were used for charging.

Once the particles are charged, the program returns to the E field calculation where the most recent charge values are used in the space charge calculation. The calculations of ionic and particulate space charge density, average field and collecting field (E field at the plate), plate current density, and particle charge are all iterated to self-consistency within each computational length increment. After the charge calculation in each iteration, if full charge has been reached (i.e., B = 1.0), the average E field is tested for convergence. If the value of E averaged across the calculation grid is within 5% of its previous value, the E/Q calculation is assumed to have converged. In modeling some ESPs, it may prove impossible to build up full particle charge without causing V/ρ nonconvergence. In this case, the particle charge is made as large as possible and the E/Q calculation is assumed to have converged with reduced charging. This usually occurs only in the first few increments of the ESP. Following the termination of the E/Q calculation, the collection efficiency is calculated for each particle size using the Deutsch equation. The number of particles in each size band remaining in the gas stream is determined, and the efficiency calculation proceeds to the next length increment in the ESP.

A comparison of the logic used in the standard and revised versions of the ESP Model may be obtained from Figures 4-8 and 4-9. Both versions of the model use iteration to achieve self-consistency in the calculation. In the standard model, an estimated value of the overall collection efficiency must be furnished as part of the input data. This estimated value is used to estimate the space charge effects, as shown in Figure 4-8. The particle charge and collecting electric field are then calculated independently of each other in each incremental length. The test of convergence is made when the overall collection efficiency is compared to the estimated value. If the two do not agree, the calculated value is taken as the new estimate and the entire process is repeated until the efficiency values do agree or the maximum number of iterations is reached.

By comparison, in the revised model, each increment is made fully self-consistent before the calculation proceeds to the next length increment (Figure 4-9). Since the space charge effects are developed within each increment, the need for an estimated efficiency is eliminated. Further, since the E field and particle charge calculations are interrelated, the fields and charges

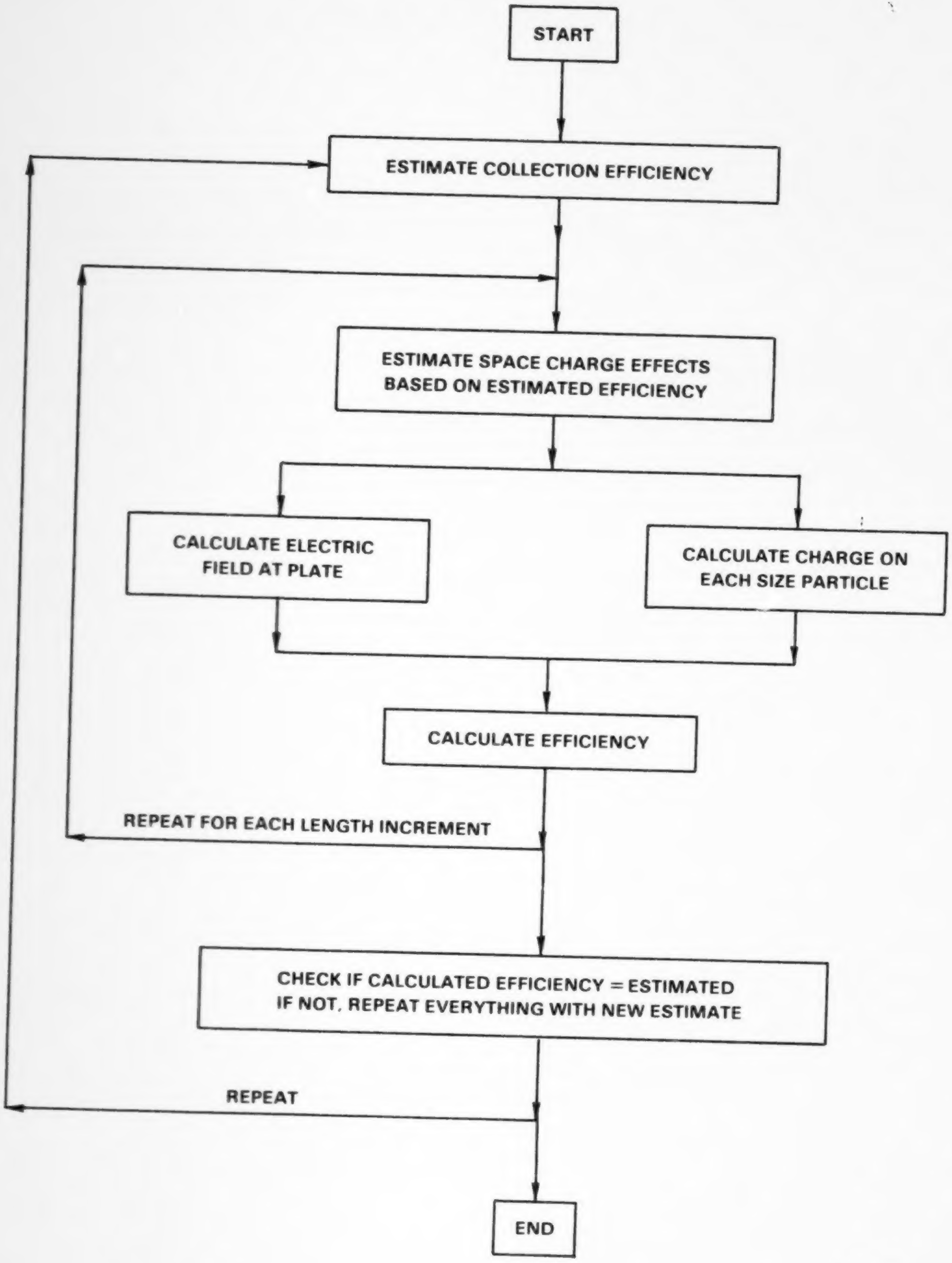
START
ESTIMATE COLLECTION EFFICIENCY
ESTIMATE SPACE CHARGE EFFECTS BASED ON ESTIMATED EFFICIENCY
CALCULATE ELECTRIC FIELD AT PLATE
CALCULATE CHARGE ON EACH SIZE PARTICLE
CALCULATE EFFICIENCY
REPEAT FOR EACH LENGTH INCREMENT
CHECK IF CALCULATED EFFICIENCY = ESTIMATED IF NOT, REPEAT EVERYTHING WITH NEW ESTIMATE
REPEAT
END

5914-77

Figure 4-8. Logic diagram for the standard version of the ESP Model (Revision 3).

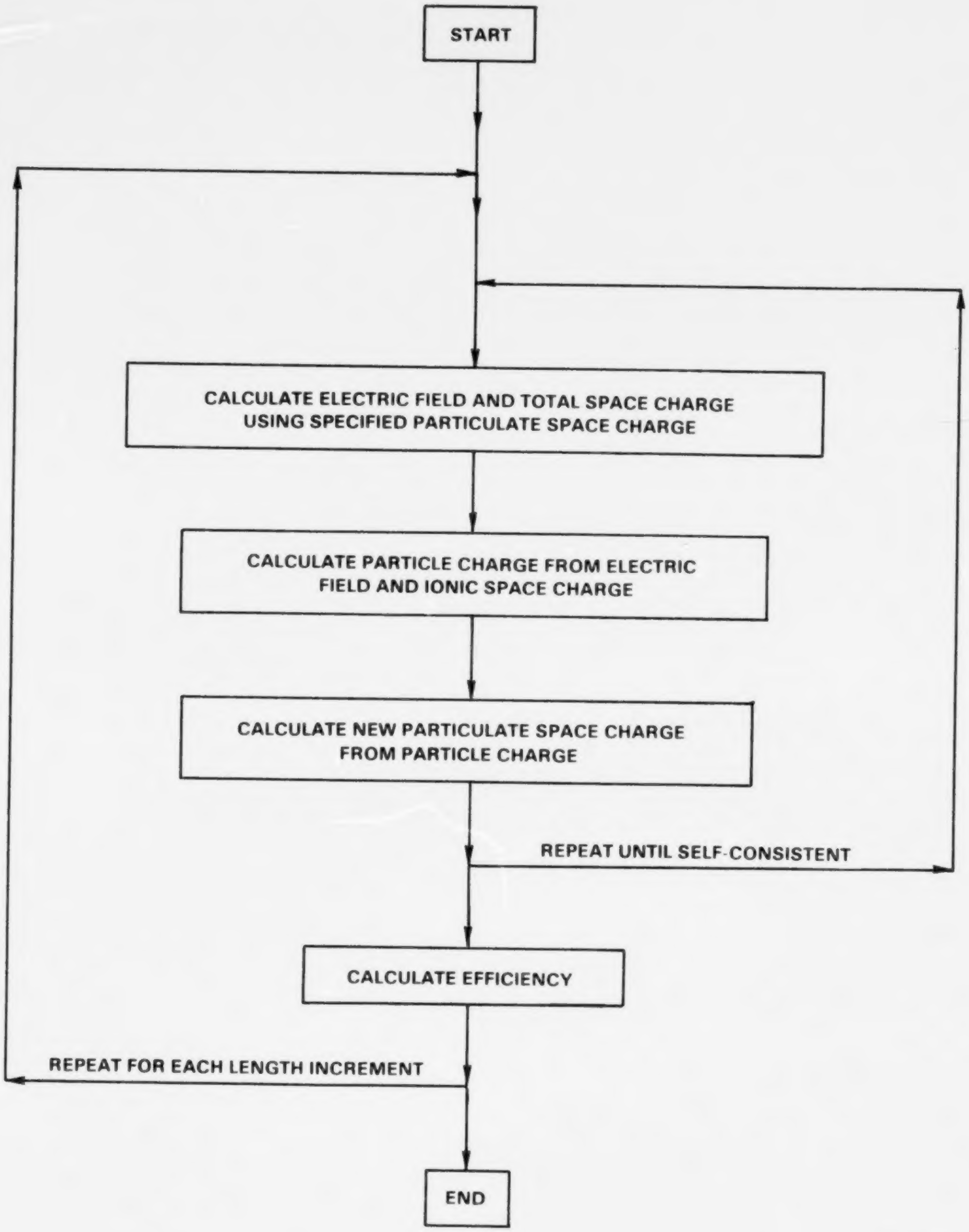
START
CALCULATE ELECTRIC FIELD AND TOTAL SPACE CHARGE USING SPECIFIED PARTICULATE SPACE CHARGE
CALCULATE PARTICLE CHARGE FROM ELECTRIC FIELD AND IONIC SPACE CHARGE
CALCULATE NEW PARTICULATE SPACE CHARGE FROM PARTICLE CHARGE
REPEAT UNTIL SELF-CONSISTENT
CALCULATE EFFICIENCY
REPEAT FOR EACH LENGTH INCREMENT
END

5914-76

Figure 4-9. Logic diagram for the revised version of the ESP Model.

increment are consistent with each other. This feature is unique to the revised ESP Model and represents a significant improvement in the state of precipitator modeling.

Comparison of Results

The evaluation of the revised version of the ESP Model (2) is based on a comparison of the standard and revised model versions using rigorous calculations of electric fields and particle charge. The comparison is made on the basis of computed changes along the length of the precipitator in values of the following parameters:

- accumulated particle charge,
- total, ionic and particulate space charge density,
- ionic and particulate plate current density,
- average electric field,
- collecting electric field,
- total particulate mass penetration.

The values of the following parameters are compared at the ESP outlet:

- fractional penetration, and
- particle migration velocity.

The results of the comparison for a pulverized-coal-fired power plant precipitator are shown in Figures 4-10 through 4-17. The ESP chosen for this comparison is the Johnsonville Unit 5 precipitator (a TVA plant). This unit features 10 in. (25 cm) plate spacing, good electrical power input, and a moderate dust loading (1.6 gr/ft^3 or 3.7 g/m^3). The ash has a moderate resistivity (2×10^{10} ohm cm) and a particle size distribution that is typical for fly ashes from eastern bituminous coal. The first three fields, divided into 1 ft (30 cm) long length increments, are shown in the data comparisons.

Figure 4-10 shows the rate of charge accumulation for three particle sizes. The reduction in the charge on the particles can be attributed to the reduced average E field used in the charging calculation (shown in Figure 4-11). The reason for the field reduction in the revised model is that the average E field is calculated by actually averaging the electric fields over the V/ρ calculation grid. In the standard version, the value of the average field is obtained by dividing the applied voltage in each field by the wire-to-plate distance, a calculation which is only valid on the wire-to-plate line. The steps in the average field curve for the standard version are due to changes in the applied voltage between fields.

Figure 4-11 also shows the enhancement of the collecting electric field (the field at the plate) due to the presence of charged particles. This effect is observable because the revised version of the model calculates the effects of space charge on the electric field explicitly. The standard version, which does not directly relate the field calculation to particle charge, does not show this phenomenon. This is an important effect due to the fact that the Deutsch migration velocity is directly proportional to the field at the plate.

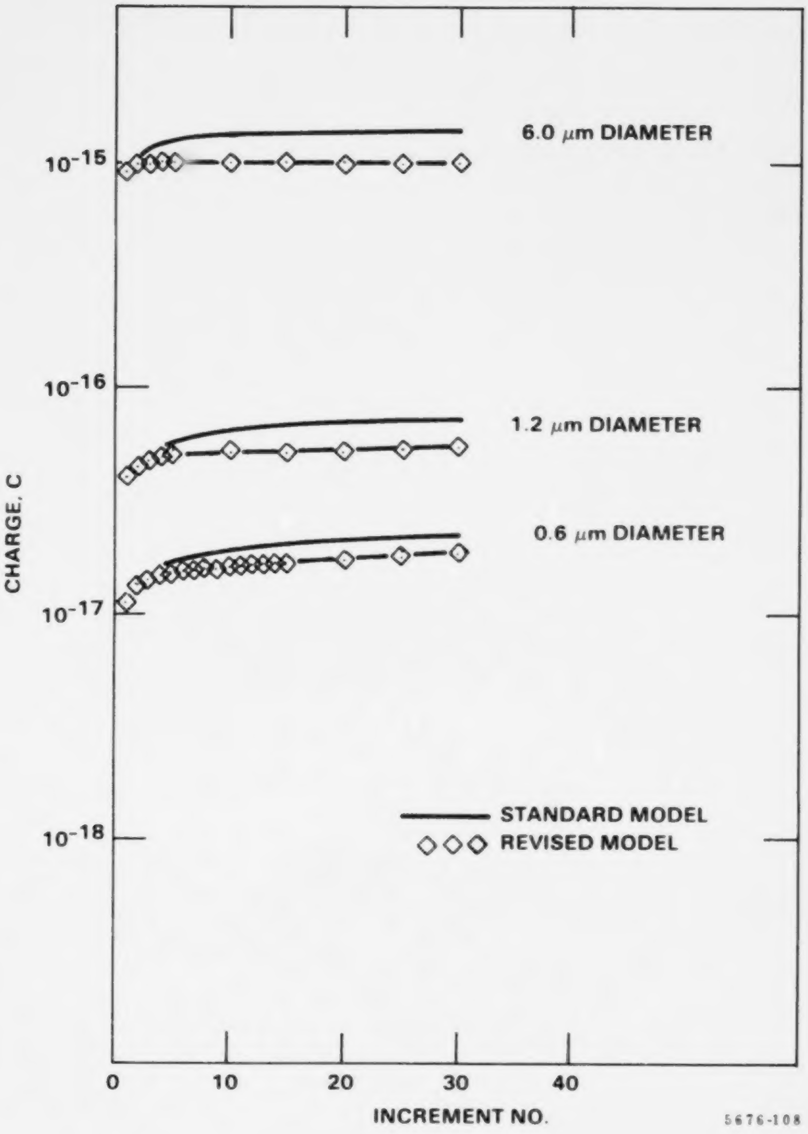

Figure 4-10. Particulate charge calculated by the standard and revised versions of the ESP Model.

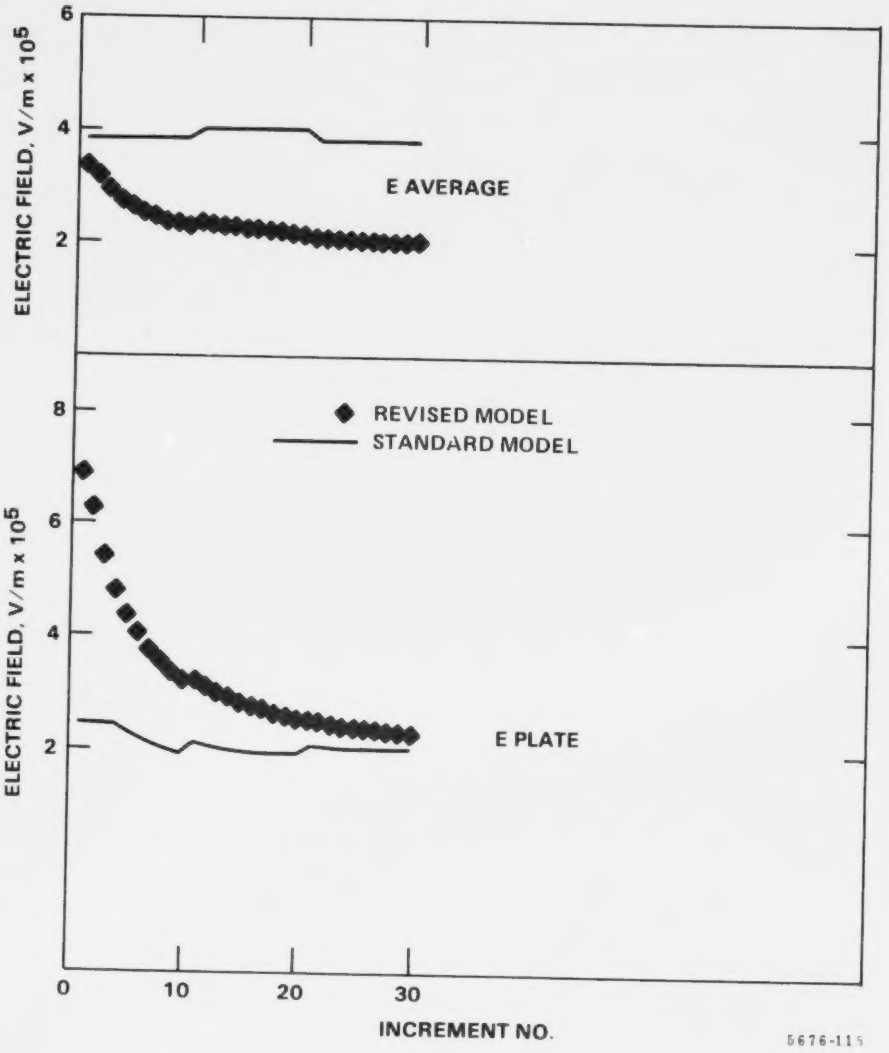

Figure 4-11. Calculated electric fields for the standard and revised versions of the ESP Model.

Figure 4-12 compares the total space charge density at the plate (directly opposite the wire) for the standard and revised versions of the model. In the standard model, no specific requirements are made on the space charge density regarding the number of charged particles present in the gas stream. The calculation is made as if only ions were present, except that an effective mobility for combined motions of ions and particles is used instead of the ionic mobility. In the revised model, where the particulate and ionic space charge are treated explicitly, the total space charge density at every point on the V/ρ calculation grid is constrained to be equal to or greater than the minimum charge density provided by a uniformly distributed, stationary cloud of charged particles. This is defined by $\rho_{min} = \sum_{\substack{\text{all particle} \\ \text{size bands}}}$ (number of particles in each size band/m^3 gas)*(charge on each size band). As shown in Figure 3-12, the space charge density starts at a high value due to the rapid charging of entrained particles and then decreases as particle collection takes place.

In Figure 4-13, the total space charge density for the revised model shown in Figure 4-12 has been broken down into its ionic and particulate components. Comparison of the figures shows that in the first half of the ESP, the particulate space charge density is the major component of the total space charge density. Only in the last few increments of this example does the ionic space charge exceed the particulate space charge. These data are not available in the combined ions and particles treatment used in the standard version of the model, but may be easily obtained from the revised model which keeps track of ions and charged particles separately.

In contrast to the dominance of the particulate space charge density, the current density on the plate is overwhelmingly ionic in nature. Figure 4-14 shows this for both the standard and revised versions of the model. Note that the particulate and ionic current densities are plotted on the same scale, demonstrating the difference in magnitude between the two components. The minimum difference is a factor of 10, with the average difference exceeding 2 orders of magnitude.

Figure 4-15 shows the incremental mass penetration calculated for the standard and revised versions of the model. The greater collecting electric field in the revised model produces a greater efficiency even though the ultimate particle charge is less than in the standard version. These curves are for the ideal efficiency only and do not contain any non-ideal effects.

Figure 4-16 shows the outlet fractional penetration calculated by the standard and revised versions of the ESP Model compared to measured data. In this figure, the effect of the empirical migration velocity correction function in the standard model is clearly shown (dashed line). The experimental data lie between the corrected and ideal (uncorrected) predictions. The penetration predicted by the revised model falls between the values predicted by the standard model but are larger than the experimental values.

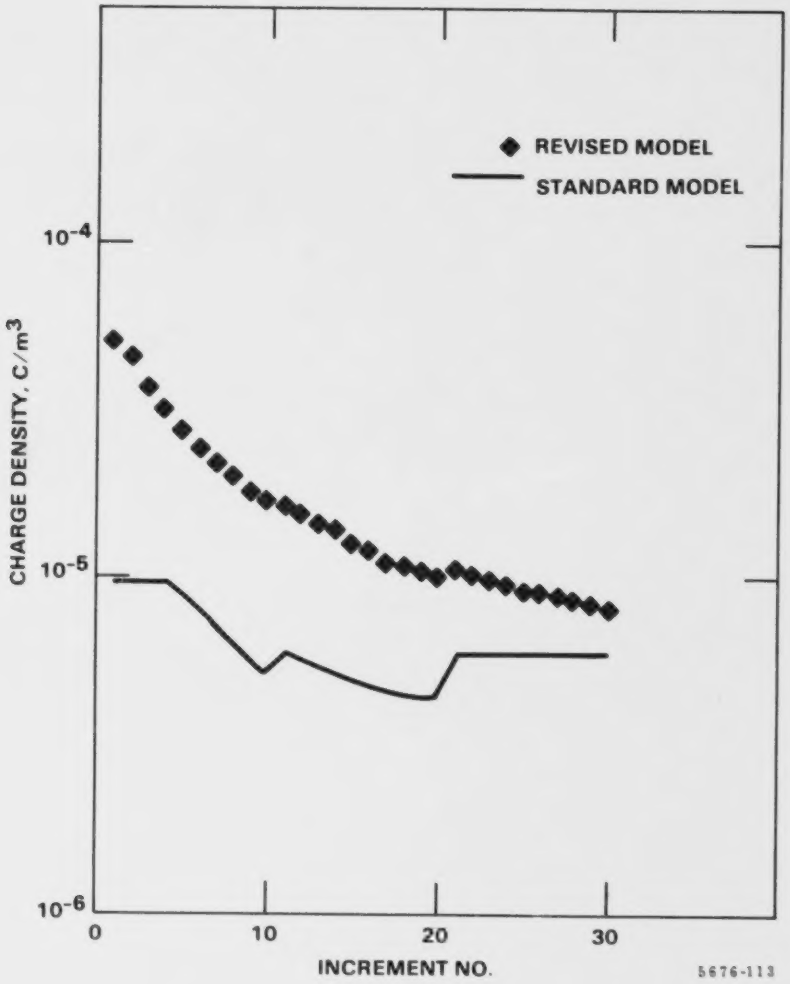

Figure 4-12. Total space charge density calculated by the standard and revised versions of the ESP Model. The calculation is at the plate directly opposite the wire.

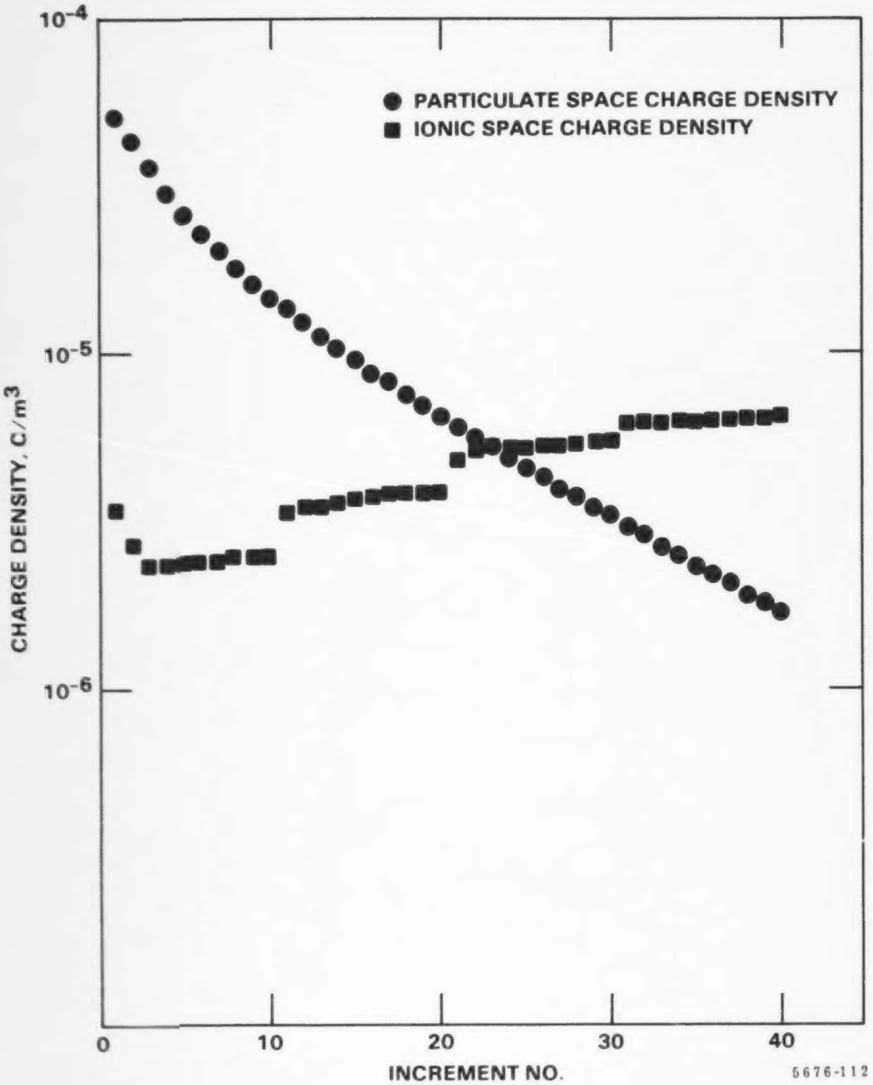

Figure 4-13. Particulate and ionic components of the space charge calculated by the revised version of the ESP Model. The calculation point is at the plate directly opposite the wire.

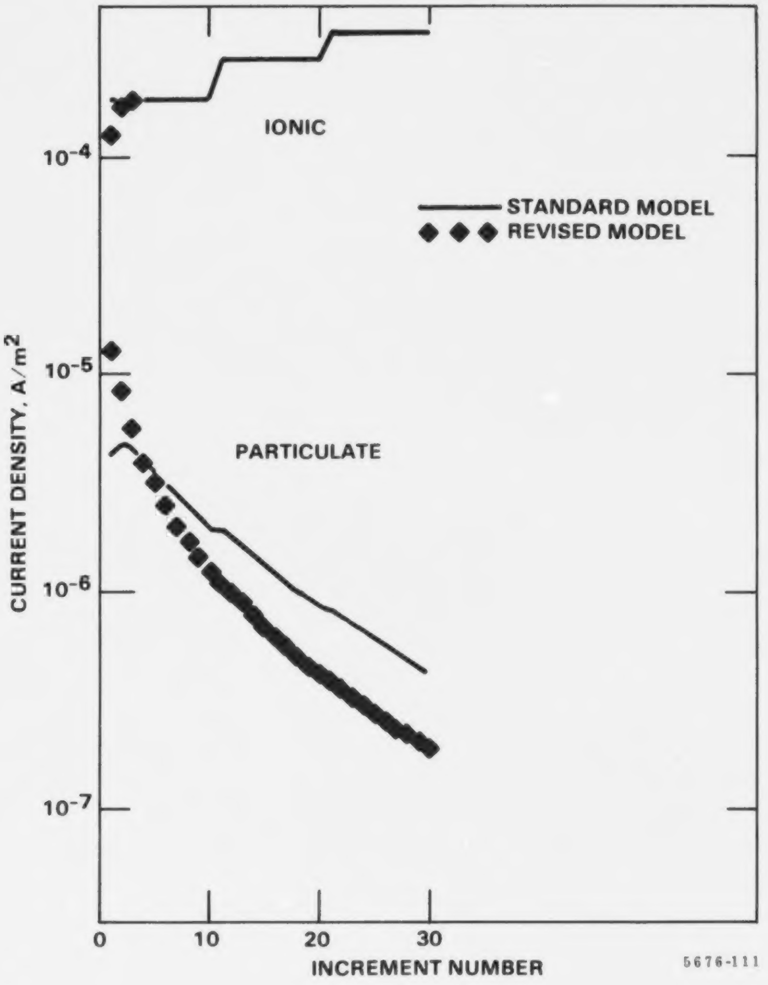

Figure 4-14. Ionic and particulate current densities predicted by the standard and revised versions of the ESP Model.

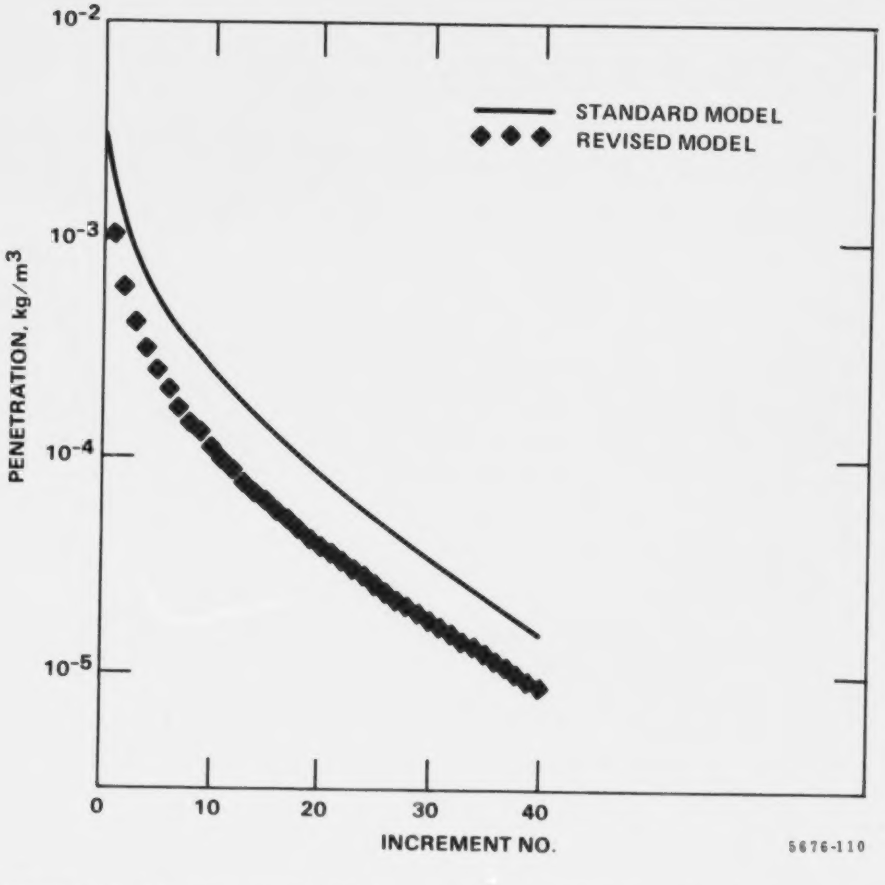

Figure 4-15. Mass penetration calculated by the standard and revised versions of the ESP Model.

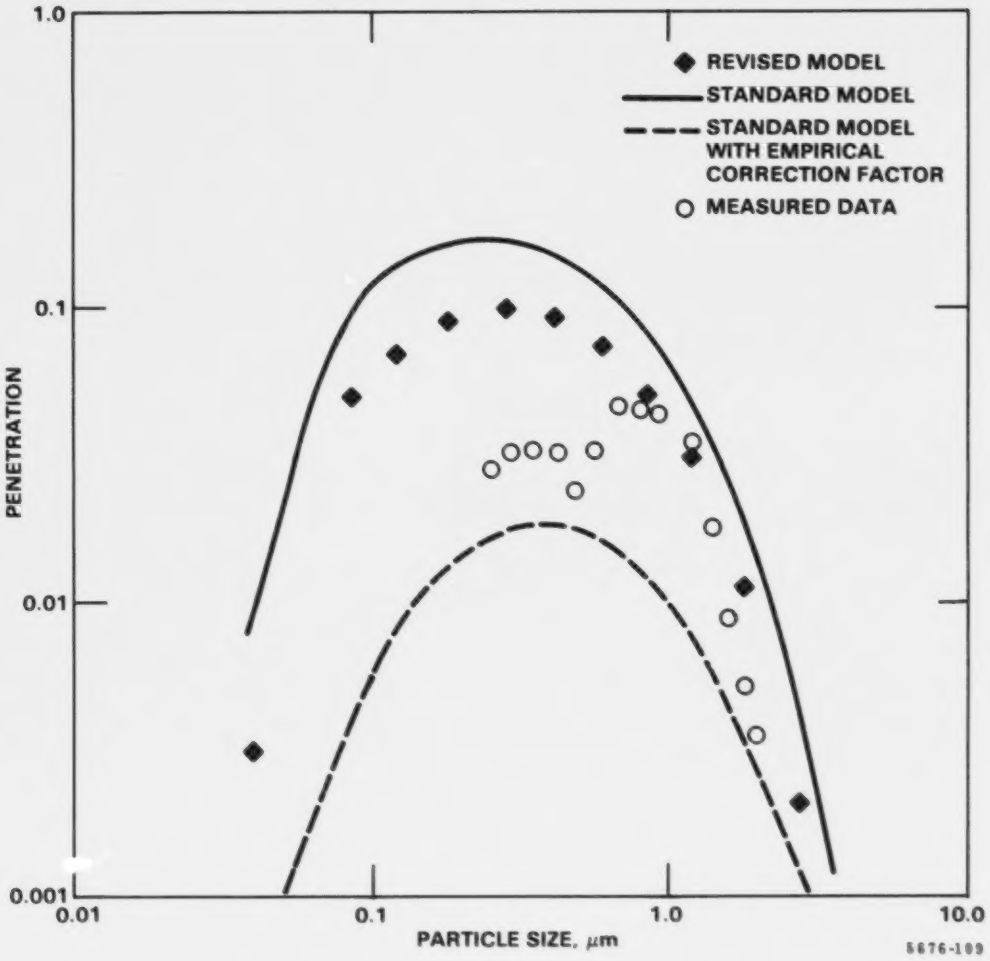

Figure 4-16. Fractional penetration calculated by the standard and revised versions of the ESP Model compared to measured data.

Figure 4-17 shows the migration velocities predicted by the standard and revised versions of the ESP Model. As with Figure 4-16, the values predicted by the revised model more closely match those predicted by the ideal calculation in the standard model than they do the values predicted using the empirical correction factor.

SUMMARY

The purpose of this task was to perform theoretical and experimental investigations into the effects of ESPs of high mass loadings typical of the LIMB process. The experimental part centered around use of a specially instrumented laboratory ESP on actual LIMB ash produced in the SRI Coal Combustion Facility. The ash entering the ESP exhibited the following properties:

1. High resistivity of (2×10^{12} ohm cm) for unconditioned LIMB ash,
2. Moderate resistivity of (2×10^{10} ohm cm) for SO_3-conditioned LIMB ash,
3. Factor of 3 increase in dust loading, and
4. Shift in the particle size distribution toward smaller particles

The results of these tests show:

1. ESP malfunction due to severe back corona using unconditioned LIMB ash, an effect of the high resistivity, and
2. Reduced current when using SO_3-conditioned LIMB ash due to space-charge suppression of the corona, a result of the high dust loading.

These data were used in the standard ESP Model (2) to project the change in outlet mass emissions which would result from adding the LIMB process to a typical ESP. The projections showed a large increase in emissions, primarily due to the increase in inlet dust loading and the shift toward small particles, where an ESP is less efficient. By comparison, the increase in emissions due to the space charge current suppression was much smaller.

The theoretical portion of this task consisted of the development of a revised version of the ESP Model. The revised version represents an improvement over the standard version in that it is responsive to a wider range of ESP operating conditions. The algorithms used in the revised model are conceptionally rigorous and the calculated fields and particle charges used to calculate the collection efficiency are fully self-consistent. The only approximation used in the revised model is the average interelectrode electric field which is used in the calculation of particle charge. However, this field is not $\Delta V/\Delta X$ as in the standard version of the model, but rather the spatial average of the field values obtained in the solution of the V/ρ grid. Considering the random motion of fine particles through regions of different field strength and the computational problem of keeping track of accumulating particle charge, this may be the best way of performing the charge calculation.

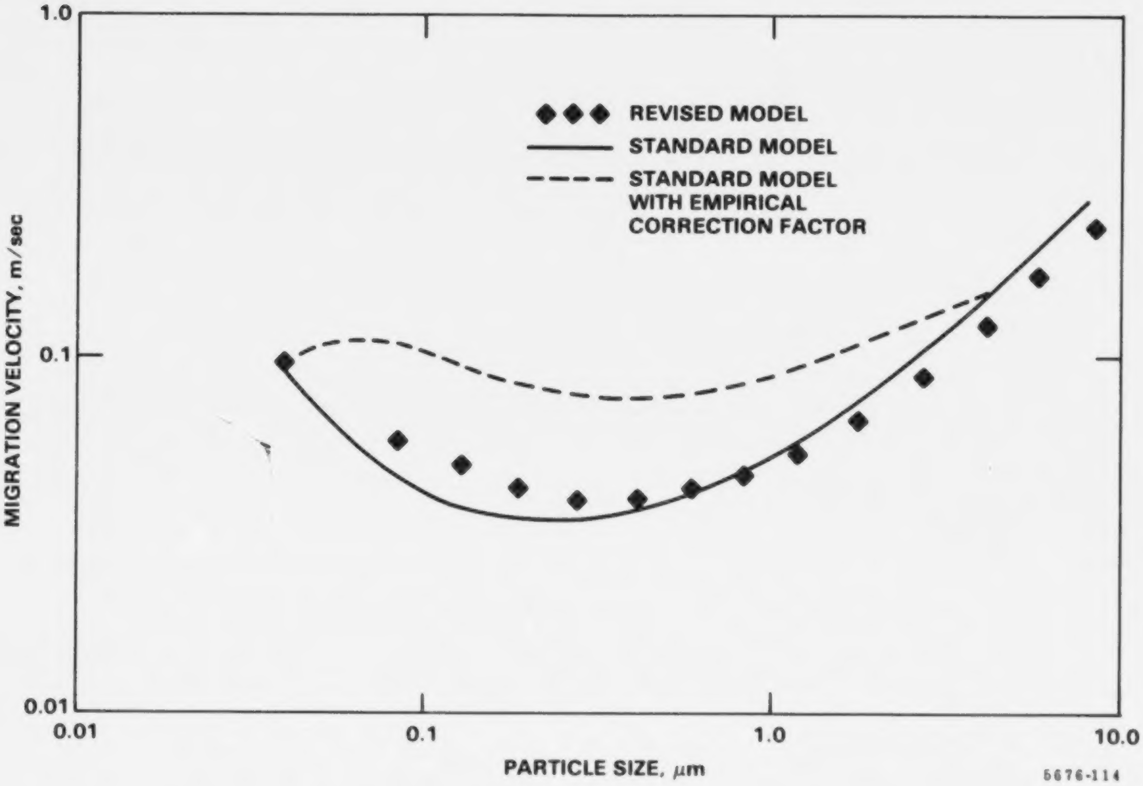

Figure 4-17. Outlet particle migration velocities calculated by the standard and revised versions of the ESP Model.

Comparisons between the revised version of the ESP Model and a limited number of field test data sets indicate that the revised model functions satisfactorily as a predictive tool. However, these data indicate that the improved algorithm has not eliminated the need for an empirical correction (usually referred to as the ramp function due to its shape) to the calculated migration velocities. Unfortunately, there are too few reliable data sets measured without plate rapping available to allow an in-depth investigation of a ramp function for the revised model. Therefore, it is recommended that the following tasks be performed on another project in order to refine the revised ESP Model:

1. A correction for the effects of rapping reentrainment must be incorporated into the model.

2. Data sets suitable for model evaluation must be selected from the SRI ESP Data Base.

3. The revised model must be used with these data to choose an appropriate ramp function.

4. The possibility of a functional connection between the calculated migration velocity error and ESP operating parameters should be investigated.

SECTION 5

TASK 3. PILOT-SCALE INVESTIGATION OF ESP PERFORMANCE WITH FURNACE SORBENT INJECTION

The objective of this task was to test the EPA's mobile pilot ESP at a site with limestone injection into the boiler to reduce SO_2 emissions. Since there were no boilers employing limestone injection technology on a continuous basis when this cooperative agreement was awarded, it was necessary to consider alternative test sites.

The first potential location examined was a ten-million-Btu/h (3-MW) furnace at the facilities of the Energy and Environmental Research Corporation near Irvine, CA. It was determined that the use of this furnace for the test program would not be advisable since it had never operated on a 24-h/day basis. A second potential site for the test program was the Homer City station of the Pennsylvania Electric Company. This organization was considering a long-term study of LIMB technology for a 650-MW(e) boiler, and the installation of the EPA mobile ESP on a slipstream drawn from this boiler was given serious consideration. However, the LIMB test program was not performed at Homer City as a result of factors unrelated to the pilot precipitator project, and it was necessary to find another test site.

An agreement was reached between the EPA and the Department of Defence of the Government of Canada concerning the installation of the EPA mobile ESP on a seventy-million-Btu/h (21-MW) heating furnace operated by the Canadian Defence Forces at Base Gagetown, located in Oromocto, New Brunswick. Unit 2 at Base Gagetown was being equipped with a limestone injection system and low-NO_x burners designed by Steinmüller of West Germany.

Denver Research Institute repaired and modified EPA's mobile ESP and began installing it at Gagetown in December 1985. The installation of the pilot ESP system was completed by DRI and SRI in February 1986. Figures 5-1 through 5-4 show the test facility and ESP location at Gagetown. Figure 5-5 is a schematic of the test facility with the associated equipment and sampling locations identified.

Testing of EPA's pilot ESP began at Gagetown in February 1986. Sampling equipment that was operated during these tests included inlet and outlet mass trains, gas sampling systems for SO_2 and SO_3, and an in-situ resistivity probe. Data were taken on February 11 and 12 without limestone injection and on February 14 with limestone injected into the furnace.

Table 5-1 presents the averaged data taken from the control panel of Unit 2. These data were recorded approximately hourly during the testing periods for the pilot ESP. Table 5-2 presents the proximate and ultimate coal analyses of samples taken from the coal feeders of Unit 2.

The data obtained from the mass trains during the three days of testing are presented as Table 5-3. Mass trains operated at the inlet sampling location are designated as BGI-xx while those at the ESP outlet sampling location are designated as BGO-xx. Single point mass train samples were taken in the Unit 2 ductwork on February 14, 1986, and are designated CFB2-xx. The sampling location for these Unit 2 samples was prior to the take-off point for the pilot ESP. Table 5-4 presents the temperature and flue gas constituents measured during the individual mass measurement tests, while Table 5-5 presents the SO_2 and SO_3 data determined by wet chemistry at the sampling location upstream of the pilot ESP inlet mass measurements.

Table 5-6 presents the chemical analysis of selected samples from the Gagetown test program during the 1985-1986 heating season. The high LOI (loss on ignition) numbers of these samples is a result of the operational problems experienced with the new burners that were installed in Unit 2. The high LOI results caused the pilot ESP electrical sections to short to ground and required opening the pilot ESP each day to clean the insulators prior to any testing. Due to the stability problems with the burners, the test program for the pilot ESP was postponed until the burners could be modified and operated reliably.

Prior to the 1986-1987 heating season, the burner contractor made modifications to the burners in Unit 2. When Unit 2 was started up in December 1986, problems with coal size caused the lower burner to slag and it was not until late January 1987 that this problem was solved. Tests of the burner in February 1987 indicated that LOI's of less than 20% could not be produced. At this time, EPA directed SRI to dismantle the pilot ESP system and transport it to Lorain, OH, for use under EPA Cooperative Agreement No. CR 812811.

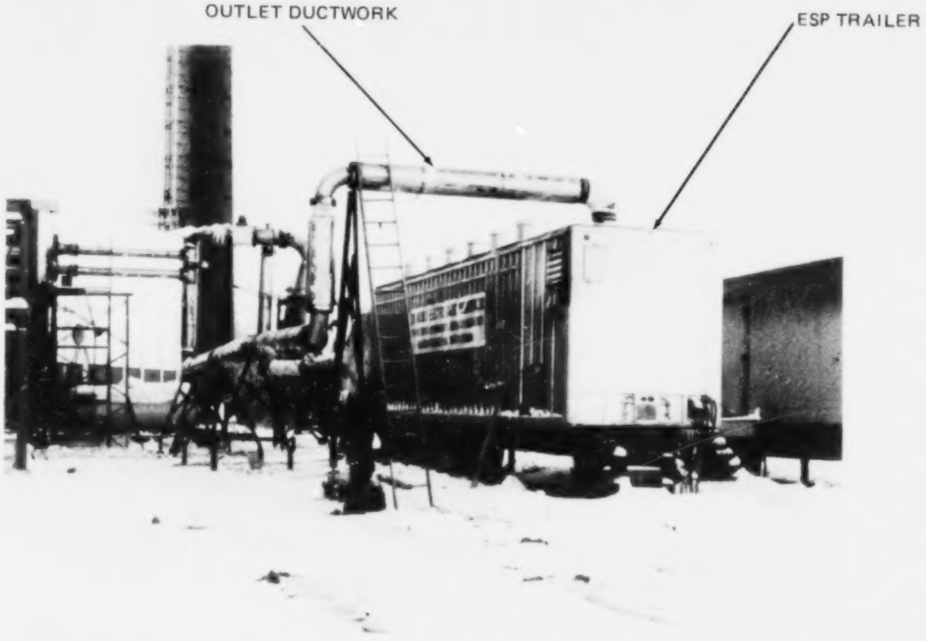
OUTLET DUCTWORK
ESP TRAILER
621-719

Figure 5-1. ESP trailer and ductwork. Base Gagetown, Oromocto, N.B.

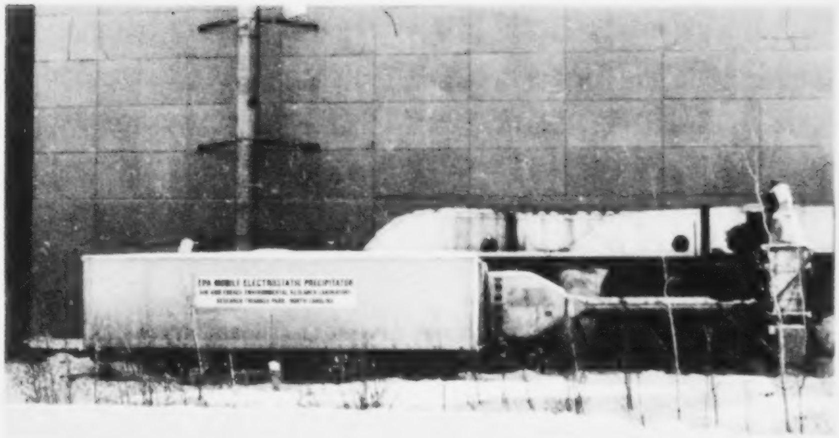
EPA MOBILE ELECTROSTATIC PRECIPITATOR
RESEARCH TRIANGLE PARK, NORTH CAROLINA

621-718

Figure 5-2. ESP control trailer and ductwork. Base Gagetown, Oromocto, N.B.

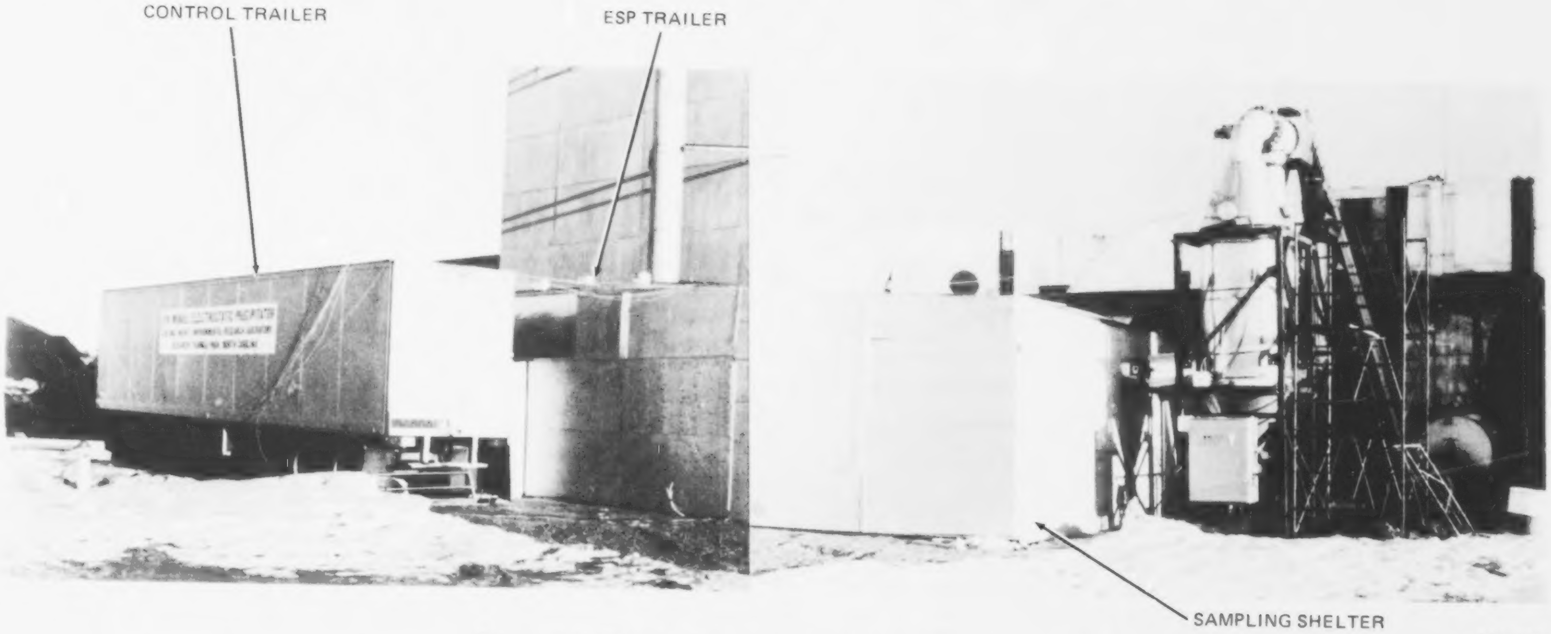
CONTROL TRAILER
ESP TRAILER
SAMPLING SHELTER

Figure 5-3. Test facility, Base Gagetown, Oromocto, N.B.

621-720

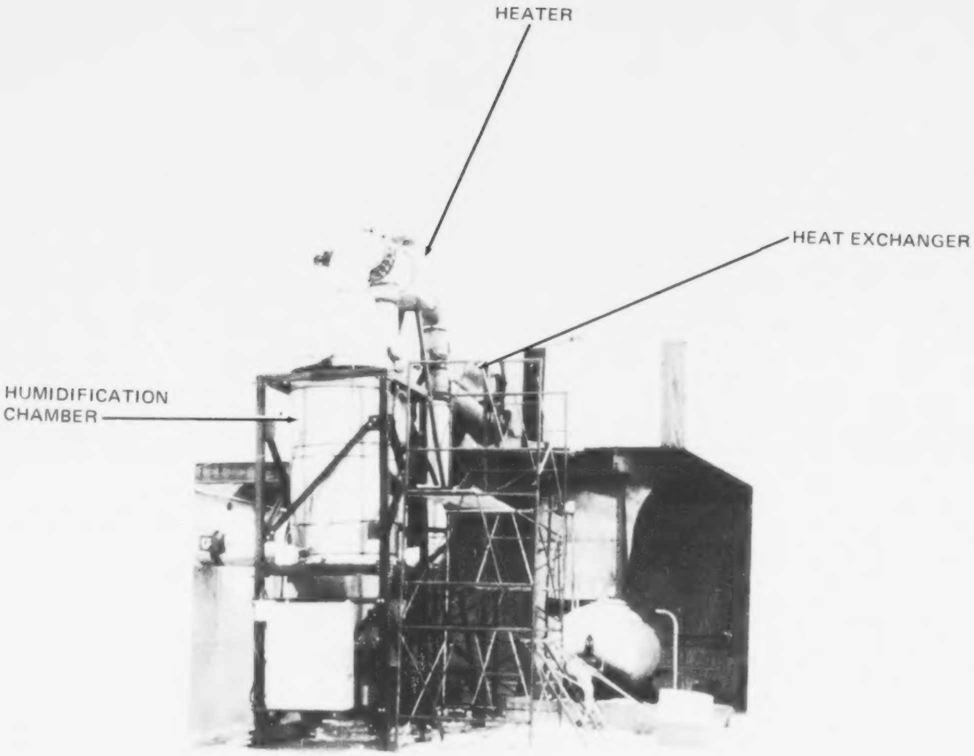
HEATER
HEAT EXCHANGER
HUMIDIFICATION CHAMBER
621-717

Figure 5-4. Inlet ductwork, heater exchanger, heater and humidification chamber. Base Gagetown, Oromocto, N.B.

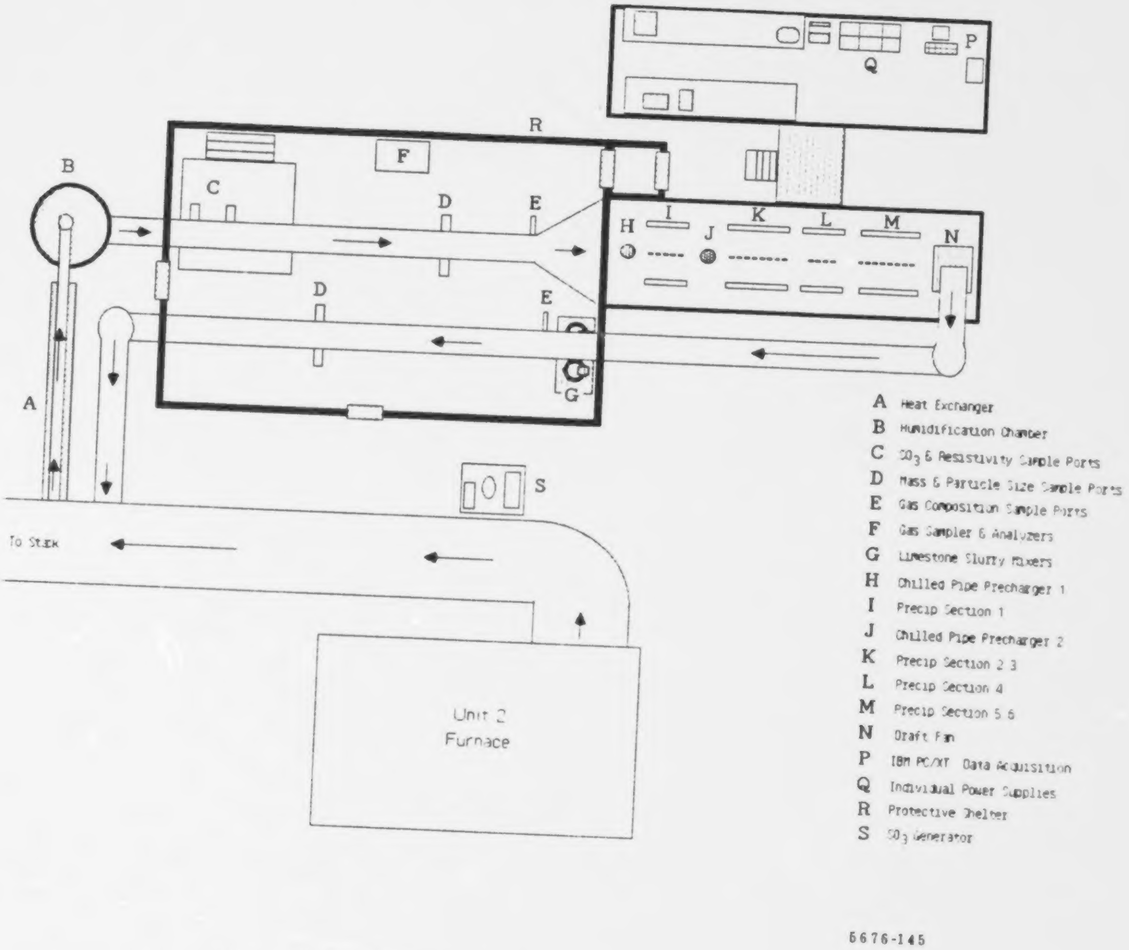
R
P
Q
B
C
F
D
E
H
I
J
K
L
M
N
D
E
G
A
S
To Stack
Unit 2
Furnace
A Heat Exchanger
B Humidification Chamber
C SO_3 & Resistivity Sample Ports
D Mass & Particle Size Sample Ports
E Gas Composition Sample Ports
F Gas Sampler & Analyzers
G Limestone Slurry Mixers
H Chilled Pipe Precharger 1
I Precip Section 1
J Chilled Pipe Precharger 2
K Precip Section 2 3
L Precip Section 4
M Precip Section 5 6
N Draft Fan
P IBM PC/XT Data Acquisition
Q Individual Power Supplies
R Protective Shelter
S SO_3 Generator
6676-145

Figure 5-5. Schematic drawing of Gagetown facility.

TABLE 5-1. GAGETOWN UNIT 2 BOILER DATA

Parameter	Feb. 11, 1986	Feb. 12, 1986	Feb. 14, 1986
Megawatt flow	18.5	17	16.8
Water flow, % of full scale	69	61	61
Air flow, % of full scale	71	67	72
Air heater temperatures, °C			
Gas in	>400	400	>400
Gas out	320	290	318
Air in	25	20	24
Air out	280	250	273
Oxygen, %	3.3	2.9	4.6
Secondary air, % open			
Upper burner	65	65	72
Lower burner	77	66	70
Primary air, % open			
Upper burner	60	63	71
Lower burner	76	63	63
Tertiary air, % open			
Upper burner	48	28	59
Lower burner	48	28	60
Coal air temperatures, °C			
Upper burner	104	100	95
Lower burner	93	96	99
Water temperature, °C			
Inlet	140	140	141
Outlet	180	182	184
Water pressure, kPa	1090	1100	1120
Furnace draft, Pa	-50	-50	-50
Mill inlet pressure, Pa			
Upper	-20	-15	-15
Lower	-15	-20	-20
Mill outlet pressure, kPa			
Upper	1.8	1.7	1.5
Lower	1.6	1.6	1.5

TABLE 5-2. GAGETOWN PROXIMATE AND ULTIMATE COAL ANALYSES

Parameter	2/12/86 As received, %	2/14/86 As received, %	2/24/86 As received, %
Proximate			
H_2O	5.97	5.31	5.25
Ash	2.78	2.65	2.96
Volatiles	33.86	34.32	33.92
Fixed C	57.39	57.72	57.87
Btu/lb	13,920	14,009	14,058
% S	1.11	1.02	1.10
Ultimate			
C	77.21	78.28	78.37
H	4.92	4.97	4.97
N	1.51	1.61	1.59
Cl	0.08	0.09	0.08
O (by diff.)	6.42	6.07	5.68

TABLE 5-3. GAGETOWN SOLIDS CONCENTRATIONS[a]

Date[b]	Test No.	gr/ft^3	mg/m^3	ESP, % eff.
2-11	BGI-01	1.134	2601.0	
	BGO-01	0.027	61.8	97.6
2-11	BGI-02	1.026	2354.5	
	BGO-02	0.027	61.3	97.4
2-12	BGI-03	1.263	2898.9	
	BGO-03	0.015	33.9	98.8
2-12	BGI-04	1.053	2415.2	
2-12	BGI-06	1.125	2581.3	
2-14	CFB2-01	1.576	3615.6	
	BGI-07	1.436	3294.2	
2-14	CFB2-02	2.250	5161.7	
	BGI-08	1.728	3964.9	
2-14	CFB2-03	2.477	5683.8	
	BGI-09	2.063	4733.4	

a. Reported for standard gas volumes.

b. February 1986.

TABLE 5-4. GAGETOWN GAS CHARACTERISTICS DURING MASS LOADING TESTS

Date[a]	Test No.	Duct temp, °F (°C)	H_2O, %	O_2, %	CO_2, %	NO_x, ppm	SO_2, ppm
2-11	BGI-01	307 (153)	5.08	7.2	10.5	343	668
2-11	BGO-01	236 (113)	2.01	10.2	8		
2-11	BGI-02	307 (153)	4.66	7.2	10.5	351	634
2-11	BGO-02	236 (113)	5.35	10.5	8		
2-12	BGI-03	314 (157)	6.06	6.9	12.5	346	664
2-12	BGO-03	235 (113)	3.71	10.5	9		
2-12	BGI-04	314 (157)	6.21	6.9	12.5	357	692
2-12	BGI-06	314 (157)	6.16	6.9	12.5	349	728
2-14	CFB2-01	547 (286)	2.49	5.4	12		
2-14	BGI-07	309 (154)	4.75	8.8	11	253	386
2-14	CFB2-02	547 (286)	5.77	5.4	12		
2-14	BGI-08	309 (154)	4.50	8.8	11	255	271
2-14	CFB2-03	547 (286)	6.31	5.4	12		
2-14	BGI-09	309 (154)	4.91	8.8	11	250	172

a. February 1986.

TABLE 5-5. GAGETOWN GAS ANALYSES AT ESP INLET

Date[a]	Time	Duct temp, °F (°C)	O_2, %	Operating conditions	SO_3, ppm	SO_2, ppm
2-11	1111-1128	310 (154)	7.2	Coal	<0.5	563
	1358-1415	311 (155)	6.4	Coal	<0.5	665
	1559-1615	302 (150)	6.9	Coal	<0.5	654
2-12	1437-1455	310 (154)	6.7	Coal	<0.5	623
	1549-1606	299 (148)	6.5	Coal	<0.5	673
2-14	1324-1340	311 (155)	8.4	Coal + limestone	<0.5	468
	1504-1520	309 (154)	8.5	Coal + limestone	<0.5	284

a. February 1986.

TABLE 5-6. GAGETOWN CHEMICAL ANALYSIS OF SOLIDS

Ash parameter Wt%	Sample Number				
	BGI-02 MT inlet	BGI-03 MT inlet	D589-11-1 ash from auger	BGI-06 MT inlet	CFB2-01 MT Unit 2 duct
Li_2O	0.03	0.03	0.03	0.03	0.02
Na_2O	0.94	0.86	0.89	0.84	0.33
K_2O	1.6	1.7	1.6	2.1	0.81
MgO	0.84	0.83	0.83	0.85	0.77
CaO	2.0	1.6	1.7	1.6	49.9
Fe_2O_3	33.4	30.6	32.1	30.0	12.1
Al_2O_3	[a]	23.6	23.1	24.1	9.6
SiO_2	[a]	38.1	36.4	38.8	16.3
TiO_2	1.8	1.7	1.8	1.8	0.67
P_2O_5	0.39	0.31	0.30	0.29	0.11
SO_3	[a]	0.81	1.1	0.48	7.9
LOI	61.2	63.9	58.7	60.0	35.0

Ash parameter Wt%	Sample Number			
	BGI-07 MT inlet	D589-14-3 limestone	CFB2-02 MT Unit 2 duct	BGI-08 MT inlet
Li_2O	0.02	0.01	0.02	0.02
Na_2O	0.43	0.05	0.27	0.31
K_2O	1.0	0.19	0.75	0.85
MgO	0.77	0.74	0.75	0.77
CaO	42.0	92.4	56.0	53.3
Fe_2O_3	15.0	0.50	9.3	11.1
Al_2O_3	11.4	1.2	7.8	9.0
SiO_2	19.3	4.4	13.1	14.9
TiO_2	0.84	<0.20	0.58	0.58
P_2O_5	0.13	<0.03	0.10	0.10
SO_3	8.2	0.19	9.8	9.3
LOI	38.8	36.2	23.6	29.1

a. Insufficient samples for determination of these components.

SECTION 6

TASK 4. STUDIES OF LIMB ASH RECYCLE, DISPOSAL, AND UTILIZATION

INTRODUCTION

LIMB ash differs from conventional fly ash in that it contains 15 to 30% by weight free lime (CaO) and 10 to 25% by weight calcium sulfate ($CaSO_4$). Under the thermal conditions that prevail in a utility boiler, small amounts of these components react with the fly ash components, forming calcium aluminosilicates, in a manner analogous to the lime-clay reactions in a cement kiln. This causes the LIMB ash to have cement-like hardening characteristics when mixed with water. This behavior can be used to enhance the stability of landfilled LIMB ash and to assist in the production of structurally sound construction materials from LIMB ash. The free lime content of the LIMB ash can also be exploited by reactivation and reinjection for additional SO_2 capture. Hydration of the LIMB ash reactivates the unused sorbent by fracturing the sulfate shell on the spent sorbent and hydrating the underlying lime. This has been confirmed by thermogravimetric analysis and BET surface area analysis of spent sorbents before and after hydration.

The LIMB process is currently being demonstrated on a 105-MW coal-fired utility boiler at the Edgewater Station of Ohio Edison Company. As part of this project, the safe handling and disposal of the LIMB ash must be demonstrated. Thus, SRI's work on LIMB ash characterization and disposal has provided the technical data and input required to ensure safe handling and environmentally acceptable disposal of the LIMB ash from the Edgewater demonstration. At the same time, the long-term issues of LIMB ash recycle and utilization must also be addressed in order to improve the economics of the process. Thus, SRI has also conducted laboratory and pilot-scale studies to examine the technical feasibility of LIMB ash recycle and utilization processes. Limited economic studies were also undertaken to investigate the potential cost savings with recycle. Due to budgetary restrictions, SRI performed no economic evaluations on processes for LIMB ash utilization.

OBJECTIVES AND SCOPE

The objectives of the LIMB ash recycle, disposal, and utilization task are enumerated below:

(1) To characterize the modified fly ash produced by LIMB,

(2) To identify potential problems with landfill disposal of the LIMB ash and suggest solutions to these problems,

(3) To develop processes for recovering, reactivating, and recycling the unused sorbent in LIMB ash, and

(4) To develop processes for utilization of LIMB ash in salable by-products or in other applications.

Objectives 1 and 2 were primarily directed at supporting the Edgewater LIMB demonstration by providing technical data relative to LIMB ash characteristics and behavior in a landfill. Objectives 3 and 4 were primarily directed at long-range optimization of the LIMB process and improvement of LIMB process economics.

Recycle. The scope of the LIMB ash recycle work included both laboratory and pilot-scale testing of various recycle concepts. Laboratory hydration studies were first performed to demonstrate that the LIMB ash could be hydrated. Thermogravimetric analysis was used to confirm that the free lime in the LIMB ash was hydrated. As an indication of the reactivation process, the change in specific surface area with hydration was determined by the BET method. The reactivity of the hydrated LIMB ash was assessed by furnace injection tests with LIMB ash hydrated in either a cement mixer or a ribbon blender. These tests were performed with LIMB ashes produced from three sorbents: Vicron limestone, Longview hydrated lime, and Tenn-Luttrell coarse limestone. In view of the large increase in particulate loading caused by recycle, various separation techniques for ash-sorbent mixtures were investigated. These studies included laboratory evaluations of inertial separation, magnetic separation, froth flotation, and steam elutriation. An in-situ cyclonic separation process using coarse limestone sorbent was also evaluated in the pilot-scale combustion facility.

Disposal. For the studies of LIMB ash characteristics and disposal, 55-gal (200-L) drums of LIMB ash were produced in the combustion facility. The temperature profile in the pilot combustor was adjusted to simulate the Edgewater boiler, and the same coal and hydrated lime were used. This simulated LIMB demonstration ash was used for a battery of characterization tests and landfill disposal simulations. Laboratory tests included the following:

(1) Chemical analysis,

(2) Leachate pH and metals analysis,

(3) Permeability measurements,

(4) Temperature-rise studies, and

(5) Wetting tests.

Based on the results of these tests, SRI projected the probable behavior of the LIMB ash under landfill conditions. The validity of this projection was investigated by full-scale conditioning and disposal tests at the Edgewater Station. About 84 tons (76 metric tons) of LIMB ash was obtained from Ontario Hydro's Lakeview Station and trucked to the Edgewater Station for the tests. The ash was conditioned at various water addition rates using the dustless unloading system at the plant. Ten different batches were prepared, with the water addition rate adjusted between batches to determine the optimum conditioning procedure. The temperature rise within each batch was monitored to ensure safe handling.

Core samples were also taken to examine the effect of hardening on in-situ permeability.

Utilization. The LIMB ash utilization studies were initiated with literature reviews and industrial contacts to establish the most promising concepts for LIMB ash utilization. Based on a critical review of these processes, further laboratory studies were focused on the use of LIMB ash in synthetic aggregate production. Laboratory production and testing of the synthetic aggregates were carried out at SRI and at the laboratories of two subcontractors: Industrial Resource Development Company (IRD) of Devon, PA, and Aardelite Holding bV of Nunspeet, The Netherlands. These tests sought to optimize the synthetic aggregate product by testing a range of water additions, pelletizing methods, curing times, and curing methods. Water additions were varied from 10 to 43% by weight in the wet ash. The latter value corresponded to the moisture level required for maximum density. Pellets were produced by compression in a laboratory hydraulic press and by rotary pelletization in the proprietary Aardelite process. The hydraulically pressed pellets were cured in humid air (95% relative humidity), carbon dioxide, and steam environments for up to 30 d. The latter two atmospheres were tested as a result of literature reports of strength enhancements in cement and concrete cured under carbon dioxide and steam. The rotary pellets were cured in the proprietary Aardelite steam process for a period of 8 h.

The structural stability of the synthetic aggregate pellets was evaluated by compressive strength tests conducted in accordance with ASTM specifications. Preliminary tests of water absorption, asphalt absorption, and scratch hardness were also made. Funding limitations prevented a thorough characterization of the aggregates. However, SRI has proposed a follow-on evaluation through the Federal Highway Administration.

RESULTS AND DISCUSSION

Recycle

Work on LIMB ash recycle began with simple laboratory tests to demonstrate that the ash could be hydrated. Thermogravimetric analysis of hydrated samples showed that very high degrees of hydration were possible with 60 to 70% excess water and 30 to 60 min of reaction time. BET analysis of the same samples before and after hydration showed that the specific surface area was simultaneously increased by 35 to 57%. This suggested that the free lime was being converted to the high-surface-area hydrate, so the product should be reactive towards SO_2. These encouraging results prompted the first crude recycle test.

Large quantities (filling 55-gal or 200-L drums) of LIMB ash were first produced in the pilot-scale combustor with both Vicron limestone and Longview hydrated lime. The resulting LIMB ash was hydrated in a cement mixer using 60 to 70% excess water. After mixing for about 2 h, analysis of the ash revealed 97% hydration and a doubling of the specific surface area. The reactivity of the hydrated product was tested by reinjection into the combustor at a flue gas temperature of 2200 °F (1200 °C). The results of these tests showed that the performance of the recycled material was roughly equivalent to that of hydrated lime, when compared on the basis of equal amounts of $Ca(OH)_2$. Thus, it was confirmed that the LIMB ash could be reactivated by hydration and reinjected for additional SO_2 removal.

A similar recycle experiment was performed with LIMB ash generated from coarse limestone (Tenn-Luttrell with a mass-median diameter of 80 μm) and the same coal (the Pittsburgh No. 8 coal selected for the Edgewater LIMB demonstration). The larger sorbent particles were thought to be more difficult to hydrate and reactivate. Surprisingly, the results were again very good, although not as good as those obtained with commercial hydrated lime. This is illustrated in Figure 6-1. Apparently, the coarse limestone LIMB ash is slightly more difficult to reactivate than the LIMB ashes produced from fine limestone or hydrated lime. This may be due to incomplete hydration of the larger underlying lime particles.

With the successful demonstration of LIMB ash reactivation, attention was then focused on the separation of the fly ash from the sorbent. This was considered necessary to avoid excessive particulate loadings in the boiler and dust collectors. A variety of separation techniques were investigated, including:

(1) Use of the existing ESP as an ash-sorbent separator,

(2) Inertial separation of fly ash from fine lime sorbent or inertial separation of coarse limestone sorbent from fly ash,

(3) Magnetic separation of high-iron ash from sorbent,

(4) Froth flotation of either lime or fly ash components,

(5) Elutriation of fine lime sorbent from ash or elutriation of ash from coarse limestone sorbent,

(6) Use of steam to provide hydration simultaneously with elutriation (i.e., steam elutriation),

(7) Dense media separation using tetrabromoethane as a medium for a separation based on the density difference between lime (specific gravity, 3.3) and fly ash (specific gravity, 2.4), and

(8) Chemical extraction using sugar to dissolve lime.

Encouraging results were obtained by inertial separation in a Bahco laboratory size classifier. With a LIMB ash produced from hydrated lime, the lime sorbent was found to be highly enriched in the size fraction below 2 μm, as shown in Figure 6-2. However, it was not considered practical to obtain such a small cutpoint in a commercial separator. Thus, a larger cutpoint was tested by using a coarse limestone as the starting sorbent. Unfortunately, it was found that the coarse limestone severely decrepitated when injected into the furnace.

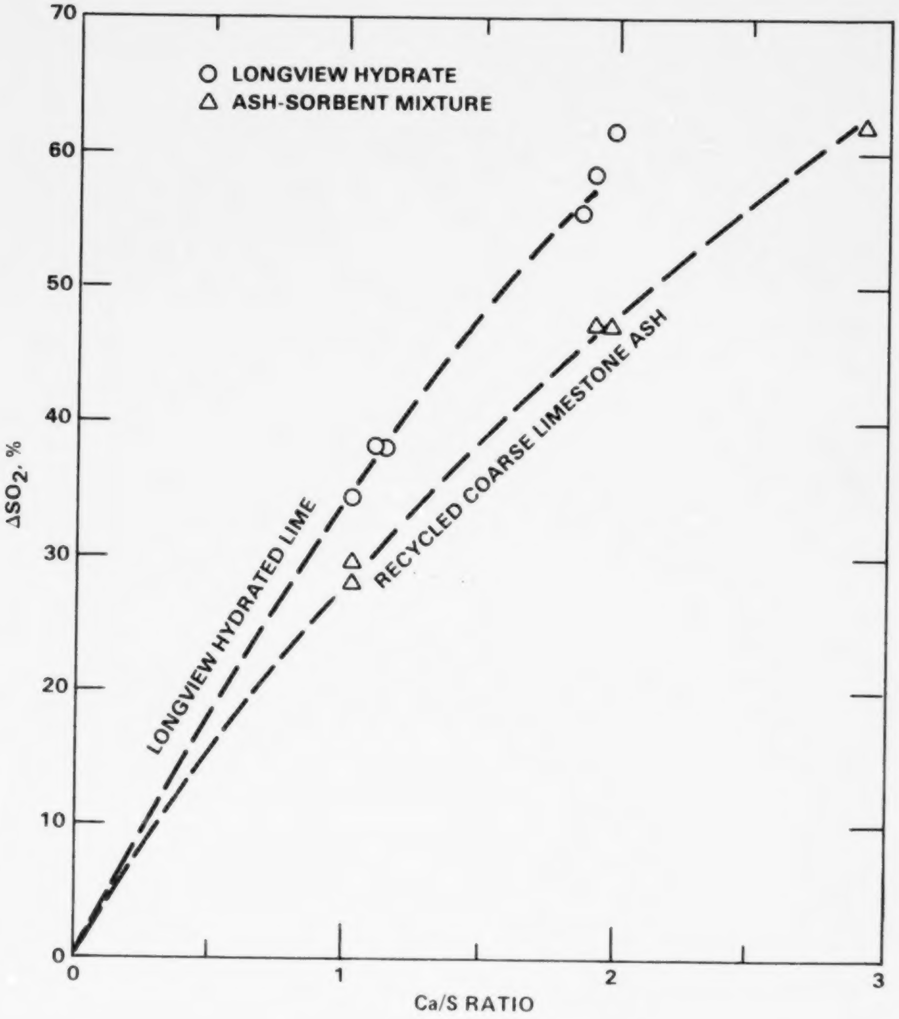

Figure 6-1. *SO_2 removal as a function of Ca/S ratio for Longview hydrate and rehydrated ash-sorbent mixture (from demonstration coal and Tenn-Luttrell coarse limestone).*

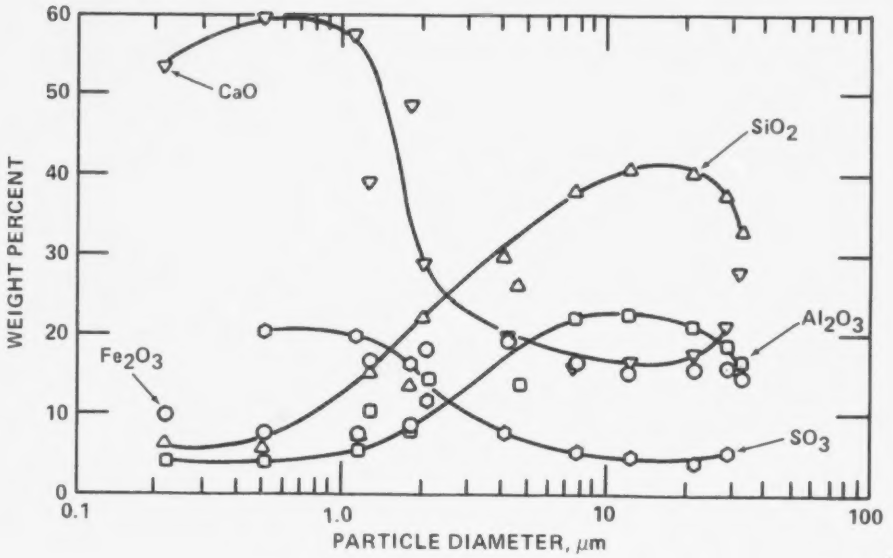

5055-89A

Figure 6-2. Size dependence of elemental concentrations in an ash-sorbent mixture produced by addition of Longview hydrated lime during combustion of Indiana coal.

This resulted in the sorbent being reduced to essentially the same size as the fly ash, making separation impossible. However, it is not known whether this would be a problem with all coarse limestones.

Some degree of ash-sorbent separation was achieved with several of the wet separation processes. For example, wet high-intensity magnetic separation produced substantial enrichment of the sorbent in the non-magnetic fraction. However, this was only true with ash produced from Hallmark coal, which is rich in magnetic iron. No effect was observed with ash from an Indiana coal. Thus, the applicability of this technique would be highly site specific. With the sugar extraction procedure, 60% of the sorbent could be recovered by dissolution and subsequent precipitation. However, this process was considered impractical due to the amount of sugar required. The dense media separation also yielded significant separation but only after settling times in excess of 4 h. The hazardous nature of the tetrabromoethane also made this process less desirable. All wet separation techniques were eventually abandoned due to problems with alkaline slurry by-products and associated water pollution problems.

Based on the results of the ash-sorbent separation studies, it appears that a dense-phase separation should be possible with LIMB ashes produced from hydrated lime. This could be accomplished in size classifying equipment similar to that used in commercial lime hydration systems. The use of the existing electrostatic precipitator (ESP) as a separator also appears to be feasible since finer particles generally tend to be collected in the back fields of the ESP. This concept will be evaluated when the LIMB demonstration comes on line and ESP hopper samples are available.

The most innovative concept for ash-sorbent separation is steam elutriation. In this process, steam is used to fluidize a bed of the LIMB ash. The steam flow, or velocity, is adjusted to elutriate only the fine hydrate particles that are formed by reaction of the steam with the unused lime. Laboratory tests of this concept were conducted by passing steam through a fritted reaction flask containing the LIMB ash. The steam was condensed and the volume of condensate was monitored to control the steam flow. The entire reaction system was placed in an oven to investigate the effect of varying reaction temperature. As shown in Figure 6-3, the degree of LIMB ash hydration increased as the temperature was reduced from 170 to 120 °C. This is reasonable since the sulfate shell on the sorbent must be penetrated by hydration, and the hydrated calcium sulfate is only stable below 130 °C. Thus, much higher degrees of hydration could probably be achieved at still lower temperatures. Unfortunately, no further experiments could be conducted due to funding limitations.

Figure 6-4 illustrates the effect of steam flow on the amount of ash elutriated. The highest degree of elutriation corresponds to the amount expected if only the hydrated lime is elutriated. By running at this steam flow rate and reducing the reaction temperature, it should be possible to optimize the process and produce good hydration with simultaneous carryover of the hydrated product.

The economics of LIMB ash recycle were investigated using modified versions of EPA's LIMB Cost and LIMB Recycle Models. Both models were modified to

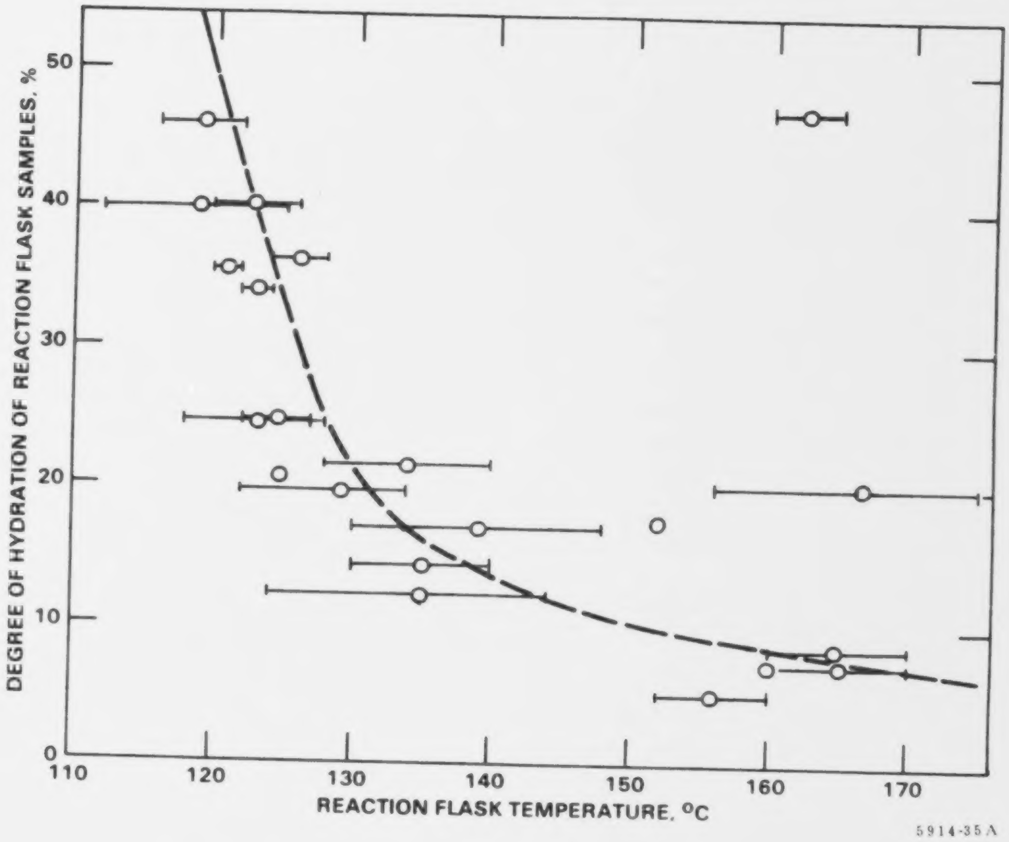

Figure 6-3. Effect of reaction flask temperature on degree of hydration.

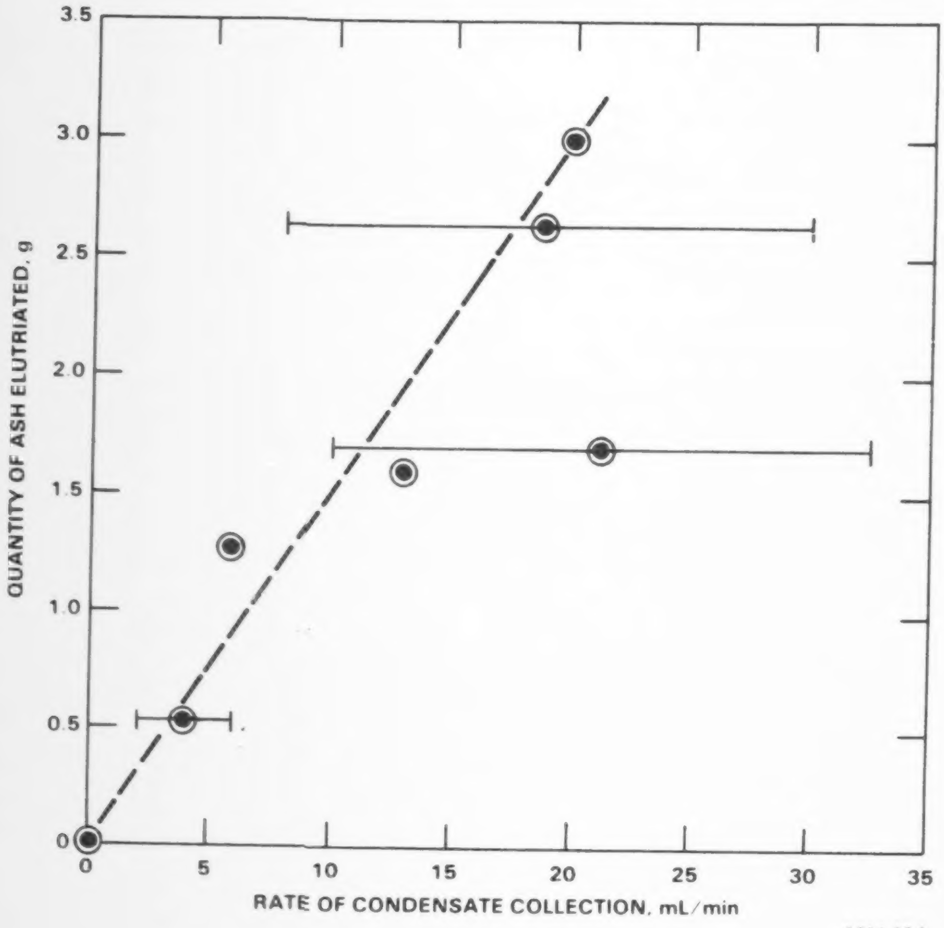

Figure 6-4. Effect of steam flow on ash elutriation.

allow direct comparisons of baseline and recycle sorbent injection cases. All required recycle equipment was included in the analysis and costed by vendor quotation. The material balance was modified to allow simulation of various degrees of ash-sorbent separation. The use of a coarse limestone sorbent with 60% recovery and recycle was found to offer a 21% savings in 15-year levelized cost, in comparison to a baseline case of hydrated lime injection. The bulk of the savings was attributable to the lower sorbent cost ($18 versus $71 per ton, or $16 versus $64 per metric ton, delivered). With on-site quicklime hydration and hydrated lime injection, recycle offered potential savings as large as 10% and 13%, respectively. However, the lowest absolute cost was projected for the quicklime-based recycle case ($682 per ton, or $620 per metric ton, of SO_2 removed).

Disposal

Landfill disposal tests were conducted with the simulated LIMB demonstration ash referred to previously (page 6-2). Chemical analysis of this ash revealed a composition of 29% free lime (CaO), 37% calcium sulfate ($CaSO_4$), and 34% fly ash. This corresponds to a molar calcium utilization of 34%, which is slightly higher than that typically obtained with hydrated lime injection. Analysis of EP leachates revealed that all eight priority metals were well below RCRA limits, as shown in Table 6-1. The main concern was the high leachate pH, which was near 12 but still below the RCRA limit of 12.5.

Potential seepage of leachates through the LIMB ash was investigated using the moist cured ash cylinders described earlier. Permeability coefficients measured by the falling head test method decreased from 3×10^{-4} cm/s after 1 d to 4×10^{-6} cm/s after 30 d. These results were obtained with wetted ash containing 28.5% moisture by weight. This moisture content was somewhat lower than the optimum determined later at the landfill test cell (about 32.4%, or a water-to-free lime molar ratio of about 5:1). In the landfill test cell, the permeability of extracted core samples was as low as 2×10^{-6} cm/s after 30 d. Thus, it appears likely that the ultimate permeability would approach that of a clay liner (ca 1×10^{-7} cm/s).

Optimum conditioning procedures for the LIMB ash were investigated by laboratory and pilot-scale conditioning tests using a 4.5-qt (4.25-L) Kitchen-Aid mixer and a 1-ft^3 (28-L) Ross ribbon blender. These tests served as a basis for assessing product consistency and heat release. The water-to-lime ratio was varied from 0.5 to 12.4, corresponding to wet mixtures containing 4.6% to 54.5% moisture. The latter condition was attained in the ASTM slaking test (ASTM C-110). The results are summarized in Table 6-2. As shown, the adiabatic temperature rise went through a maximum at a water-to-lime ratio of 1:1. Sub-stoichiometric water addition did not provide maximum reaction, while super-stoichiometric addition resulted in heat loss due to evaporation of the excess water. Based on product consistency, a ratio of 5:1 was considered to be near optimum.

In order to demonstrate the environmental acceptability of LIMB ash, the handling and disposal of a large quantity (84 tons or 76 metric tons) was demonstrated using the ash handling system at the Edgewater Plant. The ash was obtained from a full-scale demonstration of hydrated lime injection at the Lakeview Plant of Ontario Hydro. Analysis of the ash revealed an average free

TABLE 6-1. LEACHATE DATA FOR AN ASH-SORBENT MIXTURE FROM THE PILOT-SCALE COMBUSTOR

Parameter	Concentration in extract, mg/L RCRA limit[a]	 Ash-sorbent mixture
Arsenic	5	0.0145
Barium	100	4.11
Cadmium	1	0.00095
Chromium	5	0.0394
Lead	5	<0.0030
Mercury	0.2	<0.0003
Selenium	1	0.0296
Silver	5	<0.0005
pH	12.5	(12.4/12.2)[b]

a. Resource Conservation and Recovery Act, 41 CFR 35050, August 1976, enacted by Congress on October 21, 1976.

b. Before/after addition of 4 mL of 0.5 N acetic acid per 1 g of sample.

TABLE 6-2. WETTING TESTS WITH EDGEWATER DEMONSTRATION MODIFIED ASH[a]

Water-to-free lime ratio, H_2O/CaO, mole/mole	Amount of water added		Maximum adiabatic temperature, °F (°C)	Final product condition	
	As percent of dry ash, %	As percent of wet ash, %		From ribbon blender[b]	From KitchenAid mixer[c]
0.5	4.8	4.6	221 (105)	Dry powder	--
1	9.6	8.8	248 (120)	Dry powder	--
1.5	14.4	12.6	--	--	--
3	28.8	22.4	214 (101)	Dry with BB-sized clumps	--
4	38.4	27.7	--	--	Soil-like with BBs
5	48.0	32.4	199 (92.8)	Damp soil-like with BB- to marble-size clumps	
6	57.7	36.6	--	--	BB- to marble-size clumps
7	67.3	40.2	--	--	
8	76.9	43.5	151 (66.1)	Partly mud-like with later dry clumping	
9	86.5	46.4	--	--	Mortar-like
(12.4)[d]	119.6	54.5	143 (61.7)	Thick paste	--

a. All modified ash samples were produced from hydrated lime and Pittsburgh No. 8 coal fired in pilot combustor; free lime (CaO) content = 29% by weight.

b. Ribbon blender is a 1-ft^3 (28.3-L) Ross ribbon blender unit; all ribbon blender tests used 10 lb (4.5 kg) of modified ash with a mixing time of 4.5 min.

c. KitchenAid mixer tests used 200 to 800 g of modified ash with a mixing time of 4 min.

d. ASTM Slaking Test ASTM C-110.

lime content of 24%. Water addition rates were calculated based on an earlier determination of 17% free lime, so the water-to-lime ratios were lower than intended. Instead of the target range of 3.5:1 to 5:1, the actual range was 2.5:1 to 3.9:1. Using these various ratios, separate batches of the wetted ash were prepared in the Edgewater Unit 4 dustless unloader system. Each batch was placed in a separate pile in the landfill test cell, which was surrounded by a lined perimeter trench draining into a lined sump. After each rainfall, samples were taken from the trench and sump and analyzed for pH, alkalinity, solids, RCRA metals, and drinking water parameters. The results of the pH, alkalinity, solids, and metals determinations are summarized in Table 6-3. The results of the drinking water analyses are summarized in Table 6-4.

The runoff pH was initially high but was reduced to within NPDES limits (6 to 9) after several days. This was apparently the result of stabilization of the wetted ash and possibly neutralization by reaction with atmospheric carbon dioxide. The pH of the runoff collected in the sump liquid remained within narrow limits close to neutrality (6.8 to 7.7). Suspended solids in the sump liquid varied from 5 to 26 ppm, remaining below the NPDES discharge limit of 30 ppm (monthly average). The much higher levels of suspended solids in the trench are indicative of the settling that takes place in the sump. Apparently, this retention is adequate for removal of suspended solids.

As expected, all runoff analyses showed very low levels of RCRA metals due to the presence of the alkalinity. In this respect, LIMB ash appears to be environmentally superior to ordinary fly ash. With respect to all other drinking water parameters, only sulfate appears to represent a potential problem. However, the reported concentrations would be much lower in any leachates that might reach the groundwater. Dispersion modeling would be required to accurately assess the actual environmental impact in this case.

Utilization

Synthetic aggregates were produced from LIMB ash under the various conditions described on page 6-3. For the hydraulically pressed pellets, the highest compressive strengths were obtained with the CO_2 curing. Strengths in excess of 5000 psi (34 MPa) were developed in only 2 d. However, the economic feasibility of this type of curing remains to be evaluated. Steam curing did not enhance the compressive strength of these pellets. With curing in a humid air environment (95% relative humidity), strengths over 4200 psi (29 MPa) were achieved after 30 d. The maximum strengths were obtained with a mixture of 80% LIMB ash and 20% water. A mixture of 57% LIMB ash and 43% water, which yielded maximum density, was far from optimum structurally; the compressive strength was 1900 to 2500 psi (13 to 17 MPa). Thus, optimum density does not necessarily mean optimum strength.

The highest compressive strengths were obtained with the rotary pelletizing and steam curing process developed by Aardelite. As shown in Table 6-5, strengths of over 10,000 psi (69 MPa) were attained with an 80/20 mixture after only an 8-h steam curing. An economic analysis would be required to assess the relative merits of this process and the humid air curing. Both types of pellets were leached by the EP Toxicity procedure and the leachates were analyzed

TABLE 6-3. ANALYSIS OF RUNOFF FROM LANDFILL TEST SITE

Sample description		Sample analysis										
					Concentration, mg/L							
Time[a]	Location	pH	TSS[b]	Hardness[c]	As	Ba	Cd	Cr	Pb	Hg	Se	Ag
4	Trench	12.2	230									
	Sump	6.8	5.5		0.007	1.4	<0.0005	<0.005	<0.003	<0.001	<0.005	<0.0001
5	Trench	11.6	251	210	<0.002	7.1	<0.0005	0.014	<0.003	<0.001	<0.005	<0.0001
	Sump	7.1	17		<0.002	6.1	<0.0005	<0.005	<0.003	<0.001	<0.005	<0.0001
6	Trench	11.4	300	80	0.004	7.4	<0.0005	0.027	<0.003	<0.001	<0.005	<0.0001
	Sump	7.2	22	74	0.006	1.8	<0.0005	<0.005	<0.003	<0.001	<0.005	<0.0001
7	Trench	11.5	885	193								
	Sump	7.2	6.9	89	0.005	2.2	<0.0005	<0.005	<0.003	<0.001	<0.005	<0.0001
9	Trench	7.0	82									
	Sump	7.2	8.4									
10	Trench	6.9	1620									
13	Sump	7.5	26		<0.002	2.6	<0.0005	<0.005	<0.003	<0.001	<0.005	<0.0001
26	Trench	7.6	156	66	0.009	14	0.0015	0.072	0.008	<0.001	<0.005	0.0007
	Sump	7.7	8.5	92	0.003	2.1	<0.0005	<0.005	<0.003	<0.001	<0.005	<0.0001

a. Days elapsed after placement of ash-sorbent mixture in test site.
b. Total suspended solids.
c. As $CaCO_3$.

TABLE 6-4. ANALYSIS OF LIQUID AND EXTRACTS OF SOLIDS AT LANDFILL TEST SITE

	Concentration,[a] mg/L									
									Drinking water limits	
Parameter	Sump liquid	Pile 1 extract	Pile 2 extract	Pile 3 extract	Pile 4 extract	Pile 5 extract	LIMB ash extract	RCRA limit[b]	Primary[b]	Standard[b]
Arsenic	<0.005	<0.005	<0.005	<0.005	<0.005	<0.005	<0.005	5	0.5	-
Barium	1.50	2.80	3.40	4.40	1.10	2.90	14.0	100	1.0	-
Cadmium	<0.005	<0.005	<0.005	<0.005	<0.005	<0.005	<0.005	1	0.01	-
Chromium	<0.005	0.005	0.07	0.007	0.006	0.005	0.064	5	0.05	-
Lead	<0.005	<0.005	<0.005	<0.005	<0.005	<0.005	<0.005	5	0.05	-
Mercury	<0.001	<0.001	<0.001	<0.001	<0.001	<0.001	<0.001	0.2	0.002	-
Selenium	<0.001	0.001	0.002	0.003	0.005	0.003	0.005	1	0.01	-
Silver	<0.005	<0.005	<0.005	<0.005	<0.005	<0.005	<0.005	5	0.05	-
Alkalinity	173	31.3	29.4	14.9	52.7	10.8	1770	-	-	
Boron	<0.50	0.65	1.2	1.0	0.65	0.75	2.3	-	-	
Chloride	29	1.7	1.1	0.51	1.9	0.23	38	-	-	250
Color[c]	7	2	2	2	2	2	3	-	-	15 CU
Conductivity[c]	1175	785	1125	1335	538	975	8180	-	-	-
Copper	<0.05	<0.05	<0.05	<0.05	<0.05	<0.05	<0.05	-	-	1.0
Corrosivity[c]	1.2	2.0	2.2	1.4	2.6	0.6	6.0	-	-	-
Cyanide	<0.01	<0.01	<0.01	<0.01	<0.01	<0.01	0.04			
Fluoride	0.46	0.38	0.44	0.52	0.51	0.36	0.93	-	4.0	2.0
Foaming agents	<0.10	0.20	<0.10	0.20	0.29	<0.10	0.20	-	-	0.5
Hardness(as $CaCO_3$)	555	344	608	791	225	516	3050	-	-	-
Iron	<0.05	<0.05	<0.05	<0.05	<0.05	<0.05	<0.05	-	-	0.3
Manganese	<0.05	<0.05	<0.05	<0.05	<0.05	<0.05	<0.05	-	-	0.05
Nitrate	2.2	0.28	0.37	0.31	0.43	0.32	2.5	-	10	-
Odor[c]	1	1	1	10	1	10	7	-	-	3 T.O.N.
pH[c]	8.4	10.0	10.0	9.2	10.5	8.8	12.1	12.5	-	6.5 - 8.5
Sodium	58	7.2	5.3	2.6	5.3	1.3	3.3	-		-
Sulfate	441	343	620	796	199	511	1300	-	-	250
Sulfide	<0.5	<0.5	<0.5	<0.5	<0.5	<0.5	0.8	-	-	
Dissolved solids	785	516	923	1150	328	760	3580	-	-	500
Turbidity								-	1 TU	-
Zinc	<0.5	<0.5	<0.5	<0.5	<0.5	<0.5	<0.5	-	-	5.0

a. Except as noted.

b. Specification for standard.

c. Color (CU), conductivity (μmhos/cm), corrosivity (SI), odor (T.O.N.), pH (unitless).

TABLE 6-5. RESULTS OF AARDELITE'S TESTS ON LIMB FLY ASH PELLETS

Mixture	Pellet[a] No.	Pellet strength, psi (MPa)	Density, lb/ft^3 (g/cm^3)
80% LIMB ash[b] 20% Water	1	10,780 (74.3)	90.00 (1.44)
40% LIMB ash[b] 40% Holland fly ash 20% Water	9	4,775 (32.9)	88.13 (1.41)
40% LIMB ash[b,c] 40% Holland fly ash[c] 20% Water	34	6,468 (44.6)	86.25 (1.38)
24% LIMB ash[b] 32% Holland fly ash 24% Fine sand 20% Water	40	3,235 (22.3)	96.25 (1.54)

a. Forming pressure was 2,310 psi (15.9 MPa).

b. LIMB ash from the Malmo plant in Sweden.

c. Preheated to 154 °F (68 °C).

for pH and RCRA metals. The results, which are summarized in Table 6-6, indicate no potential environmental problems with these materials.

CONCLUSIONS AND RECOMMENDATIONS

The unused sorbent in LIMB ash can be reactivated by hydration and reinjected to obtain additional SO_2 removal and sorbent utilization. However, separation of the fly ash from the LIMB ash is required in order to avoid excessive particulate loadings. Future work with LIMB ash recycle should concentrate on this separation step. The most promising concepts appear to be:

(1) Use of the existing ESP as a separator,

(2) Dense-phase classification,

(3) Steam (or possibly air) elutriation, and

(4) Use of a cyclonic precollector with a coarse limestone sorbent (if the limestone does not decrepitate).

Wet separation techniques are not recommended due to the potential water pollution problems.

Both the laboratory tests and the large-scale disposal study showed that LIMB ash can be safely handled and landfilled. Cementitious reactions within the wetted ash produce a nearly impermeable product. With proper handling and conditioning, this should result in minimal potential for groundwater contamination. Analyses of both EP leachates and the test cell runoff showed that RCRA metals are of no concern at the prevailing levels. LIMB ash should not be classified as a hazardous waste under any of the RCRA criteria.

The high initial pH of the test cell runoff may indicate the need for neutralization during certain periods of operation. This could be accomplished by addition of acid to the sump or carbonation of the sump water using carbon dioxide. A sump should be provided in all cases to allow for settling of suspended solids in the landfill runoff.

A wetted LIMB ash with good disposal characteristics can be produced using existing dustless ash unloaders like the pug mill at the Edgewater Plant. A water-to-lime ratio of 5:1 appears to yield a near optimum product. With adequate compaction and stabilization, the permeability of the landfilled material should be quite low.

Synthetic aggregates represent one of the most promising uses for LIMB ash. Production of the aggregate appears to be technically feasible using existing equipment. It appears likely that the aggregates will conform to highway department specifications for use of the aggregate in wearing and base courses. Further development of the synthetic aggregate technology is warranted. Pilot-scale tests should be conducted to demonstrate the large-scale production and use of this material in a highway test section.

TABLE 6-6. EP TOXICITY DATA FOR EXTRACTS FROM LIMB ASH PELLETS

Metal	Allowable extract level, mg/L[a]	Measured extract level, mg/L					
		IRD fine aggregate 57/43 mix[b]	IRD coarse aggregate 57/43 mix[b]	IRD asphalt plug	Aardelite pellet 80/20 mix[b]	SRI pellet 80/20 mix[b] atmospheric steam cure	SRI pellet 80/20 mix[b] room temp humidified atmosphere
Arsenic	5	0.0633	0.0454	0.0322	0.0386	0.0194	0.0088
Barium	100	1.3	1.2	1.1	1.2	<0.5	1.1
Cadmium	1	<0.0002	<0.0002	<0.0002	0.0003	0.0006	0.0006
Chromium	5	0.0053	0.0041	0.0073	0.0068	0.0234	0.0090
Lead	5	<0.0003	<0.0003	<0.0003	0.0051	0.0320	0.0111
Mercury	0.2	<0.0005	<0.0005	<0.0005	<0.0005	0.0058	0.0108
Selenium	1	<0.015	<0.015	<0.015	<0.015	0.0156	0.0344
Silver	5	<0.0005	<0.0005	<0.0005	<0.0005	0.0048	0.0022

a. Allowable levels according to RCRA.

b. LIMB ash from Pittsburgh No. 8 coal and hydrated lime.

SECTION 7

TASK 5. CHARACTERIZATION OF SORBENTS THROUGH PILOT-SCALE COMBUSTOR STUDIES

INTRODUCTION

Several of the studies conducted at SRI's pilot-scale combustor (Coal Combustion Facility) were performed in direct support of the Edgewater demonstration of LIMB, now being performed at Ohio Edison's power station in Lorain, OH. An initial task was to perform screening tests on sorbents of the $Ca(OH)_2$ type that were representative of products then under consideration for use at Edgewater. Other tasks concerned ways to increase sorbent utilization, by use of an additive or by activation of the sorbent through flue-gas humidification. A final task was to evaluate water vapor and SO_3 as agents for adjusting the electrical resistivity of the ash-sorbent mixture produced from the specific coal and the specific sorbent being used at Edgewater.

Certain other pilot-scale combustor studies were of more general application. Fundamental aspects of post-furnace humidification, for example, were investigated, as well as aspects of humidification that were relevant to Edgewater. Electrostatic augmentation of sorbent activation with a water spray (a process dubbed CASH) was initially studied during this project, although more definitively studied under a later cooperative agreement between SRI and EPA (CR 812811). Finally, the activation of hydrated lime prior to furnace injection by addition of lignosulfonate was an extension of a broader investigation under Contract No. 68-02-4201 of related surfactants and dispersants (5).

OBJECTIVES AND SCOPE

The above discussion indicates that the pilot-scale combustor studies were related to specific applications at the Edgewater demonstration and to more general applications. Broadly defined, the several objectives were as follows:

- To screen a series of commercial hydrates of lime for possible application during furnace injection at Edgewater, for both guidance on a reagent choice and identification of the hydrate properties that control the effectiveness of SO_2 removal.

- To compare different lignosulfonate formulations for activating hydrated lime.

- To investigate post-furnace humidification of flue gas to achieve increased reaction of the sorbent, $Ca(OH)_2$, with SO_2. Sorbent injection and humidification may be accomplished in different ways.

  - Sorbent can be injected in the furnace and then, following calcination and partial sulfation, activated with water spray or water vapor.

  - Sorbent may be injected into a low-temperature duct and then subjected to the effects of humidification.

  - Finally, sorbent may be injected as a dry solid and then wetted by electrostatically induced collision of sorbent particles and water droplets (CASH, or "charge-augmented sorbent humidification")

- To evaluate water vapor and SO_3 as agents for lowering the electrical resistivity of ash-sorbent mixtures and improving particle collection by electrostatic precipitation.

The overall scope of the pilot-scale studies is indicated by the above discussion. The experimental results are presented below under headings that correspond to the outline of that discussion.

RESULTS AND DISCUSSION

Screening of Hydrated Limes for Reactivity with SO_2

Eleven sorbents of the hydrated lime type were obtained for the screening experiments. All were commercially produced, high-calcium products. Two were of particular interest: Sorbent A (Longview), because of its frequent use in the pilot-scale combustor experiments described elsewhere in this report, and Sorbent H (Marblehead), which was later selected as the sorbent to be used in the Edgewater demonstration.

The sorbents were analyzed for chemical composition, BET surface area, and particle-size distribution. The values of selected properties of the sorbents are listed in Table 7-1. Calcium expressed as CaO ranged from 71.1 to 73.1% in the ignited samples; magnesium as MgO ranged from 0.40 to 2.29%. The BET areas ranged from 12 to 20 m^2/g in the samples as originally received. Mass-median diameters ranged from 2.0 to 5.0 μm; more complete information on particle size distributions is given pictorially in Figure 7-1 except for Sorbents J and K (not shown) whose distributions were bounded by the curves for Sorbents D and F. The extremes in mass-median diameter and in weight percentage smaller than 1 μm are represented by Sorbents D and E, which were produced from the same limestone and were produced in identical hydrators; the difference appeared to be due to the production of Sorbent D from limestone calcined in a rotary kiln and the production of Sorbent E from limestone calcined in a vertical kiln.

Tests of sorbent reactivity with SO_2 were conducted in the pilot-scale combustor with the water-wall, high quench-rate configuration. The fuel was Pittsburgh No. 8 coal from the Boich mine, which supplies the Edgewater demonstration; the coal contained 3.1% sulfur and produced about 2200 ppm of SO_2 under the firing conditions employed (1×10^6 Btu/h or 300 kW). Each sorbent was injected in the furnace at a temperature of about 2200 °F (1200 °C) to produce a Ca/S mole ratio of 2. Sorbent reactivity was rated on the basis of utilization — the mole percent of $Ca(OH)_2$ converted to $CaSO_4$. The extent of utilization was computed from the initial Ca/S mole ratio and the quantity of SO_2 removed from the gas stream; it was not confirmed by solids analysis, which is a more reliable method for determining utilization.

TABLE 7-1. PROPERTIES OF COMMERCIAL CALCITIC HYDRATES

	Composition[a]			BET area[a]	Size distribution[b]		
Type	% CaO	% MgO	% LOI	(m^2/g)	MMD (μm)	% <1 μm	% <10 μm
A	72.5	1.74	24.4	19.0	4.0	15	69
B	71.4	0.79	25.1	15.2	3.8	5	83
C	71.1	2.29	23.6	12.4	3.0	3	93
D	72.6	0.40	24.9	18.9	2.0	21	81
E	73.1	0.44	24.8	13.7	5.0	3	87
F	72.2	0.65	24.0	16.3	2.8	6	90
G	72.8	0.44	24.6	16.8	4.2	6	85
H	71.4	0.83	24.9	14.4	3.5	4	86
I	72.1	1.53	23.6	19.6	2.6	6	90
J	72.0	1.58	24.4	14.3	2.2	17	85
K	71.2	0.90	24.7	15.0	2.6	10	87

[a] Metals determined on ignited sample and reported as equivalent wt % oxide in as-received sample. BET on as-received sample. LOI = loss on ignition at 750 °C.

[b] Single determination by sedimentation at Micromeritics Instrument Corporation.

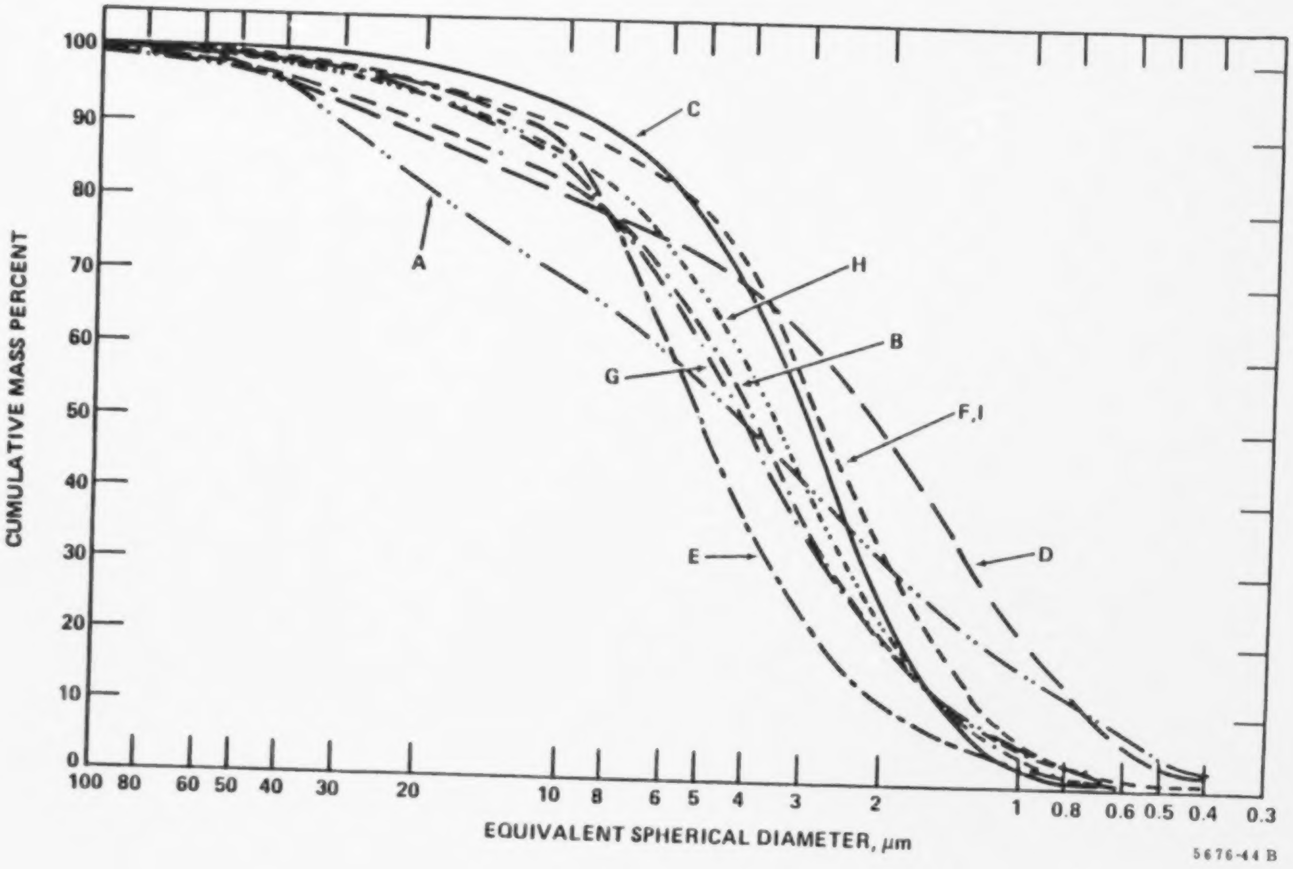

Figure 7-1. Particle-size distributions (by sedimentation) of commerical calcitic hydrates.

Calcium utilization at a Ca/S ratio of 2 ranged from a low of 25% to a high of about 30% in preliminary tests screening all eleven sorbents. Selected sorbents were then compared with a control material, in a sequence with the test materials and the control material (Sorbent I) alternated, to determine relative performance and eliminate time-dependent effects such as drift in temperature at the injection site. Four sorbents were tested using this procedure. The following rankings were obtained by taking the ratio of the calcium utilization of the indicated sorbent to the utilization observed with Sorbent I:

Sorbent	Relative utilization
F	1.18
B	1.09
C	1.04
I	1.00

Other less quantitatively certain results from the larger group of screening tests were that Sorbents J and K were of the order of Sorbent F, and that Sorbents D and E were average in performance and not distinguished from one another (notwithstanding the large difference in particle-size distributions).

The significance of the above results is that there was no obvious correlation of the properties of the raw sorbent with sulfur removal. The particle-size distributions of Sorbents F and I, for example, were indistinguishable, although Sorbent I had the higher initial surface area. The contrast in particle-size distribution and surface area between Sorbents D and E is remarkable; yet the limited tests with these sorbents did not show a definite difference in performance.

An attempt was made with impactors to measure the particle-size distributions of the calcines resulting from injection of Sorbents C and F in the combustor; this was done with gas firing of the combustor to eliminate interference from suspended fly ash. (These two sorbents had similar sedimentation-based size distributions but dissimilar utilizations.) The size distribution found with impactors was very similar to that of each raw sorbent. Unfortunately, the recovery of calcine was low; moreover, the necessity of operating impactors at relatively low gas temperature makes it uncertain whether agglomeration altered particle-size distributions between the furnace and the impactor sampling location. In short, there remains the possibility that the injection system could have produced differences in particle-size distribution that were a factor in controlling the extent of sorbent reaction with SO_2.

The greatest difference in utilization between any two sorbents was less than 20% on a relative basis. The significance of these results to a commercial boiler injection process may be summarized as follows:

- Although smaller particle size and higher surface area are the "correct" direction for increasing utilization, there is no clear correlation of utilization with these parameters even though substantial differences in these properties existed among the commercial hydrates tested.

- In view of the variety of hydrated lime sources tested, the range in utilization observed was relatively narrow. However, the potential economic significance of the variation indicates a need for source-specific evaluation of sulfation performance until a reliable predictor of calcium utilization is available.

Much later work revealed a superiority of Sorbent H (Marblehead) over Sorbent A (Longview) on the basis of the finer particle-size distribution of Sorbent H (5). The later tests, at a Ca/S ratio of 2 and an injection temperature of 2250 °F (1230 °C), gave a utilization of Sorbent H of about 32% and a utilization of Sorbent A of about 25%. These later results are not inconsistent with those given for these two specific sorbents in this section; the later data were more extensive and permitted a more exacting comparison of the two materials. Sorbents A and H were not compared directly in the series discussed in this Section, but Sorbent H did rank as one of the best sorbents in the series.

Comparison of Lignosulfonate Formulations as Additives in Hydrated Lime

Extensive experiments for EPA on the use of lignosulfonate as an additive in $Ca(OH)_2$ have been reported by SRI under Contract No. 68-02-4201 (5). Most of these experiments were conducted with the powder form of the product Lignosite from Georgia Pacific Corporation. Lignosite is a water-soluble byproduct of paper manufacturing in which the primary ingredient is calcium lignosulfate. Lignosite powder was dissolved in the water used for converting CaO to $Ca(OH)_2$; its beneficial effect on $Ca(OH)_2$ to be used by furnace injection to control SO_2 emissions is apparently due to the action of lignosulfonate as a dispersing agent, allowing the $Ca(OH)_2$ to be injected in the furnace with a finer particle-size distribution than would otherwise occur.

A limited investigation of lignosulfonate as a liquid additive to be used in $Ca(OH)_2$ was conducted as part of this project. The product was purchased as an aqueous solution consisting of 50%-by-weight dissolved solids. It was incorporated in either of two hydrated limes: Longview or Marblehead. Lime purchased from the Longview Lime Division of Dravo Lime Company, Saginaw, AL, was hydrated at SRI in a Ross ribbon blender with liquid Lignosite present. Alternatively, lime from another source was hydrated with the additive present in facilities operated by the Marblehead Lime Company, Detroit, MI. The additive level was 1% by weight in the Longview $Ca(OH)_2$ or 1.5% by weight in the Marblehead $Ca(OH)_2$.

Tests of sorbent reactivity with SO_2 were conducted at the SRI pilot-scale combustor with the Boich coal as the fuel at a firing rate of 1×10^6 Btu/h (300 kW). The furnace was operated with refractory-lined walls, at a low quench rate. The $Ca(OH)_2$ containing the Lignosite additive was injected into the furnace at several selected locations, as described below, to achieve a Ca/S mole ratio of 1 or 2. Utilization of the sorbent was calculated in either of two ways: 1) by comparing the gas-phase reduction in the SO_2 concentration with the Ca/S ratio or 2) by collecting the solid reaction product and determining the SO_4^{-2}-to-Ca^{+2} ratio therein.

Longview hydrate with and without Lignosite was tested for effectiveness of SO_2 removal with furnace injections at three temperatures and at nominal Ca/S ratios of 1 and 2. The data tabulated below summarize the results obtained for Ca/S = 2:

	% Utilization, Ca/S = 2		
Temp, °F (°C)	Without additive	With additive	Ratio
2140 (1170)	17.5	21.8	1.24
2190 (1200)	28.6	33.2	1.16
2330 (1280)	26.2	28.6	1.09

Utilizations at Ca/S = 2 are also shown graphically in Figure 7-2 as a function of temperature. Included in the figure are corresponding data from other work (under Contract No. 68-02-4201) for experiments in which the additive was used in the powder form rather than as the liquid (5). The results for both forms of the additive are obviously similar.

The first series of experiments with the Marblehead hydrates was conducted with the additive-free material injected over a wide range of temperatures to compare utilizations based on gas and solids sampling. The results are presented in Figure 7-3; the data from both sampling modes show a typical temperature dependence, with optimum utilization occurring at intermediate temperatures of 2200 to 2300 °F (1200 to 1260 °C). The utilizations based on gas or solids analysis are in good agreement for three of the five temperatures where both were available. In the cases where the agreement was not as good, the solids analysis indicated higher utilization. The higher solids utilization for these two temperatures was consistent among the two or three sample pairs yielding the average utilizations shown in the figure; the reason for the discrepancy is not known.

The effect of Lignosite on the utilization of Marblehead hydrates was then investigated with the additive-free and additive-containing materials injected at two temperatures and at two Ca/S ratios (1 and 2). The comparison of utilizations of the two materials at Ca/S = 2 is given below:

	Utilization, Ca/S = 2		
Temp, °F (°C)	Without additive	With additive	Ratio
2010 (1100)			
gas sampling	19.8	21.5	1.09
solids sampling	18.4	24.5	1.35
2320 (1270)			
gas sampling	31.0	33.1	1.07
solids sampling	33.3	(36)	(1.08)

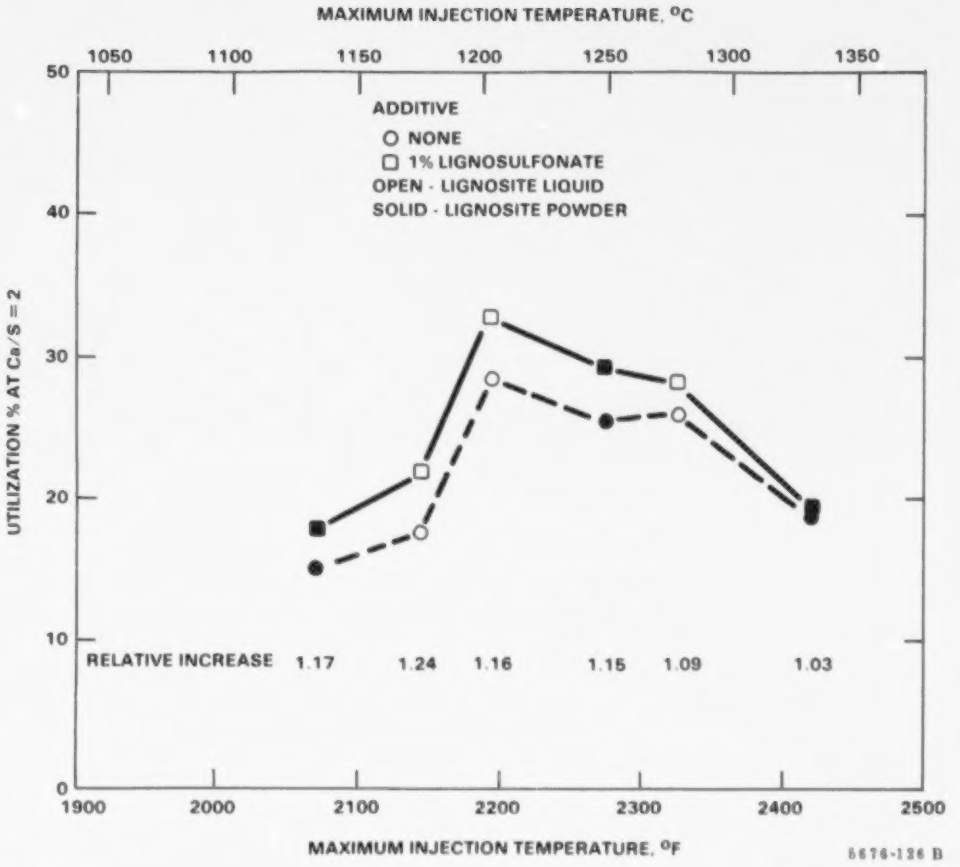

Figure 7-2. Enhancement of the utilization of Longview hydrate with Lignosite powder or liquid (Ca/S = 2).

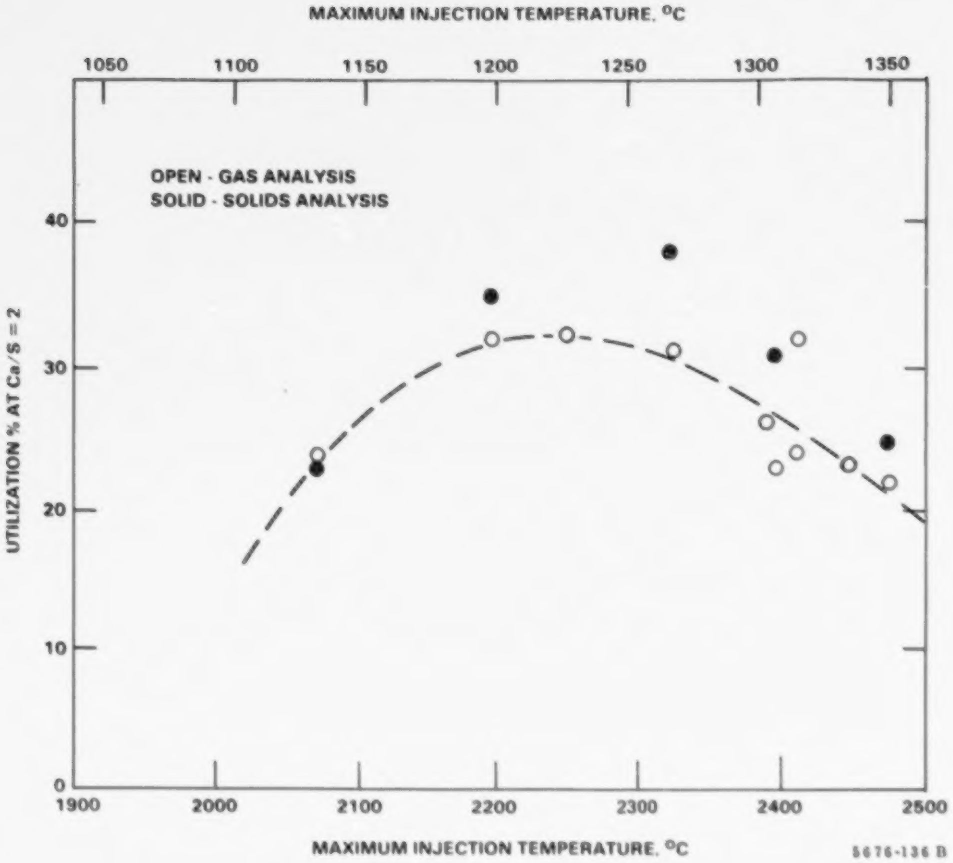

Figure 7-3. Utilization of additive-free Marblehead hydrate versus temperature as revealed by gas and solids analysis.

Two or more samples were analyzed for each experimental condition. The values above in parentheses are based on a single determination that was judged to be more reliable than the average; otherwise, the values listed are for averages. In general, the solids analyses indicate somewhat higher utilizations but generally support the gas analyses.

Utilizations of Marblehead hydrates at Ca/S = 2 with and without the liquid additive, based on gas analyses, are plotted in Figure 7-4 and compared with earlier data obtained with the powder (from Contract 68-02-4201). Again, the additive in liquid and powder forms produced similar enhancements in utilization.

In summary, the liquid formulation of Lignosite appears to be equivalent to the powder form in its effectiveness as an additive to hydrated lime. As with the powder, the relative benefit with liquid Lignosite addition to the hydration step is greater with Longview than with Marblehead lime. The utilization of both sorbents as a function of temperature confirmed previous results. Most results were based on gas-phase SO_2 removal, but solids samples supported the utilizations of both baseline and additive hydrates.

Investigation of Post-Furnace Humidification to Achieve Sorbent Activation

Post-furnace humidification is receiving a great deal of attention currently as a means of enhancing the reaction of dry calcium-based sorbents with SO_2 at relatively low gas temperatures in ducts approaching the stack. In some instances, this technique is intended to increase the utilization of sorbents that are injected into the furnace to undergo primary reaction at high temperatures; for example, Consol R & D has described a process called "BLI Activation," in which limestone is injected in the boiler and the resulting calcine is activated by humidification in a low-temperature duct to undergo further reaction with SO_2 (6). In other instances, the sorbent is only injected in the low-temperature duct; it undergoes all of its reaction in this zone and is highly dependent upon humidification to achieve significant reaction. One example of the low-temperature process has been referred to by Consol R & D as "Straight Coolside;" it is based on $Ca(OH)_2$ as the sorbent and humidification with a spray of liquid water, which evaporates to further lower the reaction temperature (6). Low-temperature or duct-injection processes are under active development by the Department of Energy as means for reducing the problem of acid rain.

One of the crucial issues associated with post-furnace humidification is whether activation can be achieved with water vapor alone or can only be accomplished by physical contact between sorbent particles and liquid water droplets prior to their evaporation. Another issue is how the effect of liquid droplets can be optimized by controlling droplet size, residence time, and other parameters. In ultimate efficiency, the interaction of sorbent particles and water droplets may approach that in a spray dryer. Comparison of vapor humidification and spray humidification with spray drying, therefore, is an appropriate way to gauge the effectiveness of the two humidification processes.

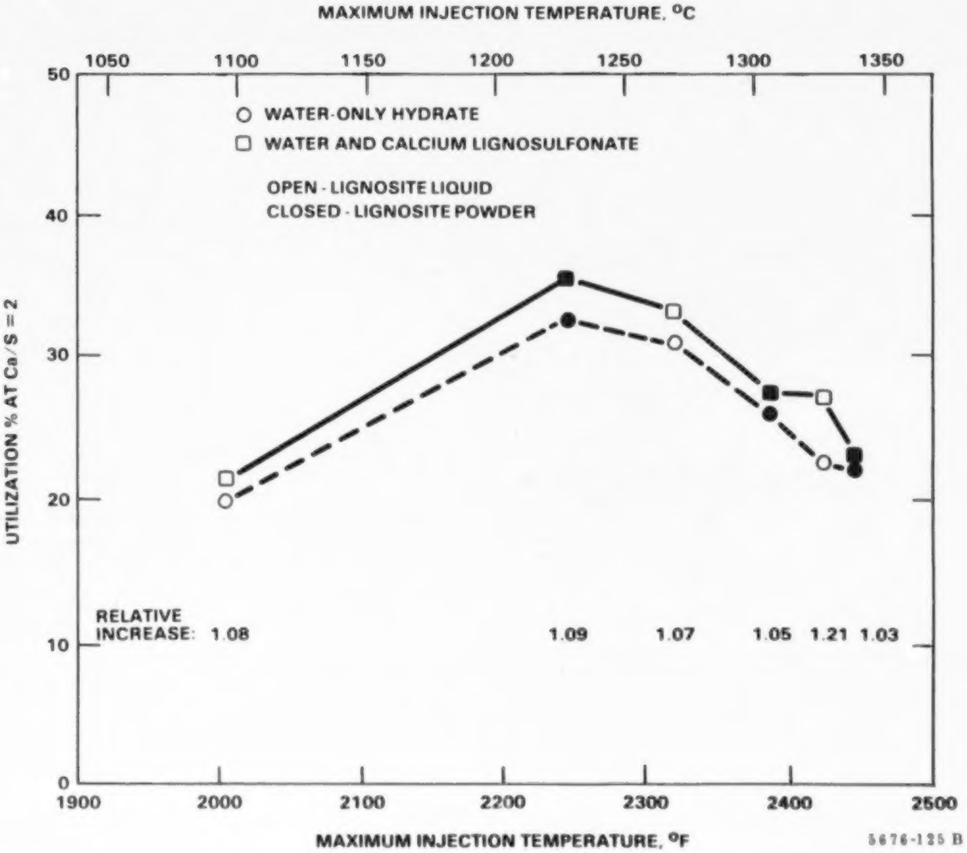

Figure 7-4. Enhancement of the utilization of Marblehead hydrate with Lignosite powder or liquid (Ca/S = 2).

Post-furnace humidification has been viewed as a possible means of increasing the utilization of $Ca(OH)_2$ sorbent in the Edgewater demonstration. Humidification will be depended upon to satisfy one other essential goal — adjustment of the ash-sorbent electrical resistivity to a lower value consistent with efficient electrostatic precipitation. Obviously, the process will be even more useful if it improves SO_2 removal. Post-humidification at Edgewater would be a process parallel to Consol R & D's "BLI Activation" process; it would differ, however, in that the sorbent at Edgewater is hydrated lime, whereas that in Consol R & D's process is limestone.

Experimental apparatus. The main component of the experimental apparatus used for the post-furnace humidification studies was a cylindrical humidification chamber on a vertical axis, which is illustrated in Figure 7-5. This chamber was inserted between segments of the 4 in. (10 cm) duct normally channeling flue gas at a temperature around 300 °F (150 °C) to the system exit. The inlet and outlet of the chamber were flared outward to a diameter of 36 in. (91 cm); the length of the chamber was about 10 ft (3 m). Thermocouples were mounted at intervals along the length of the chamber. A Sonic Development ST47 two-fluid nozzle was placed at the centerline near the inlet for injecting water or an aqueous slurry. The total residence time of flue gas in the chamber was 10 to 15 s, much longer than the time that would exist in an actual power-plant duct. The geometry, however, minimized collision of water droplets with the walls; moreover, the chief objective was to determine the upper limit of reaction. When water droplets were injected, their short lifetime (about 1 s) rather than the total gas residence time was the controlling factor on the extent of reaction.

The nozzle was operated at an air pressure of 80 psi (550 kPa) and a water flow rate of 5.75 cm^3/s. Sizing of the spray droplets with SRI's Video Droplet Analyzer indicated that the mass-median diameter was about 35 μm. The estimated time required for the droplets to undergo complete evaporation under the experimental conditions subsequently described was about 1.2 s. The ST47 nozzle was also used for slurry injection on occasion, as a substitute for water injection. Dry solids, on the other hand, were injected in a stream of air at a location immediately upstream from the humidification chamber.

A dilution probe was used to sample entrained solids at the outlet of the reactor. This probe dilutes the sample with hot, dry air through a porous wall just inside the inlet and performs the vital function of quenching reaction at the instant of sampling. A filter was used to collect solids from flue gas sampled at about 0.003 ft^3/s (0.1 L/s) and a dilution of 10:1. Analysis of these solids provided the data that were used to compute the utilization of the sorbent. This procedure was eminently superior to measurement of the change in gas-phase SO_2 concentration, which was heavily influenced by reaction with long-lived wall deposits.

An alternate sampling system — isokinetic with an in-duct filter — was used to determine the concentration of total suspended solids at the chamber outlet. It was also used on occasion at the inlet. There was no requirement at the outlet for the system to prevent further chemical reaction during sampling. On the other hand, the system was required to prevent reaction when

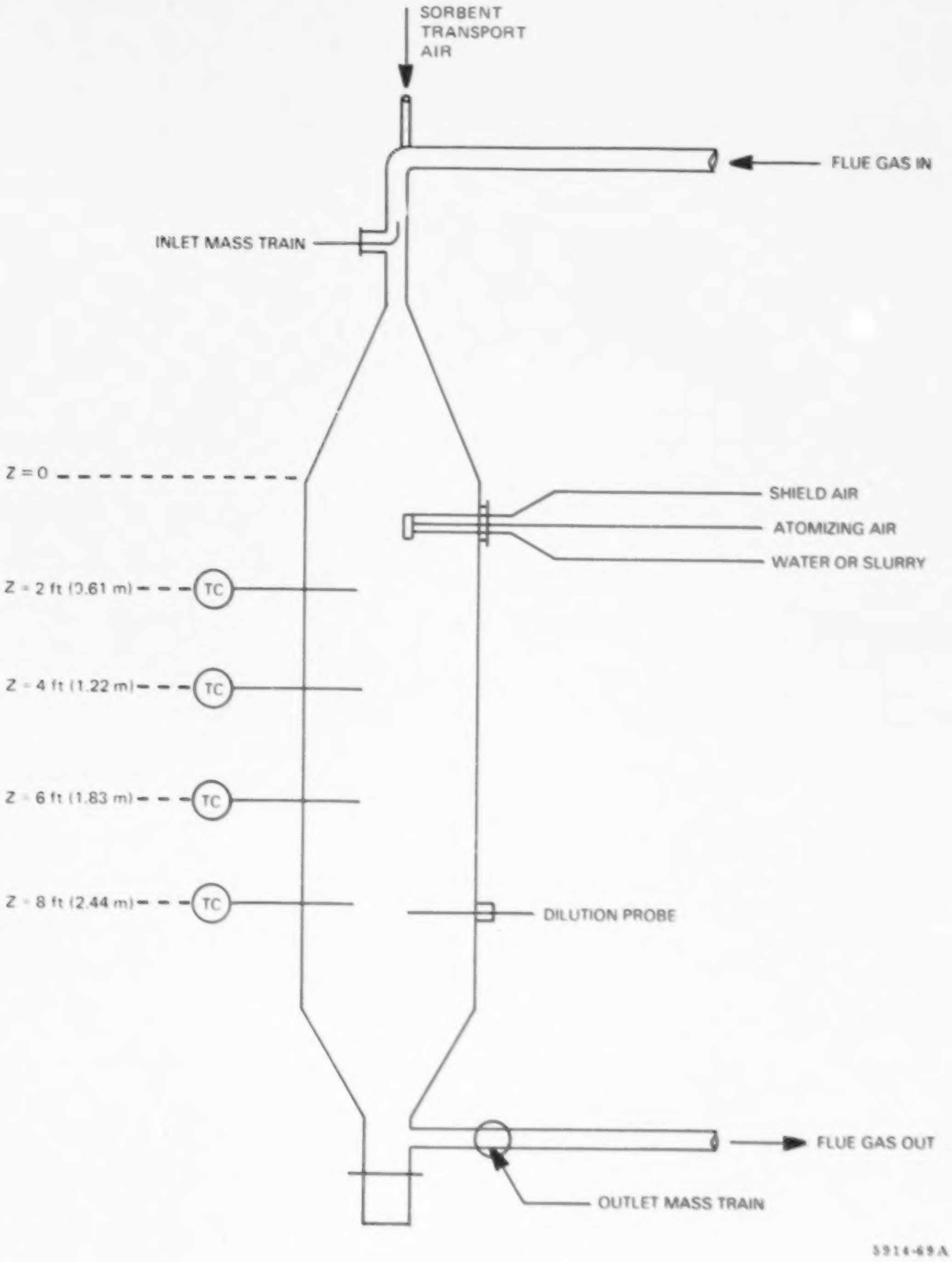
SORBENT
TRANSPORT
AIR
FLUE GAS IN
INLET MASS TRAIN
Z = 0
SHIELD AIR
ATOMIZING AIR
WATER OR SLURRY
Z = 2 ft (0.61 m)
TC
Z = 4 ft (1.22 m)
TC
Z = 6 ft (1.83 m)
TC
Z = 8 ft (2.44 m)
TC
DILUTION PROBE
FLUE GAS OUT
OUTLET MASS TRAIN
5914-69A

Figure 7-5. Humidification chamber showing injection and sampling points.

used at the inlet (when sorbent was injected upstream from the inlet, prior to injection of water); the system was found satisfactory with respect to this requirement.

Humidification of reinjected calcine. To facilitate a systematic study of humidification parameters, a large quantity of partially sulfated calcine was prepared for reinjection into the flue-gas stream immediately upstream from the humidification chamber. Reinjection of this material, followed by humidification, gave a simulation of the processes to be expected at the Edgewater demonstration if post-furnace humidification were to be adopted. The material was produced by injecting $Ca(OH)_2$ into the furnace at a Ca/S ratio of 2 during the addition of SO_2 to the combustion products from natural gas. The material was collected on the fabric filter at the exit from the combustor. Chemical analysis showed that the composition of material on the weight basis was 33% CaO, 23% $Ca(OH)_2$, 7% $CaCO_3$, 30% $CaSO_4$, and 7% other components. The calculated atom ratio Ca/S in the solid corresponded to a utilization of 18% in the furnace.

The reinjected calcine was subjected to the effects of humidification by three processes, as depicted schematically in Figure 7-6. First, the dry solid was injected into flue gas containing excess water vapor, which had been precooled to 160 °F (71 °C). At no time during this process was liquid water introduced, and thus at no time did the calcine become physically wet. Literally speaking, there was no humidification in this process, but the effects simulated humidification by vapor addition and convective cooling, with heat discharged to the surroundings. Second, the dry solid was injected into flue gas at a temperature near 300 °F (150 °C) and then liquid water was introduced as a spray to cool the flue gas to 160 °F (71 °C). Third, the solid was briefly slurried with water and then introduced as a spray at 300 °F (150 °C), which subsequently lowered the gas temperature to 160 °F (71 °C). (To facilitate spraying the slurry, a small impingement target near the exit of the ST47 nozzle, known as the resonator, was removed; the resonator was usually retained for spraying plain water.) The features common to all three processes were these: 1) the flue gas was generated by the combustion of natural gas; 2) the SO_2 was added from an external source to a concentration of 1100 ppm; 3) reaction of SO_2 with the solids occurred at the same temperature, the same humidity level, and the same approach to adiabatic saturation. The temperature was 160 °F (71 °C), which represented a 30 °F (17 °C) approach to saturation; the water vapor concentration was 0.17 mole of water per mole of dry flue gas. One of the primary differences in conditions was in the O_2 level; to make it possible to humidify the combustion gas from natural gas to the final level desired, the gas was burned with excess air when liquid water or slurry was to be injected. Another difference was in the Ca/S ratio in the humidification chamber; the ratio was 2 in the first and second methods but only 1 in the third, with slurry injection.

Determinations of sorbent utilization following humidification revealed increments in utilizations over the 18% absolute level that had occurred previously in the furnace. The results are as follows:

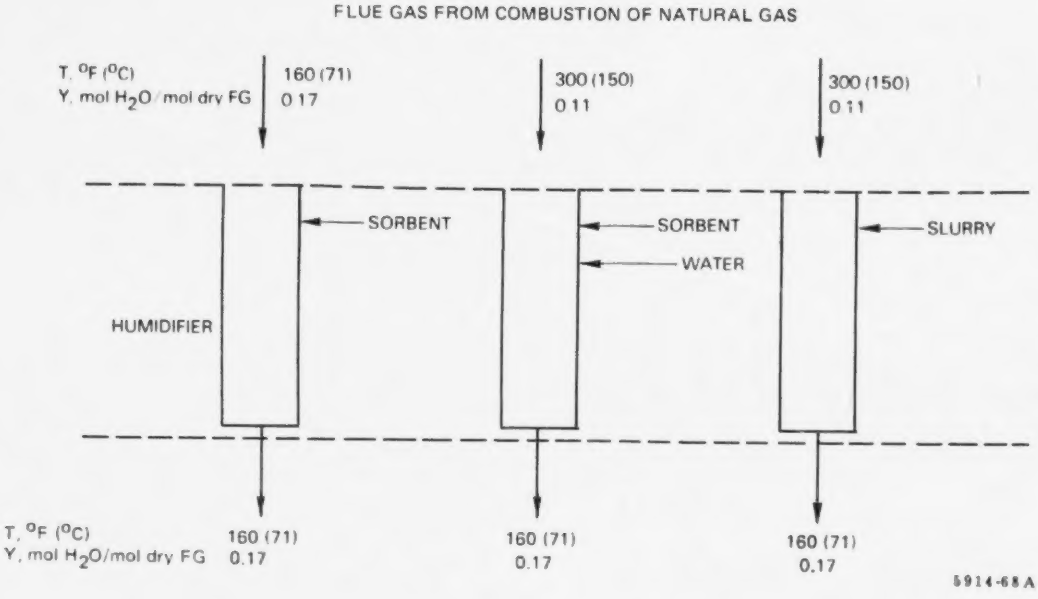
FLUE GAS FROM COMBUSTION OF NATURAL GAS
T, °F (°C)
Y, mol H2O/mol dry FG
160 (71)
0.17
300 (150)
0.11
300 (150)
0.11
SORBENT
SORBENT
WATER
SLURRY
HUMIDIFIER
T, °F (°C)
Y, mol H2O/mol dry FG
160 (71)
0.17
160 (71)
0.17
160 (71)
0.17
5914-68A

Figure 7-6. Schematic representation of humidification modes.

Humidification method	Increment in utilization
Cooling to enhance the effect of water vapor already present	1%
Cooling and humidification with a water spray	6%
Slurrying with liquid water and spray injection	33%

Very little reaction of SO_2 with the calcine occurred when only water vapor was present. A six-fold increase in reaction, giving an increment in utilization of 6%, occurred when the dry solid was subjected to the effects of a water spray. An increment in excess of 30% occurred with slurry injection. Comparison of the results obtained with the water spray and the slurry spray indicates that the extent of low-temperature reaction was controlled by the fraction of sorbent particles actually colliding with water droplets and becoming physically wet. The added increment due to the water spray (5%) divided by the increment due to the slurry spray (33%) is indicative of a collision efficiency of 15% (5/33 x 100 = 15).

The slurry was prepared on-line in order to minimize the time available for reaction of the water and calcine. Slaking tests with quicklime and sulfated calcine have shown that the latter material hydrates much more slowly, presumably due to the presence of a $CaSO_4$ layer. An initial concern was that this effect might prevent the activation of a sorbent particle in the time available in a humidifier. Although the estimated sorbent-water contact time of 30-60 s was much longer than that available in an evaporating droplet, the results show that the reaction is not inhibited to the degree indicated by the slaking tests.

Humidification of hydrated lime. To determine the effects of humidification on a sorbent that had not been subjected to high-temperature calcination, $Ca(OH)_2$ was injected into the flue-gas duct immediately upstream from the humidifier and allowed to react with SO_2 under the same conditions as those in the experiments with the partially sulfated calcine. The Ca/S mole ratio in each case was 2. The degrees of utilization observed following low-temperature reaction were as follows:

Humidification method	Extent of utilization
Cooling to enhance the effect of water vapor already present	9.6%
Cooling and humidification with a water spray	12%
Slurrying with liquid water and spray injection	28%

The results with the hydrated lime differ from those with the partially sulfated calcine primarily in terms of the effects produced by cooling only and by the combination of spray humidification and cooling. Cooling only gave a utilization of nearly 10% with the hydrated lime but an increment of just 1% with the calcine. The presence of water spray, on the other hand, increased the utilization of hydrated lime by just 2 points but increased that of the calcine by 5 points. Slurrying gave about the same result with both sorbents; this was a utilization of about 30% totally with the hydrated lime or about 30% incrementally with the calcine.

The similar effects of slurrying the calcine and the hydrated lime are particularly striking. They indicate that the shell of $CaSO_4$ product surrounding a core of unused sorbent in the calcine particles is not a strong deterrent to the promotional effects of liquid water. Evidently, the $CaSO_4$ shell sloughs off rapidly when liquid water is present and does not markedly retard the wetting and partial dissolution of the underlying sorbent.

Humidification of entrained calcine. For a more direct study of the humidification of partially sulfated calcine, $Ca(OH)_2$ was injected in the furnace, was thus subjected to calcination and sulfation in the furnace, and was then humidified at low temperature and subjected to further reaction with SO_2. Again the furnace was gas-fired and doped with SO_2 from an external source; a high level of excess air was used to produce humidity and temperature values at the humidifier that were comparable to those previously investigated. The burner was operated at either of two swirl angles for the secondary air. At 30°, there was a wide range of temperatures at the sorbent injection level — as high as 2780 °F (1525 °C), although the average was only 2070 °F (1130 °C). At 70°, on the other hand, the temperatures were more uniform at the injection level — maximum, 1990 °F (1090 °C); average, 1870 °F (1020 °C).

Utilization levels of the calcine measured at the inlet to the humidification chamber, as the result of sulfation in the furnace, were about 26%. Increments in utilization — due to humidification by the spray injection of liquid water — averaged 3.9% with 30° swirl in the furnace or 1.5% with 70° swirl in the furnace. These increments are, of course, substantially lower than that of 6% observed for reinjected calcine with the same humidification method.

Several factors may have contributed to the difference noted above for entrained and reinjected calcine. First, the reinjected calcine was less extensively utilized before humidification (18% rather than 26%). Second, the reinjected calcine was exposed to an SO_2 concentration of about 1100 ppm in the humidifier, whereas the entrained calcine reacted at a lesser concentration of about 700 ppm. Finally, the reinjected calcine was coarser in particle size — a factor that promoted more efficient particle-droplet collisions. It is reasonable to assume that, in general, humidification and cooling with a water spray will promote further reaction to a degree that is governed by the extent of prior reaction in the furnace.

Effects of wall deposits. Data on the utilization of suspended sorbent, based on analyses of solids removed in the dilution probe, usually indicated that the extent of SO_2 reaction was far below that signified by changes in the

SO_2 gas-phase concentration. Reaction of SO_2 with the solids deposited on the in-stack filter ahead of the SO_2 analyzer was not a significant contributor to this discrepancy. Hence, reaction of SO_2 with solids deposited on walls within the reaction system was assumed to be the primary cause of the discrepancy.

To test the validity of this assumption, material balances were attempted during several of the tests described above. Before each test, the humidifier chamber was thoroughly cleaned by brushing and washing. After the test, as much material as possible was removed from different areas of the walls, weighed, and analyzed to determine the amounts of calcium and sulfur in the deposits. During the test, entrained solids were collected in the dilution probe and in a mass train.

The results of material-balance determinations can be illustrated in terms of two experiments. In the first, partially sulfated calcine was injected into humid flue gas (no water was added); in the second, the dry calcine was injected and followed with a water spray. Here is a summary of the results:

- Recovery of calcium — from entrained solids, 32%; from chamber walls, 45%; total, 77%. Recovery of sulfur — from the gas phase, 82%; from entrained solids, 0.5%; from chamber walls, 11.5%; total, 94%. About 64% of the SO_2 removal from the gas phase was found in the wall deposits.

- Recovery of calcium — from entrained solids, 39%; from chamber walls, 47%; total, 86%. Recovery of sulfur — from the gas phase, 60%; from entrained solids, 5%; from chamber walls, 23%; total, 96%. Approximately 72% of the SO_2 removed from the gas phased was found in the wall deposits.

The incompleteness of calcium and sulfur recoveries does not detract from the conclusions reached. Whatever the disposition of unrecovered material may have been, the wall deposits recovered and analyzed still accounted for the fractions of SO_2 loss reported: in the first instance, 11.5/(100 - 82) or 64%; in the second instance, 23/(100 - 68) or 72%.

Conclusions. Water vapor alone is not effective for activating the removal of SO_2 by partially sulfated calcine at low temperature. Humidification of the sorbent with a water spray is more effective, but even its effectiveness is limited by the infrequency of collisions between the sorbent particles and water droplets. The rapid and extensive rate of reaction of sorbent in a slurry, even after very brief contact between sorbent and water, reveals that the key to successful humidification is increasing the frequency of sorbent-droplet collisions.

Investigation of Charge-Augmented Sorbent Humidification (CASH)

The foregoing discussion makes it clear that methods of increasing the frequency of collisions between sorbent particles and water droplets are needed to increase the effectiveness of spray humidification. Modeling studies that have been conducted under another project for EPA (under Cooperative Agreement

CR 812811) reveal that the fraction of sorbent particles that can be intercepted by water droplets increases as the droplet size increases, as the droplet velocity increases, and as the sorbent particle size increases. Another concept to be discussed here is that charge augmentation will provide another means for increasing sorbent-droplet interactions. Charge augmentation refers to a process whereby either sorbent particles or water droplets or both are given an electrostatic charge in order to increase their collision rate.

Charge-augmented sorbent humidification, or CASH, is a process conceived jointly by investigators at EPA and SRI. The initial work on this process was conducted as part of this project and then later continued under another cooperative agreement (CR 812811).

Experimental apparatus. The humidification chamber used for the CASH experiments is illustrated in Figure 7-7. The chamber was 8 in. (20 cm) in diameter and had a length of about 7 ft (2.1 m). Flue gas entered the chamber from a 4 in. (10 cm) duct at a temperature of about 300 °F (150 °C). Near the point SCI, the gas stream passed an ionizer, which imparted a negative charge to the entrained sorbent particles. Just below the ionizer, at the point SCO, the gas stream passed the spray nozzle, at which positively charged water droplets were injected. In the main part of the humidification chamber, a series of thermocouples were located at positions SC2, SC3, etc.

Beyond the humidification chamber, the flue gas stream passed again through a 4 in. (10 cm) duct and then entered a "residence-time chamber", approximately 12 in. (30 cm) in diameter and 7 ft (2.1 m) in length. The time of residence of the flue gas in this chamber was approximately 1.0 s, compared to a time of about 0.4 s in the humidification chamber. The overall system depicted in Figure 7-7 was in operation before the larger humidification chamber previously illustrated in Figure 7-5 became available; with a higher ratio of surface area to gas volume, it suffered to a greater degree from wall deposits.

Sorbent concentration and charge. Determination of the concentration of entrained sorbent particles was made to ensure that an adequate quantity of sorbent was transported from the furnace to the humidifier. Samples were withdrawn at the outlet of the humidifier both with and without particle charging. Quantities of sorbent recovered, relative to the quantities injected, were in the range 40 to 50%, which were typical for this combustor. There was no evidence that particle charging and any resulting particle precipitation significantly lowered the concentration.

Sorbent particles were charged negatively with a sharp-edged disc ionizer, with a diameter of 2.2 in. (5.6 cm), which was located in the centerline of the inlet duct to the spray chamber. Particle charge was determined by collecting particles at the humidifier outlet on an electrically isolated filter and measuring the accumulated charge. With the ionizer at the usual voltage setting, -20 kV, and the water flow rate at a typical value around 4 cm^3/s, the particle charge was in the range 5 to 9 $\mu C/g$, compared to a baseline value of 0.25 $\mu C/g$ with the ionizer not operating.

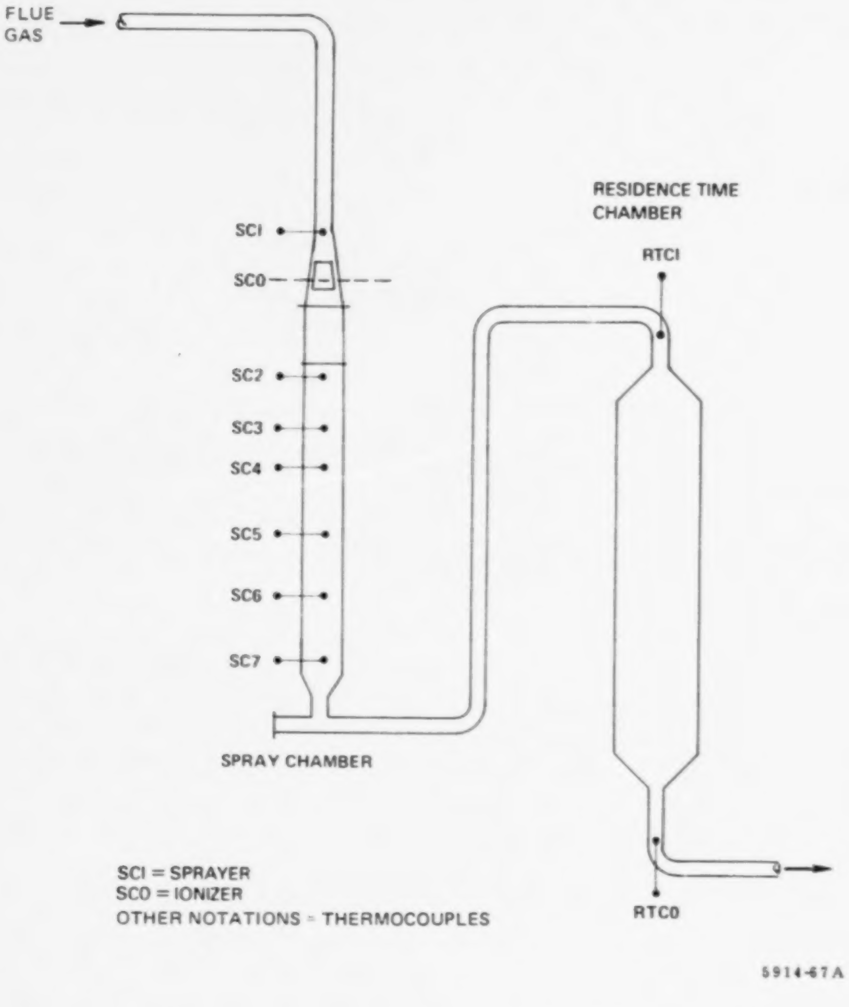
FLUE GAS
RESIDENCE TIME CHAMBER
RTCI
SCI
SCO
SC2
SC3
SC4
SC5
SC6
SC7
SPRAY CHAMBER
SCI = SPRAYER
SCO = IONIZER
OTHER NOTATIONS = THERMOCOUPLES
RTCO
5914-67A

Figure 7-7. Spray chamber and residence time chamber.

Water injection and droplet charging. A water spray was introduced with a Sonic Development ST47 two-fluid nozzle. The characteristics of the spray obtained with this nozzle have already been discussed in connection with other humidification studies.

The spray droplets were charged and the quantity of charge was measured with the system shown in Figure 7-8. The nozzle was electrically isolated from ground by channeling the water to the nozzle through plastic tubing; it was energized with a Spellman DC power supply. For measurement of charge, the spray was directed to a bed of steel wool, and the charge thus collected was discharged to ground through a microammeter. The ratio of charge to droplet mass was calculated from the ratio of current to water flow rate. The results were in the range 0.8 to 2.0 μC/g at nozzle voltages of 10 to 20 kV. The actual data were obtained with a negative polarity on the nozzle; the specific charge was assumed to be about the same with the positive polarity used for most of the humidification tests.

SO_2 removal. Tests were performed to compare SO_2 removal by three procedures: sorbent injection without humidification, sorbent injection with humidification but without charging, and sorbent injection with humidification and with charging. In some tests, limestone was injected in the furnace at 2300 °F (1260 °C); in others, hydrated lime was injected downstream from the furnace at 400 °F (200 °C). Firing was always with natural gas; it produced a water vapor concentration of 0.184 mole per mole of dry gas, which was increased by 0.054 mole per mole of dry gas when humidification was in progress (approach to saturation, 20 °F or 11 °C). SO_2 was added from an external source to produce a concentration of 2000 ppm. Changes in SO_2 concentration were used to calculate sorbent utilization; no solids analysis was performed to evaluate utilization by the more direct and reliable approach.

For limestone injection at Ca/S = 2.3 without humidification, the reduction in SO_2 concentration was approximately 30%, which corresponds to a utilization of 13%. Again for limestone injected but with humidification, the apparent utilization increased slightly, to about 14%. Both procedures were accompanied by a significant degree of wall reaction. When sorbent injection terminated, the SO_2 concentration did not return to the initial value, and it lagged even more during the experiments with humidification.

The effect of charge augmentation was determined by operating for a time with humidification and then activating the two charging devices. The results of one such experiment are presented in Figure 7-9. Charge augmentation had no observed effect on SO_2 removal. Similar experiments were conducted with a variety of experimental conditions:

- Charging conditions
    - no charging of sorbent particles; negative charging of water droplets
    - negative charging of both sorbent and water
    - negative charging of sorbent; positive charging of water.

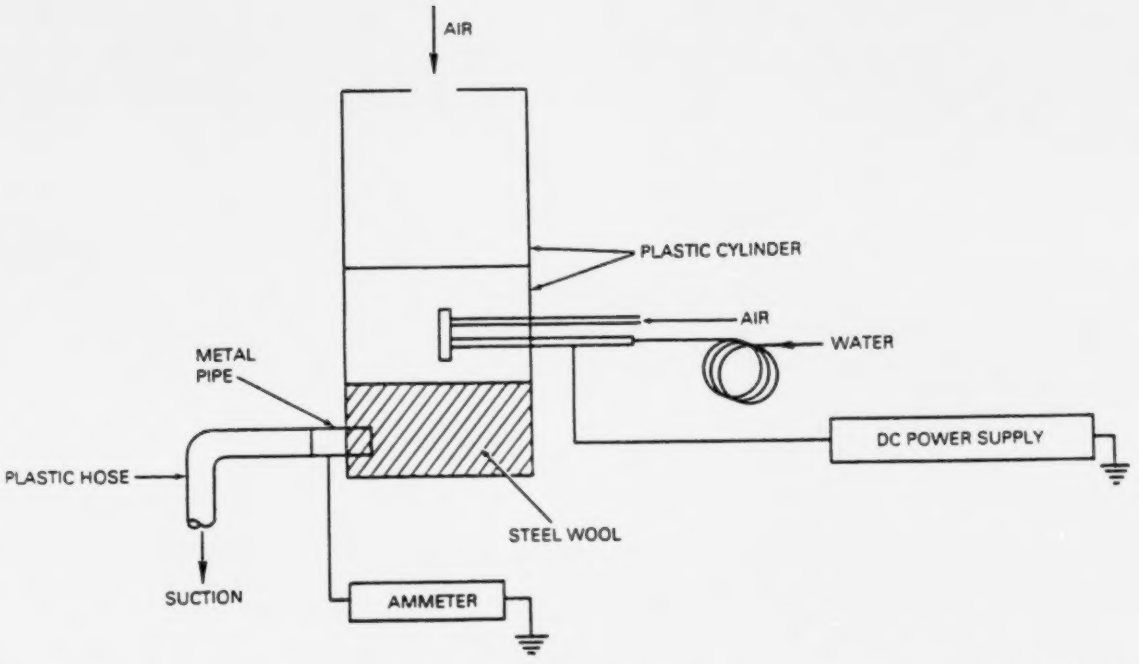
AIR
PLASTIC CYLINDER
AIR
WATER
METAL PIPE
DC POWER SUPPLY
PLASTIC HOSE
STEEL WOOL
SUCTION
AMMETER

5676-101A

Figure 7-8. Apparatus for drop charging and charge measurement.

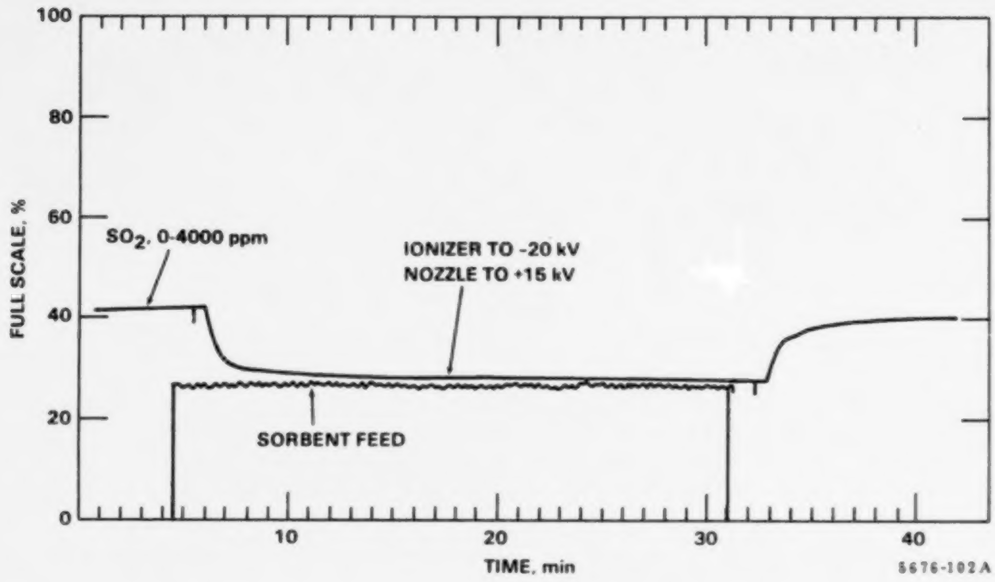

Figure 7-9. Charge augmentation of humidification to enhance SO_2 capture with limestone injection.

- Nozzle conditions
  - operation with the resonator in place (this device is a small impingement target near the exit)
  - operation with the resonator removed, which extended the droplet lifetime.

Under none of these conditions did charging increase the extent of SO_2 removal.

For hydrated lime injected at Ca/S = 1.8 without humidification, sorbent utilization was about 5%. When water was injected, utilization increased to 15%. When water was added and charging was also initiated, no further increase in utilization occurred. Thus, CASH was found equally ineffective for both limestone and hydrated lime.

Conclusions. In the preliminary studies of CASH described here, the effect on sorbent utilization was immeasurable. Even in further studies under Cooperative Agreement CR 812811 (now terminated), no favorable effect has ever been discerned. The reasons for this disappointing result are not clearcut. One possible explanation, however, is that the attractive force between oppositively charged sorbent particles and water droplets is small; it decreases with the square of the separating distance and is small in comparison with other electrical forces except when the separating distance is of the order of the particle-dimensions. The other electrical forces arise from the lack of precise electrical balance between positive and negative charges. In the absence of zero as a net charge in the cloud of particles and droplets, an electrical force operates on each, bringing about a separation and deposition on the container walls.

Study of Conditioning for Ash Resistivity Control

Preliminary tests during the Edgewater demonstration showed that the performance of the ESP was severely degraded by sorbent injection. This problem had been anticipated and plans made for humidification of the flue gas with a water spray, both to lower the temperature and to lower the ash resistivity. At the time of the work described here, the humidification system at Edgewater was not to be operable for several months; meanwhile, there was the need to determine whether either a temporary SO_3 conditioning system or a temporary humidification system might relieve the problem and allow sorbent injection trials to proceed in the interim.

Both SO_3 and water vapor conditioning were investigated. The effect of both on the resistivity of ash-sorbent mixtures was determined; also, the effect of water vapor on the voltage-current relationships of a pilot-scale ESP was determined. Ash resistivity was measured with a point-plane probe; this device normally provides two measurements: 1) "V-I" resistivity, which is based on a comparison of voltage-current curves for the probe with and without a precipitated dust layer and 2) "spark" resistivity, which is based on the electric field and current density where electrical breakdown occurs in the dust layer, when located between parallel planar electrodes.

SO_3 conditioning. Tests with a slipstream at the Edgewater plant revealed that the ash-sorbent mixture had a resistivity of 5×10^{12} ohm cm but that SO_3 injection could lower the value decisively. A concentration of 40 to 50 ppm gave a result of 4×10^{10} ohm cm; a concentration of 110-130 ppm gave 4×10^{9} ohm cm. The crucial question, however, was whether these resistivity reductions could be attained under the more unfavorable temperature conditions anticipated — for example, a temperature of 380 °F (195 °C).

The pilot-scale combustor in Birmingham was operated with the Edgewater demonstration coal as the fuel at 1×10^{6} Btu/h (300 kW) and with the Edgewater sorbent (Marblehead hydrated lime) as the sorbent with furnace injection. At an injection temperature of about 2100 °F (1150 °C) and a Ca/S ratio of 2, the sorbent was 25% utilized. The resistivity of the ash-sorbent mixture was not determined precisely but was found to be at least 1×10^{13} ohm cm at 350 °F (177 °C); this value is to be compared to 1×10^{10} ohm cm for the ash alone.

The SO_3 concentration from the furnace when sorbent was not injected was 31 ppm. This value increased to 82 ppm when SO_3 was added at a nominal rate of 60 ppm. This injection rate continued when sorbent injection was underway; the actual concentration present when sorbent was added, however, was not measured, since no method that is reliable under these conditions is known. The SO_3 was injected at a port about 1.4 s in transit time upstream from the port used for resistivity measurements; it was injected at a temperature 20 to 40 °F (11 to 22 °C) higher than that at the measurement site.

The results of the resistivity measurements for ash alone and for ash-sorbent mixtures with and without SO_3 conditioning are plotted in Figure 7-10. The data are for the range 300 to 380 °F (150 to 195 °C); all are based on the spark method, since the results by the V-I method were much more erratic. Obviously, injecting 60 ppm of SO_3 gave far less reduction in resistivity than was needed to compensate for the effect of the sorbent. Injecting more SO_3 was considered impractical in these tests and was not attempted.

Water vapor: effect on resistivity. A water spray was injected with one of the Sonic Development ST47 nozzles mentioned previously in this report. The nozzle was located in a chamber 8 in. (20 cm) in diameter, which was inserted in place of a segment of the usual 4 in. (10 cm) duct. The resistivity probe was placed in a 12 in. (30 cm) chamber downstream, beyond two 180° turns in the 4 in. (10 cm) connecting duct. This geometry and the residence time (1.6 s) should have minimized transport of water droplets into the probe.

Both spark and V-I resistivity data for ash-sorbent mixtures are plotted in Figure 7-11 as a function of the approach to saturation. Except for three outlier data points for spark resistivity near an approach of 20 °F (11 °C), the data indicate a trend toward a resistivity of 1×10^{11} ohm cm at saturation. The contrast between the resistivity of the unconditioned ash-sorbent mixture and the resistivity values of the conditioned (and cooled) ash-sorbent mixtures is depicted in Figure 7-12.

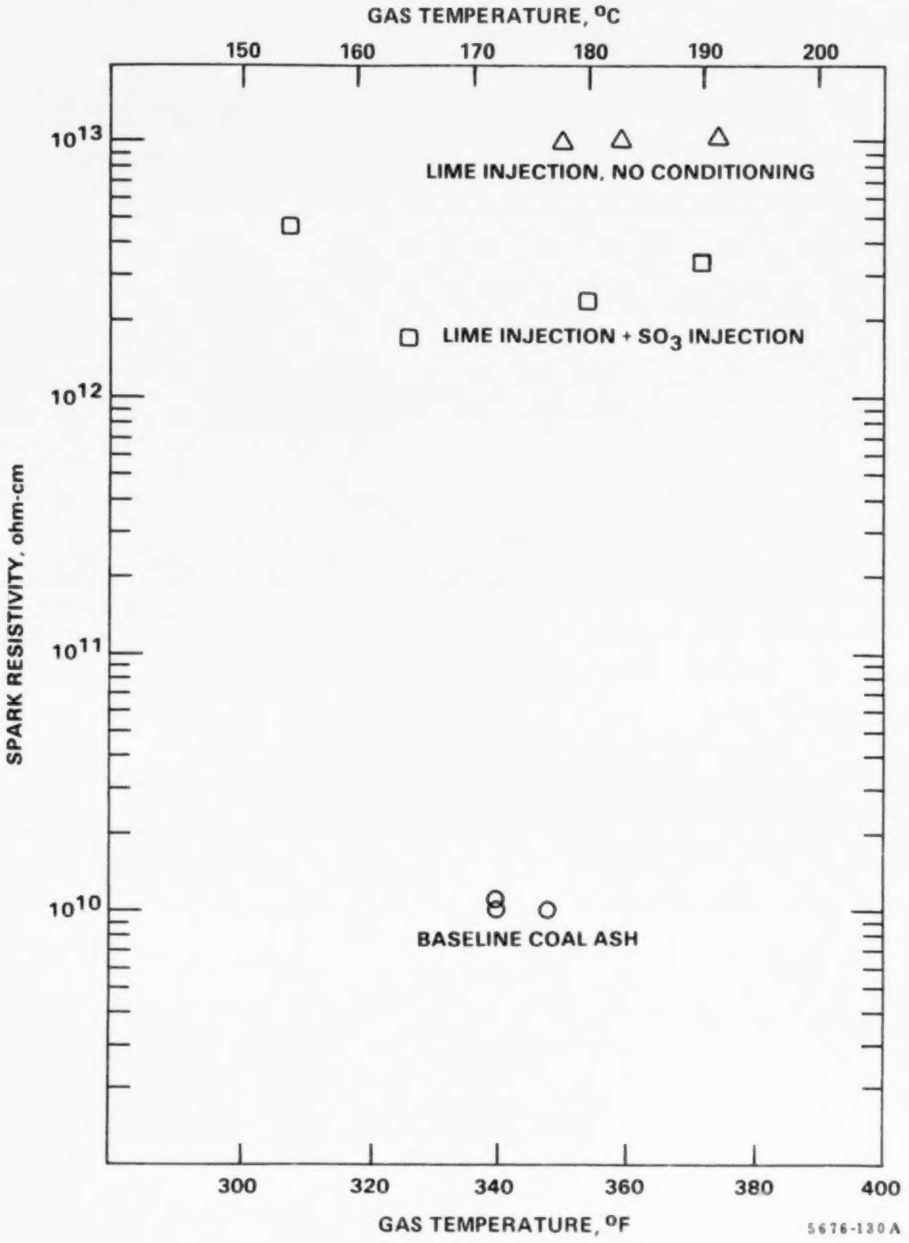

Figure 7-10. Resistivity of fly ash and ash-sorbent mixture with and without SO_3 conditioning.

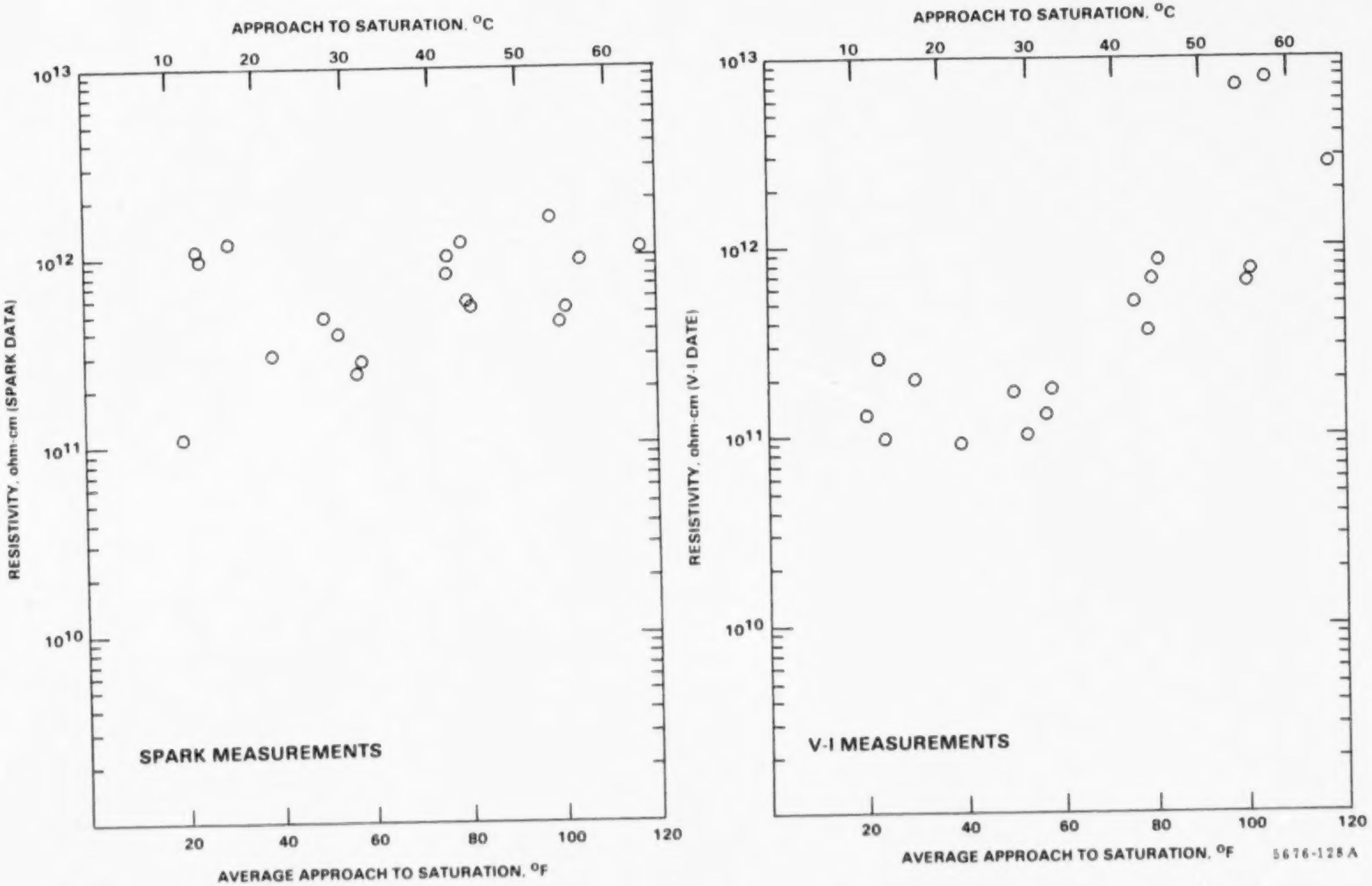

Figure 7-11. Resistivity of ash-sorbent mixture with water conditioning.

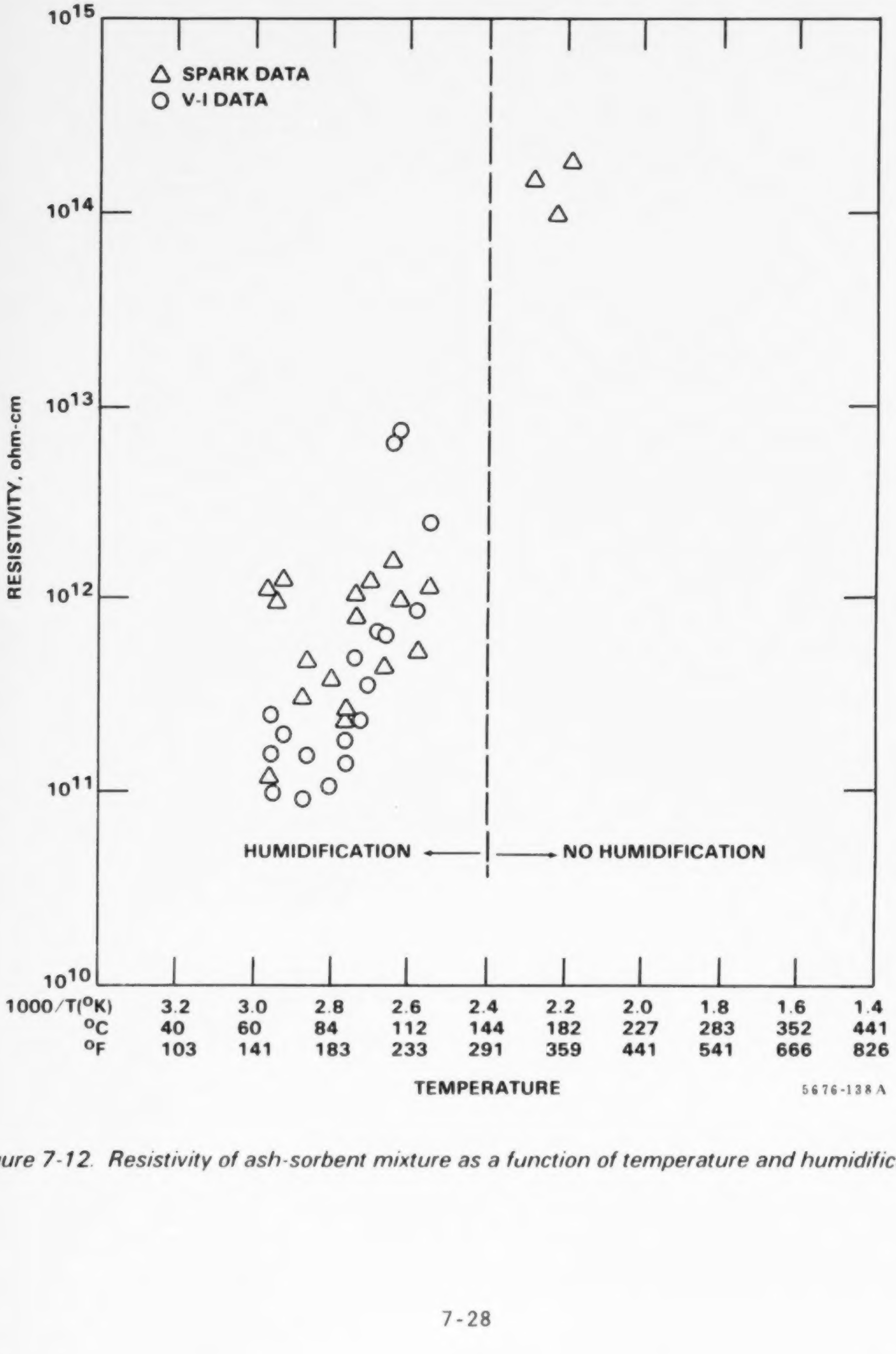

Figure 7-12. Resistivity of ash-sorbent mixture as a function of temperature and humidification.

Water vapor: effect on pilot-scale ESP. The pilot ESP is a single-lane wire-plate unit with two plates 26 in. (66 cm) high and 48 in. (122 cm) long in the direction of gas flow. It has a plate spacing of 9 in. (23 cm) and a wire separation of 6 in. (15 cm). Its specific collecting area is atypically low — 63 $ft^2/[1000\ ft^3/min]$ ($12\ m^2/[m^3/s]$); this makes the unit inappropriate for measurements of collection efficiency but does not preclude meaningful measurements of electrical conditions.

Voltage-current data from the ESP for ash alone and for ash-sorbent mixtures with and without water conditioning are shown in Figure 7-13. With the ash alone or with the water-conditioned ash-sorbent mixture, the data are indicative of favorable operating conditions. The lower current densities for the latter are, at least in part, a reflection of the partial current quenching by the finely-divided suspended fly ash in the interelectrode space; the lower current densities do not necessarily imply that the deposited ash has a higher resistivity. With the unconditioned ash-sorbent mixture, the data are indicative of unfavorable conditions; the sharp rise in current density between 45 and 50 kV suggests incipient back corona and sparking.

A plot of current density versus time, which is given Figure 7-14, gives further indications of the unfavorable effect that sorbent injection initiates and that subsequent water injection relieves. During the interval of sorbent injection, the current density was erratic; decreases in the voltage were required to suppress sparking. After conditioning was started, the current density rapidly decreased to more stable values; the temperature only gradually approached a new stable value, as a consequence of the thermal inertia of the system. Intermittent rapping of wires and plates removed deposits and permitted temporary operation at higher current densities.

Conclusions. In previous work, SO_3 has appeared to be a promising agent for lowering the resistivity of ash-sorbent mixtures. In this work, however, the agent gave only minimal effects at 60 ppm. The untreated mixture had a resistivity of 1×10^{13} ohm cm or greater; the treated mixture still had a value above 1×10^{12} ohm cm. The addition of a water spray, on the other hand, gave far better results. A water addition that lowered the temperature to 20 °F (11 °C) above the adiabatic saturation point and increased the water vapor concentration from 0.054 to 0.10 mole per mole by dry gas gave a resistivity of 1×10^{11} ohm cm. The favorable effect of water addition was confirmed by measurements of the voltage-current characteristics of a pilot-scale ESP.

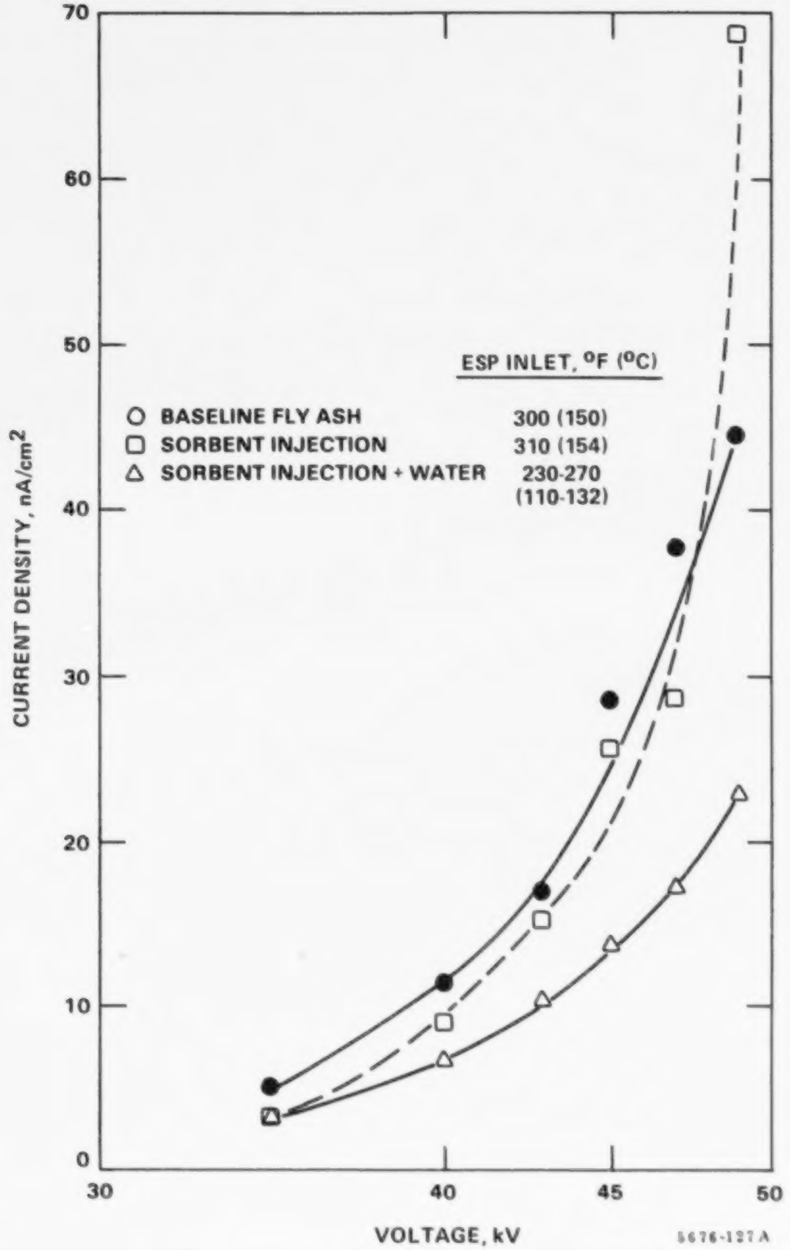

Figure 7-13. Pilot ESP voltage-current curves.

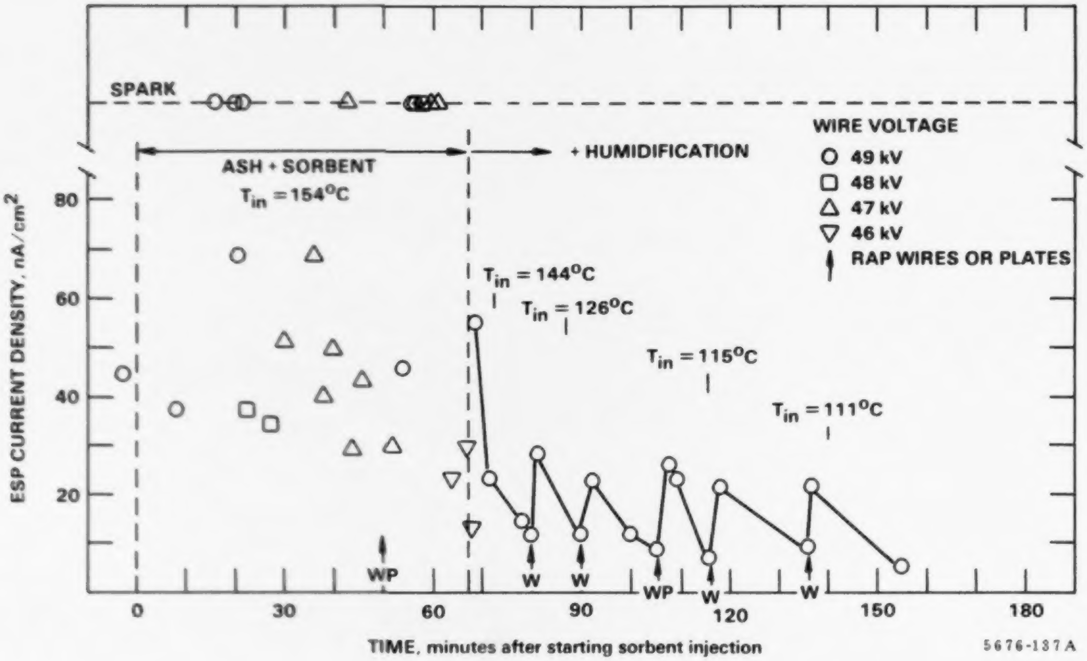

Figure 7-14. ESP electrical performance during sorbent injection, with and without humidification.

SECTION 8

REFERENCES

1. Bickelhaupt, R.E. A Technique for Predicting Fly Ash Resistivity. EPA-600/7-79-204 (NTIS PB80-102-379). U.S. Environmental Protection Agency, Research Triangle Park, North Carolina. 1979.

2. Faulkner, M.G., and J.L. DuBard. A Mathematical Model of Electrostatic Precipitation (Revision 3). EPA-600/7-84-069a,b,c. (Volume I, Modeling and Programming: NTIS PB84-212-679; Volume II, User's Manual: NTIS PB84-212-687; FORTRAN Source Code Tape: NTIS PB84-232-990). U.S. Environmental Protection Agency, Research Triangle Park, North Carolina. 1984.

3. Ballinger, D.W. (editor). Methods for Chemical Analysis of Water and Wastes. EPA-600/4-79-020 (NTIS PB 297686). U.S. Environmental Protection Agency, Cincinnati, Ohio. 1979.

4. Franson, M.A.H. (editor). Standard Methods for the Examination of Water and Wastewater. American Public Health Association, Washington, D.C. Fifteenth Edition, 1981. 1134 pp.

5. Gooch, J.P., R. Beittel, and E.B. Dismukes. Investigation for "Super-Sorbent" Processing. EPA-600/7-88-016 (NTIS PB). U.S. Environmental Protection Agency, Research Triangle Park, North Carolina. 1988.

6. Yoon, H., M.R. Stouffer, W.A. Rosenhoover, and R.M. Statnick. Laboratory and Field Development of Coolside SO_2 Abatement Technology. Second Annual Pittsburgh Coal Conference, Pittsburgh, Pennsylvania. September 1985.

APPENDIX

QUALITY CONTROL EVALUATION REPORT

Quality Assurance Project Plans

The work described in this report was performed in accordance with three separate Quality Assurance Project Plans (QAPPs). Work on Tasks 1, 2, and 5 was done in accordance with the QAPP submitted on June 1, 1985, and approved by EPA in January 1986. Due to the nature of the other two tasks (3 and 4), separate QAPPs were required by EPA. These QAPPs were submitted to EPA on November 15, 1985, and March 26, 1986, respectively. The QAPP for Task 4 was approved by EPA on May 1, 1986. No review was received on the QAPP for Task 3. The entire project and all tasks were designated as EPA QA Category III, and all QAPPs adequately addressed the seven critical areas of QA for Category III projects.

Management and Technical Systems Audits

On July 15, 1985, EPA conducted a Management Systems Audit (MSA) and a Technical Systems Audit (TSA) on the project and all associated tasks. Based on the results of these audits, the program was rated as "Acceptable, with Qualifications." The major qualifications were that separate QAPPs be prepared for Tasks 3 and 4 and that Standard Operating Procedures (SOPS) be more thoroughly documented for certain measurement systems. SRI responded by upgrading existing SOPs and writing some new SOPs. Separate QAPPs for Tasks 3 and 4 were also prepared and submitted as described above.

Evaluation of Measurement and Analytical Systems

All measurement and analytical systems were operated in accordance with the procedures given in the QAPPs. Accuracy was checked using NBS Standard Reference Materials (SRMs) and additional primary standards when appropriate. Precision was checked by use of duplicate runs and sample replicates. In general, the precision and accuracy of each system was found to be within the data quality objectives specified in the appropriate QAPP. For example, the precision and accuracy of the SO_2 measurements, which represent one of the most critical data elements in the project, were 6% and 3.6%, respectively. These are well within the objectives of 10% and 5%. Multipoint calibrations revealed excellent linearity in the instrument response.

Coal and sorbent feedrates. Coal and sorbent feedrates to the SRI pilot combustor were checked by weighing the amount of material discharged during a fixed time interval. The actual coal feedrate was found to be typically within 1% of the set point on the gravimetric feeder. Sorbent feedrates were slightly less dependable due to the smaller amount of material being fed. The accuracy of these data were not really an issue, however, because the test results were based on actual Ca/S ratios determined by chemical analysis.

Chemical analysis of ash and sorbent samples. All chemical analyses of ash and sorbent samples were checked for accuracy by the use of NBS SRM fly ash (SRM No. 1633a) and limestone (SRM No. 1c). Accuracies on all elements were well within the data quality objectives. Precisions were checked by replicate analyses of an Eastern U.S. fly ash. All relative standard deviations (RSDs) were under 2.5% except for sulfur trioxide, which had an RSD of 12%. This exceeded the data quality objective of 9%, which was based on past experience. This difference was not considered to be critical since sorbent utilization is based on soluble sulfate rather than sulfur trioxide.

Measurements of sorbent specific surface area. Specific surface area measurements were checked using two standards supplied by Quantachrome Corporation. The measurement accuracy was determined to be within 6.2% at the low surface area range (ca. 5 m^2/g) where the accuracy was 2.7%. Precision based on replicate determinations was 0.8 to 2.5%, expressed as relative standard deviation.

CHN and TGA analysis of hydrated LIMB ash. Two other analytical procedures, CHN elemental analysis and thermogravimetric analysis (TGA), were subjected to extensive QC evaluations due to their importance to the work on Task 4. Measurement accuracy was assessed using synthetic mixtures on reagent-grade materials (calcium oxide, calcium sulfate, calcium hydroxide, and calcium carbonate) mixed with NBS fly ash. The TGA was used to analyze for the sulfate, hydroxide, and carbonate. Accuracies for each component were determined on six different synthetic mixtures with differing compositions. For the sulfate and hydroxide, the relative errors compared to the known weight percentages were below 20 and 10%, respectively. For the carbonate, the relative error was as high as 165%. This large error was traced to the inability of the TGA to accurately determine low levels of calcium carbonate (less than 2% by weight). This error was inconsequential, however, due to the low levels of carbonate in all ash/sorbent samples.

EP toxicity extraction tests on LIMB ash. The atomic absorption (AA) analysis of the EP Toxicity extracts produced under Task 4 was calibrated by the method of standard additions, following an initial three-point calibration to verify proper optical alignment. These procedures were used prior to each set of analyses. No problems with accuracy or precision were encountered. Production of leachates by the TCLP procedure, which was under consideration at the time of project initiation, was not utilized due to uncertainties in the procedure.

Permeability measurements. For the permeability measurements under Task 4, the free moisture content of the sample cylinders was checked by weighing before and after drying at 110 °C. This method confirmed the reaction of the free lime with the water that was added for conditioning and stabilization prior to the permeability measurements. Thermocouples used for measuring temperature rise in the wetted LIMB ash were calibrated at the freezing and boiling points of water and checked against a mercury-in-glass thermometer.

Analysis of fractions from separation tests. Analysis of the steam elutriation tests under Task 4 were based on the CHN and TGA analyses described previously. These procedures were subjected to extensive QC as discussed previously. Results of magnetic separation and flotation tests were determined from chemical analyses of the separated fractions. These chemical analyses were subjected to the accuracy and precision checks described previously.

Aggregate strength evaluations. Compression testing equipment used for aggregate strength testing under Task 4 was calibrated by Southern Calibration and Service, Inc. in accordance with ASTM E4. Calipers used to measure pellet size were calibrated by Starett Co. using standards traceable to NBS. The Carver hydraulic press used to make the aggregate pellets was not calibrated since pelletizing pressure was not a variable in this study.

Auxiliary sampling equipment. Calibration of auxiliary sampling equipment included checking the RAC StakSamplr boxes with dry and wet test meters, checking tolerances on all sampling nozzles, checking resistivity probe electrode spacings with calipers, checking tolerances on cascade impactor hole sizes and jet-to-plate spacings, calibrating impactors with known aerosols, and calibrating the electrobalance used to weight particulate catches. These procedures were repeated at intervals on six months to one year in order to ensure the maintenance of reliable data throughout the project.

Sample Custody and Tracking

Sample custody and tracking requirements were met as specified in the QAPPs. All samples were assigned unique SRI notebook numbers referring to the page and section in which they are described in the laboratory notebook. Sample containers were marked with the corresponding numbers and other appropriate identifying information.

Internal Audits, QC Checks, and Corrective Measures

An internal audit by the SRI QA Manager revealed no serious deficiencies in the internal QC checks and data reduction. However, recommendations were made to standardize the use of laboratory notebooks for recording data during field measurement activities. This replaced the use of loose-leaf binders and loose forms. In cases where the forms were desirable, they were attached in the notebook. This facilitated access to the data for subsequent QC checks.

Limitations of Use of Data

The most significant limitation on the use of these data is that they should not be applied outside the range of the conditions studied. For example, the SO_2 removal data should not be used to predict the performance of a full-scale LIMB retrofit unless the boiler temperature profile and injection conditions are known to be similar to those given here. Similarly, the resistivity and particle size data would only be applicable to units firing the same coal and sorbent combinations under the same conditions. However, the general trends in the data would still apply.

The various LIMB ash utilization and separation techniques investigated under Task 4 are in a very early stage of development. Therefore, the results should not be extrapolated to commercial applications at this time. However, the results are still useful in assessing the relative merits of the various utilization and separation concepts.